

THESIS FOR THE DEGREE OF DOCTORAL OF PHILOSOPHY

**Agonist binding directs dynamic competition among nuclear
receptors for heterodimerization with their common partner,
retinoid X receptor**

By: Lina Fadel, Pharm.D, MS

**University of Debrecen
Doctoral school of Molecular Medicine**

Debrecen, 2022

THESIS FOR THE DEGREE OF DOCTORAL OF PHILOSOPHY

**Agonist binding directs dynamic competition among nuclear
receptors for heterodimerization with their common partner,
retinoid X receptor**

By: Lina Fadel, Pharm.D, MS

Supervisor: György Vámosi, PhD



University of Debrecen

Doctoral school of Molecular Medicine

Debrecen, 2022

Table of Contents

LIST OF ABBREVIATIONS	4
1. INTRODUCTION	7
2. THEORETICAL BACKGROUND	8
2.1. History of research on nuclear receptors (NRs)	9
2.2. Nuclear receptor superfamily classification	19
2.2.1. Classical classification of NRs	19
2.2.2. Genealogical classification of NRs	21
2.3. Structure of NRs	23
2.4. Mechanism of activation	24
2.4.1. Steroid receptors (SR) subfamily	24
2.4.2. RXR partners subfamily	25
2.5. Retinoid X Receptor (RXR) as a promiscuous partner	28
2.6. Crosstalk between nuclear receptors (NRs)	29
3. OBJECTIVES	32
4. MATERIALS AND METHODS	34
4.1. Cloning protocol	35
4.2. Plasmid Construction	39
4.3 Translocation assay (competition assay)	49
4.3.1. Generation of TagBFP-RXR α stable cell line	51
4.3.2. Cell culture	53
4.3.3. Immunofluorescence labelling and flow cytometry	53
4.3.4. Western Blot	53
4.3.5. Transfection	54
4.3.6. Limiting pool of RXR and RXR overexpression conditions	54
4.3.7. Ligand treatment	56
4.3.8. Microscopy	56

4.3.9. Analysis of microscopy data	56
4.3.10. Statistics	57
4.4. SPIM-FRET-ALEX-FCCS	58
4.4.1. Samples preparation.....	58
4.4.2. Microscopy setup	59
4.4.3. Fluorescence (Cross-)Correlation Spectroscopy, F(C)CS	59
4.4.4. Förster resonance energy transfer, FRET	60
4.5. Chromatin immunoprecipitation (ChIP).....	63
4.5.1. ChIP Protocol.....	63
4.5.2. VDR ChIP in THP1 cells.....	67
4.6. Fluorescence recovery after photobleaching, FRAP	69
4.6.1. Cell culture and transfection	70
4.6.2. Applied treatment.....	70
4.6.3. FRAP microscopy setting	70
4.6.4. Data analysis	71
5. RESULTS.....	73
5.1 RXR dependent nuclear accumulation of NRs as a pre-requisite step to apply our three-color imaging model system	74
5.2 Competition between RXR partners revealed by three-color imaging model system 80	
5.2.1. Competition between PPAR γ and RAR α	80
5.2.2. Competition between RAR α and VDR.....	83
5.2.4. Competition between PPAR γ and VDR	85
5.2.5. Competition of VDR/ <i>nls</i> m, as NR1, with RAR α or PPAR γ	88
5.2.6. Overexpression of RXR α abrogates competition between its potential heterodimerization partners	90
5.3. The effect of specific agonist treatment on RXR homodimerization revealed by SPIM-ALEX-FRET-FCCS	91
5.4. Chromatin binding of NRs is dynamically regulated by specific agonist treatment .	96

5.5. Doxorubicin effect on the mobility of RARα	100
5.5.1 Doxorubicin affects the binding of EGFP-RAR α to DNA	100
5.5.2. Doxorubicin had no effect on EGFP dimer diffusion	103
6. DISCUSSION	104
6.1. NLS1 mutants as a model system to study heterodimerization with RXR	105
6.2. Competition of NRs for their common partner, RXRα	106
6.3. Similarities and differences in the localization of NRs	109
6.4. Ligand-induced chromatin binding of VDR and heterodimerization with RXR are correlated	110
6.5. Doxorubicin effect on the DNA binding of RARα	111
Summary.....	113
REFERENCES	116
APPENDICES	133
I. LIST OF THE FIGURES	134
II. LIST OF THE TABLES	136
III. KEYWORDS	137
IV. Authenticated list of candidate's publications	138
V. Conferences' presentations and posters related to the dissertation topic	139
VI. ACKNOWLEDGMENT	140
VII. Publications related to the dissertation	Error! Bookmark not defined.

LIST OF ABBREVIATIONS

AF-H: Activation function helix
AF-1: N-terminal transcription activation function domain
AF-2: C-terminal ligand-dependent transcription activation function domain
AR: Androgen receptor
B: Tag-BFP, Blue fluorescent protein
C: mCherry, red fluorescent protein
cal: Calcitriol, VDR specific agonist
CAR: Constitutive Androstane Receptor
CEBPA: CCAAT enhancer-binding protein alpha
ChIP-seq: chromatin immunoprecipitation-sequencing
CNS: Central nervous system
COUP-TF: Chicken ovalbumin upstream promoter-transcription factor
DAX1: Dosage-sensitive sex reversal-adrenal hypoplasia congenital critical region on the X chromosome, gene 1
DBD: DNA-binding domain
DMEM: Dulbecco's Modified Eagle's Medium
Dox: Doxorubicin
DRs: Direct repeats
ER: Estrogen receptor
ERs: Everted repeats
FCS: Fluorescence correlation spectroscopy
FCCS: Fluorescence cross-correlation spectroscopy
FFA: Free fatty acids
FP: Fluorescent protein
FRAP: Fluorescence recovery after photobleaching
FRET: Förster resonance energy transfer
FXR: Farnesoid X receptor
G: EGFP, Enhanced green fluorescent protein
G418: Geneticin, antibiotic

GBS: Genomic binding site
 GCNF: Germ cell nuclear factor
 GR: Glucocorticoid receptor
 HEK293: Human embryonic kidney cells
 HEK293^{B-RXR α} : HEK293 cell stably expressing Tag-BFP RXR α
 HNF4: Hepatocyte nuclear factor 4
 HRE: Hormone response element
 IL15R α : Interleukin-2 receptor alpha
 IL2R α : Interleukin-2 receptor alpha
 IR: Inverted repeat
 LBD: Ligand-binding domain
 LBP: Ligand-binding pocket
 LRH-1: Liver receptor homology 1
 LSM: Light scanning microcopy
 LXR: Liver X receptor
 MOI: Multiplicity of infection
 MR: Mineralocorticoid receptor
 NCR: Nuclear-to-cytoplasmic ratio
 NES: Nuclear export signal
 NLS: Nuclear localization signal
*nls*m: Mutation in the NLS
 NOR1: Neuron derived orphan receptor
 NR: Nuclear receptor
 NR/*nls*m: Nuclear receptor with a mutation in its NLS
 NR1: The homogenous version of the RXR partner, or the studied partner
 NR2: The wt version of the RXR partner, or the competing partner
 Nurr1: Nur-related factor-1
 Nurr77: Nur-related factor-77
 PNR: Photoreceptor-cell-specific nuclear receptor
 PPAR: Peroxisome proliferator-activated receptor
 PR: Progesterone receptor

PTM: Post translational modification
PU.1: Purine-rich box 1
PUFA: Polyunsaturated fatty acid
PXR: Pregnane Xenobiotic Receptor
RAR: Retinoid acid receptor
RE: Response element
RevERB: Reverse ERB
ROI: Region of interest
ROR: RAR-related orphan receptor
RSG: Rosiglitazone, PPAR γ specific agonist
RUNX1: Runt-related transcription factor
RXR: Retinoid X receptor
RXR/*znm*: RXR with a mutation in its two zinc fingers motifs
SF-1: Steroidogenesis Factor-1
SHP: Short heterodimeric partner
SPIM: Selected plane illumination microscopy, Light sheet microscopy
TF: Transcription factor
THP-1: Immortalized monocyte-like cell line
TLX: Tallies homology orphan receptor
TR2: Testicular orphan receptor
THR: Thyroid hormone receptor
TR: Thyroid receptor
VDR: Vitamin D receptor
Wt.: Wild type
znm: Mutation in the two-zinc finger motif

1. INTRODUCTION

Nuclear receptors (NR) are a superfamily of structurally related proteins, which serve as the largest group of transcription factors in eukaryotes. They exert their transcriptional activity as a response to binding to their ligands; hence they are classified as ligand dependent transcription factors.

This family of receptors comprises 49 NRs in humans, and they sense a wide variety of ligands e.g. steroids, hormones, vitamins, metabolites, xenobiotics, etc. Many further molecules are being identified as ligands for NRs such as the signaling molecules; phospholipids and heme, which had extended the known types of ligands recognized by NRs.

Through binding to their ligands, NRs control a vast variety of biological process like development, cell differentiation, metabolism, and cell death. Consequently, dysfunctions in these pathways may end up with critical pathological issues ranging from simple metabolic diseases to cancers. Governing important signaling pathways spotlighted nuclear receptors as important druggable targets and a plethora of studies have been focusing on this field.

The initial observations on the molecular mechanism of NR action have been made by using “bulk” molecular biological and biochemical techniques. Numerous fluorescence microscopy studies on single cells have advanced our understanding of the molecular mechanism of NR activation by observing protein-protein and protein-DNA interactions and dynamics. Previously we have shown by fluorescence correlation spectroscopy that specific agonists increase chromatin binding of retinoic acid receptor alpha (RAR α) and retinoid X receptor alpha (RXR α) in a coactivator-dependent manner. We have also proven by light-sheet microscopy-based FRET and fluorescence cross-correlation measurements (SPIM-FRET-FCCS) that dimerization of RAR α and RXR α and chromatin binding of the dimer, as well as homodimerization of the RXR ligand binding domain (RXR-LBD) are enhanced upon agonist treatment.

Typically, multiple heterodimeric partners of RXR are present in certain cell types. In cells where there is a limiting or sequestered pool of RXR combined with the expression of several RXR heterodimerization partners, the mechanism by which RXR partner selection is mediated remains unclear. We hypothesized that there is competition between RXR partners for binding to RXR and that binding of a specific agonist increases the affinity of a given NR to RXR and favors their heterodimerization. RXR α and three NR partners were included in this study: Peroxisome proliferator-activated receptor gamma (PPAR γ), vitamin D receptor (VDR) and RAR α .

2. THEORETICAL BACKGROUND

2.1. History of research on nuclear receptors (NRs)

There is a debate about the origin of the nuclear receptors. One of the hypotheses claims that the ligands of NRs were evolved interdependently from the NRs while the other supports the notion that NRs were first “designed” for other biological processes and ligand binding is a gain of function¹.

In 1923, estrogen was first isolated from the urine of a pregnant woman as a crystalline compound². Soon after, other sex steroid hormones were identified like estradiol, progesterone and testosterone and a vast knowledge has accumulated concerning their similarity in structure and physiological activities on mammalian tissues and organs.

Despite this rich knowledge, the mechanism by which these compounds exert their functions remained unclear and it took scientists more than 30 years to isolate, using biochemical methods, a protein which could bind to estrogen, which was referred to as estrogen receptor (ER); in 1961, ER was the first NR to be identified³.

The revolution in the NR field emerged in 1985 when the cDNA of glucocorticoid receptor (GR) was cloned⁴. It was the first NR to be cloned and this revolutionary finding paved the way to the discovery of dozens of other evolutionary related proteins; the estrogen receptor (ER)⁵, the progesterone receptor (PR)⁶, the mineralocorticoid receptor (MR)⁷, the androgen receptor (AR)⁸, estrogen-related receptors (ERR)⁹ and *v-erbA*-related receptors¹⁰.

Based on homology in the sequence, another nuclear receptor responding to thyroid hormone was identified; thyroid hormone receptor (THR) is a gene encoded by *c-erbA*¹¹. This discovery laid the foundations for identifying another set of NRs, which can respond to non-steroid ligands.

In 1987, vitamin D receptor, VDR was first cloned by McDonnell et al¹² and retinoic acid (vitamin A) receptor, RAR, by Giguere et al¹³. The cDNA of these receptors showed a conserved evolutionary template, it also helped to delineate their structure and function and the concept of a superfamily of nuclear receptors emerged¹⁴.

Based on the homology in the sequences, many nuclear receptors had been discovered even before their endogenous ligands have been identified; thus, they were classified as orphan receptors. The discovery of orphan receptors foreshadowed the presence of undiscovered ligands and undescribed signaling pathways.

Several discovered orphan receptors are still waiting for an adoption while some others have characterized ligands by now.

RXR was the first adopted orphan receptor; its clone was first isolated in 1990 by Mangelsdorf et. al¹⁵ and in 1992, Heyman R.A et. al identified the 9-*cis*-retinoic acid as a high affinity ligand for RXR¹⁶.

Similarly, and in a short period of time, other NRs were isolated first as orphans and their cognate ligands were identified soon after. E.g., in 1990 Issemann & Green isolated peroxisome proliferator-activated receptors (PPARs), the name coming from their capability to induce peroxisome proliferation¹⁷. In 1992, fatty acids were identified as ligands for PPARs, and this study showed that PPAR activation promotes the transcription of acyl-CoA oxidase gene, the rate limiting enzyme in β oxidation¹⁸. This gave a glimpse into the importance of PPARs in fatty acid homeostasis.

In 1993, the concept of the RXR heterodimer was first described. Keller et al revealed the engagement of both RXR and PPAR in the regulation of the peroxisomal β oxidation of fatty acids¹⁹.

Evans & Mangelsdorf defined the discovery of RXR heterodimerization as the “Big Bang” because it had an explosive impact on the discovery of new signaling pathways²⁰. The RXR network expanded, and now it is considered as an obligatory partner for more than twenty other NRs²¹.

Besides these identified RXR partners, two other NRs known as xenobiotic receptors were cloned; the constitutive active/androstane receptor (CAR), which was named MB67 at first, and the Pregnane X receptor (PXR) were first cloned in 1994²² and 1997²³⁻²⁷, respectively.

In 1996, a very unique NR was cloned, which lacks a DBD and interacts with several other NRs as revealed by yeast two-hybrid system. This receptor was called the Short heterodimeric partner (SHP)²⁸.

The link between the ligand of the NR and the functional signaling pathway governed by this receptor urged scientists to find the ligand of other orphan receptors, i.e., in 1996 the oxysterols for liver X receptors (LXRs)²⁹ and in 1999 the bile acids for farnesoid X receptor (FXR)³⁰. In 2007 heme was first identified as a ligand for the orphan NRs; REV-ERB α and REV-ERB β ³¹.

In brief, we can say that soon after the identification of the GR sequence, discoveries accelerated, and the efforts of researchers intensified, and the NR family expanded to include 49 NRs in humans shown in *Table 1*. Naming nuclear receptors was agreed to reflect the names of their cognate ligands.

Table 1. Mammalian nuclear receptors and their cognate ligands.

Receptor name	Abbreviation	Endogenous ligands	Main biological function
Dosage-sensitive sex reversal-adrenal hypoplasia congenital critical region on the X chromosome, gene 1.	DAX 1	Orphan	Normal development and function of the hypothalamic-pituitary-adrenal-gonadal (HPAG) axis ³² .
Short heterodimeric partner	SHP	Orphan	<p>A negative regulator of other NRs' signaling pathways.</p> <p>Regulation of metabolic pathways, stress and inflammatory response, detoxification and cell cycle control.</p> <p>It has several interacting NR partners; LRH-1, HNF4, ERRs, LXRs, PPARs, GR, ERs, TRβ, RARα, FXR, PXR, CAR, AR, Nur77 and RXR.</p> <p>Direct binding to NRs is through AF-2 domain implying competition with coactivator binding and transcription inhibition of its partners³³.</p>

Receptor name	Abbreviation	Endogenous ligands	Main biological function
Thyroid hormone receptors	TR α TR β	Thyroid hormones.	Brain, bone and intestine development, lipid and carbohydrate metabolism, fetal development, growth, CNC myelination, cardiovascular and reproductive systems function ³⁴⁻³⁷ .
Retinoic acid receptors	RAR α RAR β RAR γ	all- <i>trans</i> retinoic acid (RA) 9- <i>cis</i> -RA 9- <i>cis</i> dihydro-13,14-RA, and n-3 polyunsaturated fatty acids ^{38,38}	Differentiation, proliferation and maintenance of immunity, homeostasis during inflammatory responses ³⁹ . It modulates the synthesis and metabolism of lipids and bile acids in hepatocytes, regulates cholesterol transport in macrophages, and represses fibrogenesis in hepatic stellate cells ⁴⁰ . It is essential for the eye health and development; for normal optic vesicle and anterior segment formation ⁴¹ .
Farnesoid X receptor	FXR α FXR β	Bile acids.	Bile acid homeostasis ⁴² .
Liver X Receptors	LXR α LXR β	Oxysterols.	Cholesterol homeostasis ^{43,44} .

Receptor name	Abbreviation	Endogenous ligands	Main biological function
Peroxisome Proliferator Activator Receptors	PPAR α PPAR β/δ	Fatty acids, Oxidized phospholipids, and Oxidized LDL.	Fatty acid oxidation, ketogenesis, lipid transport, gluconeogenesis, glycogen metabolism, and inflammation ⁴⁵ .
	PPAR γ	linoleic acid, fatty acids.	Regulates inflammation, and glucose and lipid metabolism ⁴⁵ .
Reverse-Erb	RevERB α RevERB β	Heme.	These two receptors regulate similar genes controlling metabolism, development, immunity and the circadian rhythm. Both receptors bind to ROR response element; ROR activates the transcription while RevERB represses it ⁴⁶ .
RAR-related orphan receptors	ROR α ROR β ROR γ	Sterols.	
Vitamin D receptor	VDR	1 α ,25-dihydroxyvitamin D3 and lithocholic acid.	Calcium and phosphor homeostasis, bone homeostasis, cell proliferation and differentiation to many tissues, oral health and regulation of apoptosis ^{47,48} .
Constitutive androstane receptor * Also known as MB67	CAR	Xenobiotics.	Protection of the liver from xenobiotic induced injury. Energy metabolism; glucose and lipid metabolism ⁴⁹ .

Receptor name	Abbreviation	Endogenous ligands	Main biological function
<p>Pregnane X receptor</p> <p>* Also known as steroid and xenobiotic receptor (SXR)</p>	<p>PXR</p> <p>* SXR</p>	Endobiotic and Xenobiotic.	<p>Detoxifying the body by eliminating xenobiotics and endobiotic.</p> <p>Anti-inflammatory effect; it inhibits NF-κB expression, and it maintains the intestinal wall integrity by regulating inflammation in hepatocytes and the small intestine.</p> <p>It increases cell motility which is beside enhancing drug metabolism could account for poor prognosis in cancers⁵⁰.</p>
Hepatocyte nuclear factors 4.	<p>HNF4α</p> <p>HNF4γ</p>	Fatty acids	<p>Master regulator of hepatic differentiation. It controls glycolysis, gluconeogenesis, ureagenesis, bile acid synthesis, drug metabolism, fatty acid metabolism, apolipoprotein synthesis, and blood coagulation⁵¹.</p>
Retinoid X receptors	<p>RXRα</p> <p>RXRβ</p> <p>RXRγ</p>	9-cis retinoic acid and docosahexanoic acid	<p>Obligatory heterodimerization partner for 20 other NRs²¹.</p> <p>It is still unclear if it has its “private” signaling pathway⁵².</p>

Receptor name	Abbreviation	Endogenous ligands	Main biological function
Testicular orphan receptor	TR2 TR4	Orphan * Polyunsaturated fatty acids (PUFAs).	Share ligands and HRE with PPAR γ but they have opposing effects on different signaling pathways ⁵³ .
Tallies homology orphan receptor	TLX	Orphan.	Functioning mainly through transcription repression. Maintains neural stem cell self-renewal in developing and adult brains ⁵⁴ .
Photoreceptor-cell-specific nuclear receptor	PNR	Orphan * Biliverdin ⁵⁵ .	Important for retinal photoreceptor development and maintenance; it represses the promoter of cyclin D1 attenuating the proliferation of S-cone cells ⁵⁶ . Anticancer effect by stimulating P53 acetylation ⁵⁶ .
Chicken ovalbumin upstream promoter-transcription factors	COUP-TF α COUP-TF β COUP-TF γ	Orphans.	Potent repressors of several NRs; RAR, TR, VDR, PPAR and HNF-4 ⁵⁷ . It is an important regulator of differentiation. The lack of its function is correlated with several diseases; infertility, diabetes and abnormality in vascular system ⁵⁸ .

Receptor name	Abbreviation	Endogenous ligands	Main biological function
Glucocorticoid receptor	GR	Glucocorticoids, Cortisone.	Metabolism and anti-inflammatory response ⁵⁹ .
Estrogen receptor	Er α Er β	Estrogens.	Functioning in both females and males. Responsible for: metabolism, reproductive organ development, bone re-modeling, cardiovascular system function and behavior ⁶⁰ .
Progesterone receptors	PR A/B	Progesterone.	Female reproductive functions; sexual behavior, menstruation, pregnancy and milk secretion ^{61,62} .
Androgen receptor	AR	Androgens; testosterone and dihydrotestosterone.	Male sexual differentiation, bone growth, muscle homeostasis, and development ⁶³ .
Mineralocorticoid receptor	MR	Aldosterone, Mineralocorticoids and glucocorticoids.	Controlling of electrolytes, extracellular volume, intracellular pH and blood pressure. It also contributes to cardiovascular and renal disease ⁶⁴ .

Receptor name	Abbreviation	Endogenous ligands	Main biological function
Estrogen related receptors	ERR α ERR β ERR γ	Orphan *cholesterols may be potential ERR α ligands ⁶⁵ .	Critical role in lipid and carbohydrate metabolism and mitochondrial function under both physiological and pathological conditions ^{66,67} .
Neuron derived orphan receptor 1	NOR-1	Orphan.	<p>They exert anti-inflammatory function.</p> <p>In macrophage, these NRs reduce inflammatory responses and lipid loading.</p> <p>This provided protection form atherosclerosis by inhibition of macrophage differentiation to foaming cells⁶⁸.</p> <p>In glia cells, Nur1 and Nur77 inhibit inflammatory effect of NF-κB⁶⁹.</p>
Nur-related factor -1	Nurr1	Orphan.	
Nur-related factor -77 * Also known as nerve growth Factor 1B or TR3.	Nurr77 * NGF-B1 * TR3	Orphan (Unsaturated fatty acids ⁷⁰)	
Steroidogenesis Factor-1	SF-1	Phospholipids ⁷¹	It plays a role in early sexual differentiation and in steroid hormone biosynthesis ⁷² .

Receptor name	Abbreviation	Endogenous ligands	Main biological function
Liver receptor homology 1.	LRH-1	Phospholipids ⁷³ .	<p>Differentiation and development, reverse cholesterol transport, bile-acid homeostasis, and steroidogenesis⁷³.</p> <p>It upregulates proliferation and tumor growth markers like c-Myc; it enhances cell migration, wound healing and invasion⁷⁴.</p> <p>It promotes cancer formation and confers it an aggressive malignancy by enhancing the metastasis. It has multiple effects on activating ER signaling pathway promoting breast cancer⁷⁵⁻⁷⁷.</p>
<p>Germ cell nuclear factor.</p> <p>* Also known as retinoid receptor-related testis-associated receptor.</p>	<p>GCNF</p> <p>* RTR</p>	Orphan.	<p>Transcriptional repressor essential for normal embryonic development⁷⁸.</p>

2.2. Nuclear receptor superfamily classification

The 49 identified nuclear receptors in humans are a superfamily of ligand dependent transcription factors, which may share a similar structure, a similar mechanism of activation, a similar nature of ligands, or a sequence alignment.

As the criteria of classification differ, the number of NR subfamilies described in the literature varies.

Here we present both the:

- i) The classical classification of NRs into four subgroups based on their dimerization, DNA binding specificity and ligands^{79,80}, shown in *Fig. 1*.
- ii) The genealogical classification where the structure and the function of the NRs were added to the classification criteria, rendering the NR superfamilies divided into seven subgroups as can be seen in *Table 2*⁷⁰.

2.2.1. Classical classification of NRs

Subgroup 1, steroid receptors (SRs):

Members of this subfamily are activated upon binding to cholesterol-derived steroid hormones such as androgen, estrogen, progesterone and corticosteroids.

They recognize a specific DNA sequence called a hormone response element (HRE), this HRE is composed of inverted repeats (IRs) (two NR-binding sequences with opposite orientations) and bind to their specific DNA sequence as a homodimer.

Receptors belonging to this subfamily: AR, GR, MR, ER, PR.

Subgroup 2, RXR partners:

The ligands of these receptors are non-steroids, rather they recognize a wide variety of ligands; hormones and vitamins. All the members of this family require heterodimerization with RXR as a pre-requisite step for their proper transcriptional activity. On the DNA they recognize specific response elements composed of two direct repeats (DRs) (two NR-binding sequences with identical orientation separated by several base pairs).

Receptors belonging to this subfamily: PPAR, VDR, RAR, TR, LXR, FXR, CAR, PXR, COUP-TF.

Subgroup 3, homodimeric orphan receptors:

Structurally the members of this family are similar to other NRs but differ in the DNA specific binding sequences; they bind to both inverted repeats (IRs) and direct repeats (DRs), and there is also no defined endogenous ligand for their own activation; hence, they are classified as orphans.

Receptors in this category can bind to similar target genes as NRs and therefore they can play an important role in the activation of alternative pathways; e.g., binding of RevERbA α to its response element acts as a transcriptional repressor for genes regulated by RXR-RAR receptors.⁷⁹ Before identifying 9-cis retinoic acid as an endogenous ligand for RXR, RXR was recognized as a homodimeric orphan receptor⁸⁰.

Receptors belonging to this subfamily: RevERb, ROR, GCNF, HNF-4, TLX, TR2.

Subgroup 4, monomeric orphan receptors:

Similar to subgroup 3, activation of NRs of this subgroup doesn't require ligand binding. More studies are needed to understand the structure and the function of orphan receptors.

RevERbA and ROR are classified as both dimeric⁷⁹ and monomeric⁸¹ orphan receptors.

Receptors belonging to this subfamily: SF1, NUR77, RevERb, ROR, ERR.

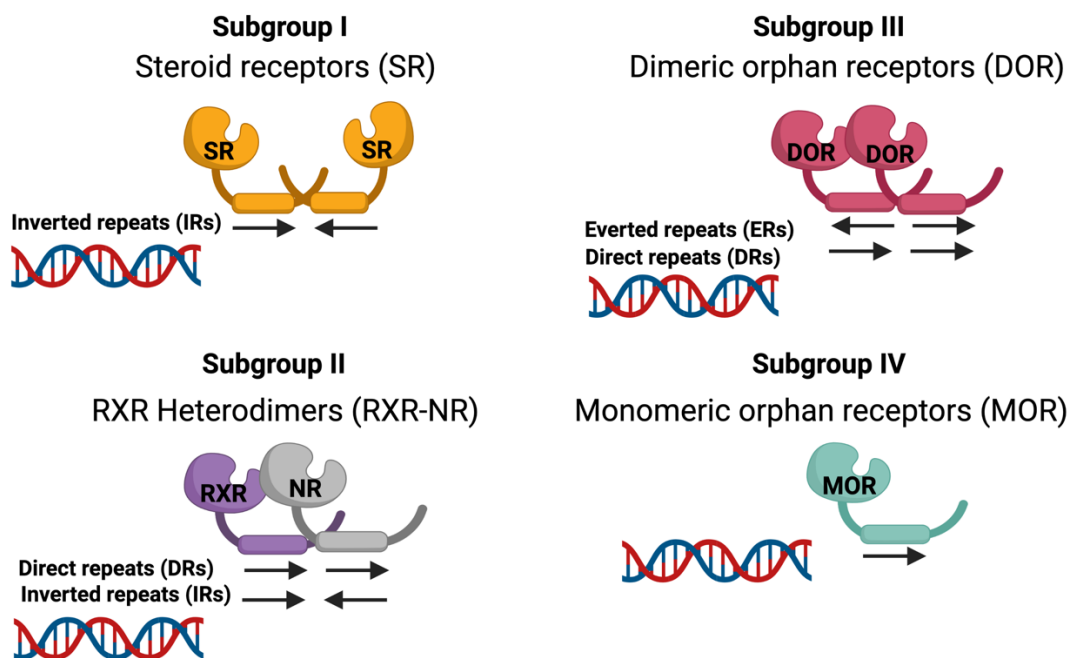


Figure 1. Nuclear receptors classical classification into four subfamilies.

Created with BioRender.com

2.2.2. Genealogical classification of NRs

In 1999, the Nuclear Receptors Nomenclature Committee recommended this classification to be the base for a new unified nomenclature for the members of this superfamily.

Table 2. Nuclear receptors classification into 7 subfamilies⁷⁰.

Subfamily name		Receptors members	Classification criteria are based on their:
Subgroup 0	NR0B	DAX1 SHP	Shared structure: these two atypical receptors consist of only an LBD. Their LBDs fold in a similar manner to those of other NRs and have similar motifs to the ones seen in NR coactivators; they can interact with other NRs.
Subgroup 1	NR1A	TR α , TR β	<p>Nature of the ligand: These receptors are activated by a wide variety of non-steroid lipophilic molecules.</p> <p>The HRE they recognize: On the DNA they can recognize direct repeats (DRs).</p>
	NR1B	RAR α , RAR β , RAR γ	
	NR1C	PPAR α , PPAR β/δ , PPAR γ	
	NR1D	RevERB α , RevERB β	
	NR1F	ROR α , ROR β , ROR γ	
	NR1H	LXR α , LXR β FXR α , FXR β	
	NR1I	VDR PXR (SXR)	

Subfamily name		Receptors members	Classification criteria are based on their:
Subgroup 2	NR2A	HNF4 α , HNF4 γ	<p>Ligands and function: classified as orphans but structural studies have shown that these receptors are able to bind to fatty acids even though it is not clear yet if they can drive a ligand dependent regulation as other NRs.</p>
	NR2B	RXR α , RXR β , RXR γ	
	NR2C	TR2, TR4	
	NR2E	TLX PNR	
	NR2F	COUP-TF α , COUP-TF β , COUP-TF γ .	
Subgroup 3	NR3A	Er α , Er β	<p>Ligands nature: steroids. Function: regulators of metabolism, reproductivity and development.</p>
	NR3B	ERR α , ERR β , ERR γ	
	NR3C	AR GR MR PR	
Subgroup 4	NR4A	NGF1-B (Nurr77, TR3) Nurr-1 NOR-1	<p>Function: These neuron derived orphan receptors are required for neuron development.</p>
Subgroup 5	NR5A	SF-1 LRH1	<p>Ligand nature: Both can be activated by phospholipids. Function: These receptors are important for development, metabolism and steroidogenesis.</p>

Subfamily name		Receptors members	Classification criteria are based on their:
Subgroup 6	NR6A	GCNF (RTR)	Structure: Only one receptor in this subgroup. GCNF shows a critical difference in its structure. Its LBD does not contain activation function helix (AF-H).

In conclusion, the classification of the receptors will keep being updated as many subtleties of the molecular mechanism of activation are being clarified and alternative mechanisms are being suggested. Moreover, more endogenous ligands are continuously being identified taking the receptors out from the orphan category.

2.3. Structure of NRs

Nuclear receptors share a common structure composed of several functional domains: a N-terminal transcription activation function domain (AF-1), a DNA-binding domain (DBD), a flexible hinge region and a ligand-binding domain (LBD) also functioning as a ligand-dependent transcription activation function domain (AF-2) at the C terminus ^{82,83} (*Fig. 2*).



Figure 2. Schematic representation of nuclear receptors structure.

Created with BioRender.com

The length of the AF1 varies among NRs; it is the least conserved domain. Its activation is ligand independent. The majority of the posttranslational modifications (PTM) which modulate the function of NRs and correlate it to the pathology of several disease. Phosphorylation, acetylation and SUMOylating, occur mainly in the AF1 domain⁸⁴.

DBD is a conserved domain maintaining the structure and the function of the NRs. The DBD is composed of two zinc finger motifs working together as a single functional domain to maintain the structure of the DBD. Between the two motifs, there is a nuclear localization signal termed

NLS⁸⁵. Importin proteins recognize the NLS and shuttle the NRs from their place of synthesis, the cytoplasm, to their place of action, the nucleus. There is also a proposed nuclear export signal, NES, near the carboxylic end of the DBD. The DBD of RXR and its partners also contributes to receptor heterodimerization.

DBDs recognize a specific sequence on the DNA called a hormone response element (HRE)⁸⁶. These sequences could form direct (DR), inverted (IR), everted (ER), or palindromic (pal) repeats.

RXR heterodimers recognize HREs composed of two AGGTCA half-sites arranged as direct repeats (DRs) and separated by a spacer of 0 to 8 base pairs termed DR0 to DR8^{87,88} (*Fig. 3*).

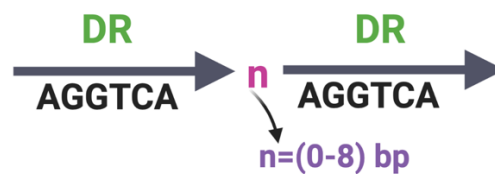


Figure 3. Schematic representation of REs recognized by RXR heterodimers.

Created with BioRender.com

The LBD is also a conserved domain, and it accommodates the core function of nuclear receptors. It contains the ligand-binding pocket (LBP) and the AF-2, the ligand dependent transactivation domain. It is responsible of dimer formation, coregulator binding and ligand-dependent transactivation⁸⁹.

2.4. Mechanism of activation

The mechanism of activation is well characterized for both steroid receptors and RXR partners subgroups of NRs. The receptors in subgroups III and IV are mainly orphans and more studies are needed to clarify their mechanism of activation.

2.4.1. Steroid receptors (SR) subfamily

In the absence of ligand treatment, some of these receptors like GR and MR reside constitutively in the cytoplasm while ER is mainly nuclear. Whether nuclear or cytoplasmic, these receptors bind to chaperon proteins; Hsp90 and Hsp70, the co-chaperone p23, and TPR proteins like FKBP52, FKBP51.

The classical model of activation of these receptors supports the notions that soon after ligand binding, conformational changes occur and lead to dissociation of SRs from the chaperon complex and subsequent translocation into the nucleus. Liganded SRs bind as homodimers to specific DNA sequences in the regulatory regions of their target genes. The hormone-free SRs are exported back to the cytoplasm and kept engaged in this nuclear-cytoplasmic cycle. Besides the receptors' cycle, the chaperon also undergoes an accompanied nuclear-cytoplasmic cycle⁹⁰.

According to the classic model, chaperons are not involved in the nuclear translocation of the receptors, the translocation is merely ligand dependent.

Recent observations have stated that dynein/dynactin motor complex associates with the Hsp90-FKBP52 complex bound to GR and MR. This led to the suggestion of a new molecular model in which the receptor translocates into the nucleus in a chaperon-bound state opposing the classic model. The new model can be explained by the immunophilin exchange; upon steroid binding, FKBP51 is released from the receptor complex and replaced by FKBP52⁹¹ besides the observations that the dynein/dynactin motor complex associates with the Hsp90-FKBP52 complex bound to MR⁹² and GR⁹³.

Previous studies have shown that FKBP51 interacts very weakly with dynein/dynactin⁹⁴ while FKBP52 has a strong interaction^{95,96}. Thus, the displacement of FKBP51 by FKBP52 enhances the binding of the receptors to dynein/dynactin and subsequently their nuclear translocation. In other words, steroids bind to their cognate receptors while it is still binding to chaperons and the whole heterocomplex, steroid-steroid receptor-chaperon protein, translocates into the nucleus.

In brief, the main differences between the classic and the alternative model is that in the new model the chaperons not only stay bound to the receptors while the receptors shuttle to the nucleus but also the chaperon can facilitate this translocation.

This alternative new model of activation has been approved for GR and MR and further studies are needed to support this model and to generalize it to the other members of this subfamily of nuclear receptors.

2.4.2. RXR partners subfamily

RXR and its partners share a common mechanism of activation described in a molecular switch model⁹⁷ as illustrated in *Fig. 4*. In brief, it is a conformational change in the receptor in response to ligand binding from an apo form, in the absence of ligand or in the presence of antagonist

binding, to a holo form, upon binding to agonists. Apo receptors have a high affinity for binding corepressors like SMRT/TRAC or NCoR/RIP13, rendering them transcriptionally repressed. Agonist binding releases the receptors from corepressor binding and enhances the interaction with coactivators like DRIP and the subsequent transcription initiation and target gene expression^{97,98}.

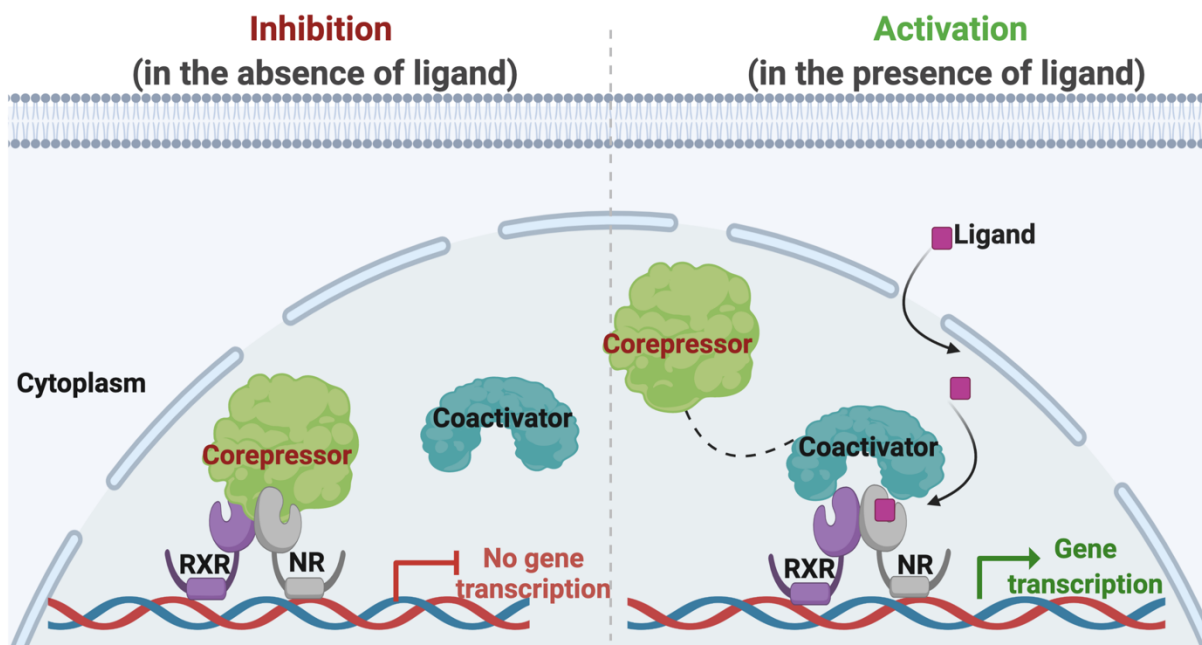


Figure 4. Activation mechanism of RXR partners subfamily according to the molecular switch model

NRs binding to DNA in the repression state (left) and in the activation state (right). Created with BioRender.com

Comparing the structure of the apo RXR and the liganded holo RAR showed a major structural rearrangement of H12 upon agonist binding. This change in structure was described by the mouse-trap model where agonist binds to the LBP and H12 bends to close the pocket⁹⁹.

Later on, other NRs' LBD structures have been identified and it has been shown that the LBD does not make a large movement in the H12, given LRH-1 as an example. Besides, the LBD of other NRs like LRH-1, PPAR, ER, and GR get stabilized upon ligand treatment. These urged the scientists to propose a more dynamic model, the dynamic stabilization model, which can substitute the old mouse trap model^{70,100-102}.

The mechanism of switching coregulators is also accompanied by changes in the chromatin status of activation; corepressors have histone deacetylase activity whereas coactivators have among others histone acetyl transferase activity¹⁰³.

Recently, ChIP-seq data revealed a more diverse pattern of nuclear receptors binding to DNA. Data showed that RXR partners not only bind to DNA as a heterodimeric complex with RXR but can also bind to non-specific regions on the DNA as monomers in the absence of agonist treatment, giving VDR as an example¹⁰⁴. Fluorescence microscopy based biophysical techniques suggested that NRs spend a significant fraction of their time diffusing (or moving) in the nucleus^{105,106}.

These observations suggested a more dynamic model of activation, the hit-and-run model. A transcription factor needs to be bound to the chromatin only for the time period needed to carry out its function, then it can disassociate. This model can explain why in some cases the binding of a TF cannot be detected, although its biological response is present; the TF senses the signal and hit its specific binding sites, serving as a trigger or catalyzer TF, then it is released to other binding sites leaving a room for other TFs to bind and maintain the transcriptional activity, serving as auxiliary TFs^{107,108}.

From another aspect, after reviewing the literature including our previous studies, we can highlight several points that could improve our understanding of the mechanism of activation of RXR partners.

i) Heterodimerization with RXR has been found to increase the nuclear accumulation of several RXR partners: VDR¹⁰⁹, Nur77¹¹⁰, PXR and CAR¹¹¹. *ii)* Specific agonist treatment can augment the heterodimerization of their cognate receptors with RXR^{104,112}. *iii)* Specific agonist treatment can enhance the DNA-bound fraction of their receptors^{105,112}. *iv)* Specific agonist treatment increases the specific DNA-binding of their receptors¹⁰⁴. *v)* Heterodimerization with RXR causes an increase in the affinity between the heterodimer and the coactivators¹¹³.

Putting things together, we can summarize these observations and extend the molecular switch model to cover the following points: receptors in their holo form have a higher DNA-associated fraction than in their apo form; receptors in their holo form have a higher tendency to heterodimerize with RXR; DNA binding also enhances heterodimerization and heterodimerization can enhance coactivator binding. These encourage us to propose a new matrix model of activation where all the participants: the availability of RXR and its partners, the ligands, and the coactivators, the heterodimerization, and the proper DNA binding, contribute synergistically to bringing the heterodimers into an active status.

2.5. Retinoid X Receptor (RXR) as a promiscuous partner

Starting with the nomenclature, the X in RXR refers to the mystery when it was first identified in 1990 as a receptor that can be activated by ATRA but is not able to bind it. Two years later, 9-*cis* RA was identified as an endogenous ligand for RXR.

Structural studies have shown that most of the selective ligands of RXR have a characteristic bent structure; the ligand binding pocket (LBP) of RXR is very restrictive. 9-*cis* RA with its twisted polyene side-chain can fit in the LBP of RXR while ATRA with its elongated polyene side-chain is excluded¹¹⁴.

There are three isotypes of RXR: RXR α , RXR β , and RXR γ encoded by three different genes RXRA, RXRB, and RXRG, respectively, and they display different tissue distribution.

RXR plays a pivotal role as a transcription regulator, it serves as an obligatory heterodimerization partner for twenty other nuclear receptors: CAR, FXR, LXRs α and β , NUR77, NURR1, PPARs α , β/δ and γ , PNR, PXR/SXR, RARs α , β and γ , RARs α , β and γ , SHP, TRs α and β , and VDR¹¹⁴.

Besides forming heterodimers with other NRs, RXR is also able to bind to DNA as a homodimer.

RXR and its partners exert transcriptional activity controlling a wide variety of biological processes related to development, cell differentiation, immunity, metabolism and apoptosis.

In the heterodimeric complex, RXR-NR, RXR could be either *i)* a silent partner; the heterodimeric complex of RXR-NR does not respond to RXR ligand, or it could respond to it only in the presence of the partner ligand. These heterodimeric complexes are called non-permissive, e.g., VDR, RAR and TR. *ii)* an active partner; the heterodimeric complex of RXR-NR responds to either the ligand of RXR or the ligand of its partner. These heterodimeric complexes are called “permissive”, e.g., PPAR and LXR. Douglas J. Kojetin et al 2015 defined in their study that the difference between permissive and non-permissive heterodimers is structural; in the non-permissive dimer, the partner allosterically silences RXR¹¹⁵.

RXR has both a nuclear localization signal (NLS) and a nuclear export signal (NES) rendering it to shuttle between the nucleus and the cytoplasm but with a preferred nuclear localization. Its cytoplasmic presence allows RXR to transport via a piggyback mechanism some of its heterodimeric partners from the cytoplasm to the nucleus like NUR77¹¹⁰ and VDR¹⁰⁹.

Several RXR heterodimerization partners could be expressed in one tissue, given the liver as an example where almost all RXR partners are expressed¹¹⁶; thus, in a cell where there is limiting

availability of RXR and several RXR partners are expressed, a competition between these NRs for RXR binding could be suggested. (Fig. 5).

In this study, we will focus on detecting the interactions between RXR and three of its partners: PPAR γ , VDR and RAR α , trying to unravel the mechanism behind RXR partner selection.

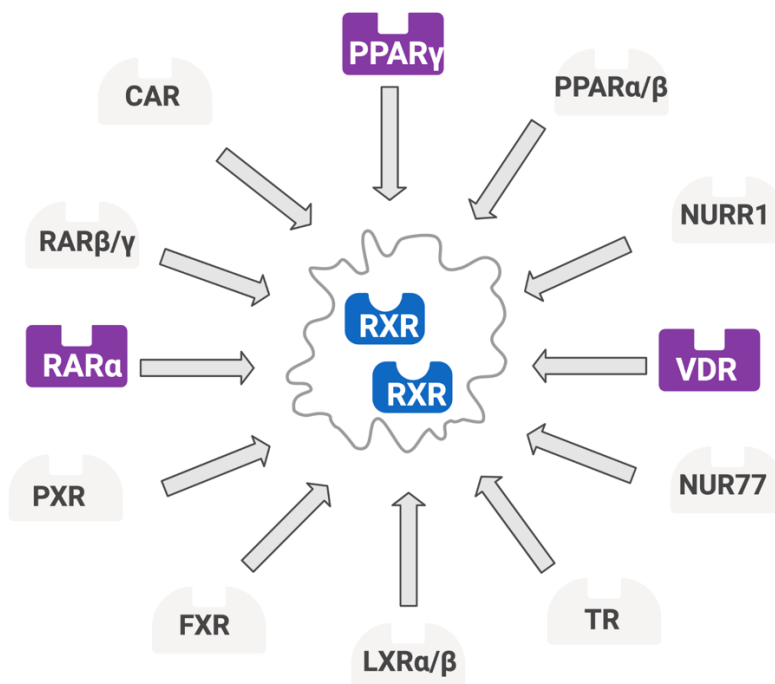


Figure 5: Schematic representation for several RXR partners sharing a limiting pool of RXR.

Created with BioRender.com

2.6. Crosstalk between nuclear receptors (NRs)

Nuclear receptors are excellent targets for drug intervention, and their ligands are widely applied drugs in many diseases. In recent clinical trials, unexpected side effects have been observed despite the high specificity of the drug-NR interaction.

Understanding the crosstalk between NRs could add more clues to solve the puzzle and help to circumvent the drawbacks correlated with NR-ligand treatment. This may also help to improve the treatment strategies using already FDA-approved drugs.

The similarity in structure, mechanism of activation and sharing of coregulators (corepressors and coactivators) suggested a crosstalk between NRs²¹.

Bosscher et al defined dual NR crosstalk as “the phenomenon whereby two concomitant nuclear receptor-associated signaling pathways are intertwined, which results in the triggering of a unique signaling and gene expression profile”¹¹⁷. Generally, we could say that crosstalk between NRs is a complicated phenomenon. It could occur on the upstream or the downstream levels of regulation or even at the DNA binding level.

PPAR γ was shown to dominate the signaling pathway of VDR, it attenuated 1,25-dihydroxyvitamin-D3 mediated transactivation of VDR in human breast cancer cells,¹¹⁸ and it also suppressed TR signaling in epiphyseal chondrocytes.¹¹⁹

Expression of TR in embryonic carcinoma cells suppresses the RA-dependent transactivation mediated by endogenous RAR β ¹²⁰. PPAR/RXR binding to the response element of PPAR was shown to be reduced in the presence of LXR α or LXR β ¹²¹.

Retinoic acid treatment of undifferentiated mouse embryonic stem cells decreases the expression of LXR target genes as well as decreases RXR binding at LXR response elements (RE), while inducing RXR redistribution to RAR target genes¹²².

Besides direct transcription regulation, NRs have also been reported as modifiers of intracellular signal transduction pathways by interacting with the components or participants of the signaling cascade. RAR has been found to modulates the activation of signaling pathways in the cytoplasm by interacting with Akt, p38, WNT and ERK¹²³⁻¹²⁵. In bone cells, the effects of ATRA and Vit D on bone cells differentiation and WNT pathway, can also indicate a crosstalk between RAR and VDR.

While Retinoic acid treatment was found to inhibit the WNT signaling by upregulating the WNT inhibitor DKK1¹²⁶, Vitamin D could strongly decrease the expression of WNT inhibitor *DKK1* and *sFPR2* and activate the expression of *LRP5* (it is the co-receptors of WNT)¹²⁷.

In contrast to the classical application of NRs-ligands in clinic, the use of ligands targeting more than one NR could serve as a more efficient strategy than targeting only one NR at a time. This could be the case in diseases where many NRs are identified to be relevant for therapeutic intervention. Evans et al proposed in their study a novel approach to treat type 2 diabetes mellitus, insulin resistant patients with a simultaneous activation of PPAR α , PPAR γ and PPAR δ ¹²⁸ whereas the classical approach is to apply thiazolidine, a PPAR γ specific agonist. This will encounter the

direct causative factor and enhance the tissue sensitivity for insulin which is obtained at the price of developing several side effects, e.g. obesity.

Despite a plethora of knowledge on NRs exists as a result of extensive research in the field, many gaps in our understating of NRs mediated gene control are still present and many points are yet to be clarified.

Here, based on our results on the ligand dependent competition of NRs for heterodimerization with RXR, we bring forward a rational approach applying cotreatment strategies, which could address the unmet treatment goals and answer the unexpected side effects associated with single treatment strategies.

3. OBJECTIVES

In cells where there is a limiting or sequestered pool of RXR^{21,97,129,130} combined with the expression of several RXR heterodimerization partners (NRs), the mechanism of RXR partner selection remains unclear. Previous data suggested that specific agonist treatment could enhance heterodimerization and chromatin binding of RXR and RAR^{121 105,106 112}.

Here in, we aimed to answer the following questions:

- I. Is there competition between RXR partners for binding to RXR?**
- II. Does binding of a specific agonist increase the affinity of a given receptor to RXR and favor their heterodimerization?**

To study these questions, we developed a nuclear translocation assay for monitoring the heterodimerization of RXR and its NR partners specifically; PPAR γ , VDR and RAR α , and competition was detected at different treatment conditions.

As heterodimerization is a prerequisite step for proper transcriptional activity of NRs, we also aimed to the answer:

- III. What is the effect of specific agonist treatment on the direct DNA binding of NRs?**

Chromatin immunoprecipitation sequencing was applied to unravel the changes in the genomic binding sites of VDR upon specific agonist treatment.

Better understanding of RXR α partitioning between its different heterodimeric partners may help to improve the therapeutic application and reduce the side effects of drugs triggering different specific signaling pathways and explain how targeting a NR pathway can interfere indirectly with a seemingly distinct NR pathway.

Intercalators like doxorubicin influence the superhelicity and dynamics of chromatin¹³¹, which may affect the binding of nuclear proteins to their specific response elements. Previous studies have suggested that treatment with specific RAR agonists like ATRA could reduce the cardiotoxicity¹³² of doxorubicin and increase its efficacy¹³³. Thus, we set out to investigate:

- IV. How does doxorubicin affect the DNA binding of RAR α ?**

To this end, we monitored mobility changes of RAR α upon treatment with different doses of doxorubicin, in the absence or presence of specific RAR α agonist. Changes in DNA-binding of NRs may interfere with their transcriptional activities and could account in part for the side effects caused by doxorubicin.

4. MATERIALS AND METHODS

4.1. Cloning protocol

Nuclear receptors were cloned into the pCMV-C3 vector; NR used as an insert “PCR product” while EGFP-C3 or mCherry-C3 as a vector.

The restriction map and multiple cloning site (MCS) of pEGFP-C3 vector is shown in *Fig 6*. and of pRSET-B-mCherry C-1 in *Fig. 7*. Both plasmids were purchased from Clontech Laboratories (Mountain View, CA).

mCherry-C3 vector was prepared as described previously¹⁰⁵. In brief, EGFP seq was cut out using NheI and ScaI restriction enzymes and replaced by the insertion of mCherry-C3 sticky ends amplicon. To prepare the mCherry-C3 amplicon, proper primers were used to correct for the frame shift and to insert NheI and ScaI restriction sites using mCherry-C1 vector seen in *Fig. 7* as a template.

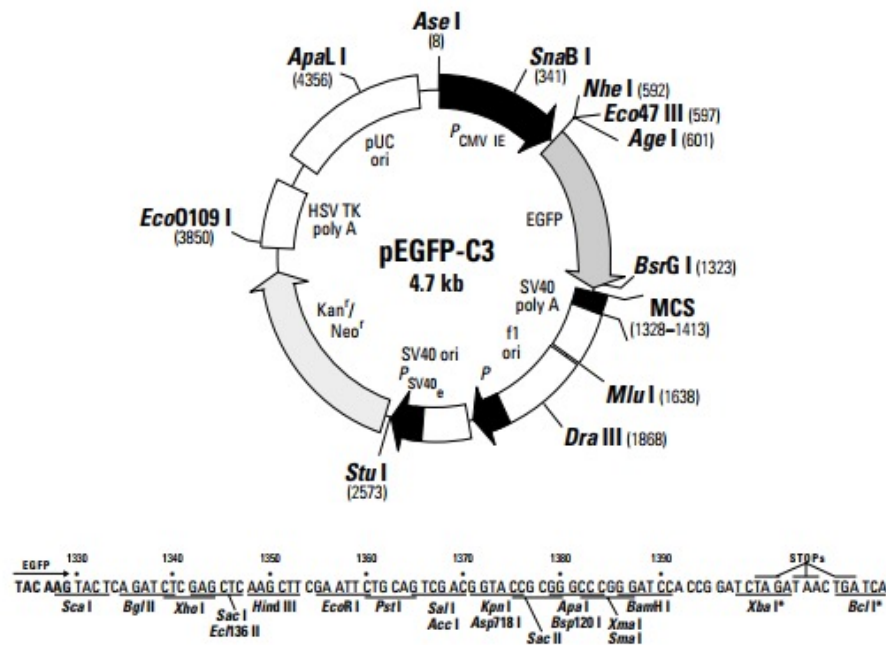


Figure 6. The restriction map and multiple cloning site (MCS) of the pEGFP-C3 vector

(<http://www.qualityard.com/upload/2019-05-24/ba70773f9c55f6a36d8e8a88ca963c27.pdf>)

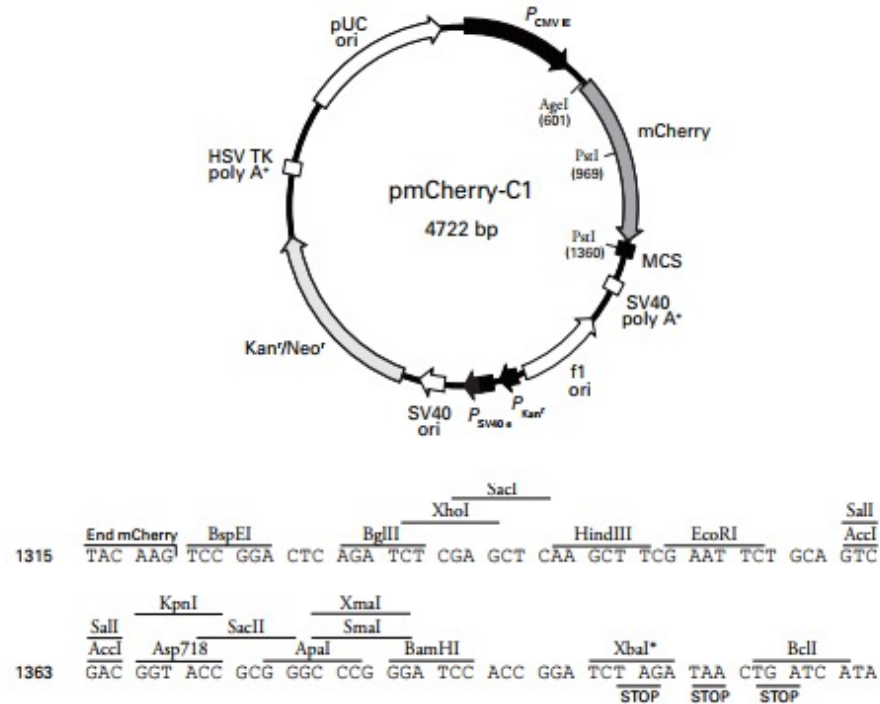


Figure 7. The restriction map and multiple cloning site (MCS) of the pRSET-B-mCherry C-1

(<https://www.scribd.com/document/242560824/PmCherry-C1-Vector-Information>)

Primer design

The complementary DNA of homo sapiens NRs was checked on <https://www.ncbi.nlm.nih.gov/nucleotide/> and the sequence was aligned with the amino acid sequence of splice variant 1 from <https://www.uniprot.org/uniprot> website using Serial Cloner 2-6-1 program.

Primers were designed manually taking into account the following criteria: no frame shift, the GC content between 40-60%, hairpin: no more than 4 bps, dimer formation: no more than 6 bps, base pair repeat not to exceed 4, length of the specific part of the primer: 18-21 bp.

Primers were checked using Oligo Analyzer software (<https://eu.idtdna.com/calc/analyzer>) and purchased from Integrated DNA Technologies (Coralville, IA, USA).

PCR, polymerase chain reaction

The PCR reaction was prepared as follows: First, primer mix was prepared (40 µl NFW + 5 µl FW primer, 100 µM, + 5 µl REV primer, 100 µM). Second, master mix was prepared (60 µl NFW + 20 µl HF buffer + 5 µl primer mix + 5 µl dNTP + 5 µl having 150 -250 ng DNA template). Third,

master mix was divided into 5 PCR tubes (19 µl per each) and 0.2 µl fusion DNA polymerase (Thermo Fisher Scientific, Waltham, MA, USA) was added to each tube. *Table 3* shows the PCR settings applied.

Table 3. PCR setting

No of cycles	Step	Time	Temperature
1 cycle	Preheating	3 min	98 °C
33 cycles	Denaturation	30 sec	98 °C
	Annealing	30 sec	50 °C
	Elongation	60 sec	72 °C
1 cycle	Elongation	10 min	72 °C

The PCR product was run on 1% agarose gel (1 g agarose powder in 100 ml TE 1X) for 1 h, 110 V. Proper length bands were cut out from the gel and cleaned up using PCR clean-up kit (MN, Germany) according to the manufacturer's recommendation.

Double digest

Both the cleaned PCR product (insert) and the vector were double-digested with the proper restriction enzymes. The digestion was carried out in 200 µl digestion mixture for 3-5 h at 37 °C. Then both the digested insert and the digested vector were run on 1% agarose gel; 1 h, 110 V. Proper length bands were cut out from the gel and cleaned up using PCR clean-up kit (MN, Germany).

Concentration of the cleaned up digested, sticky ends insert (PCR product) and vector DNA were determined using a NanoDrop™ 1000 spectrophotometer (Thermo Fisher Scientific).

Ligation

20 µl ligation mixture was prepared as follows: x µl insert, y µl vector, 2 µl ligase buffer, 1 µl T4DNA ligase (Thermo Fisher Scientific), NFW (up to 20 µl).

The amount of the insert and the vector were calculated according to the following equation:

$$insert [ng] = 5 \cdot \frac{insert\ length [bp]}{vector\ length [bp]} vector [ng] \quad (eq. 1)$$

Ligation mixture was incubated overnight at 4 °C.

Transformation

20 µl ligation mixture was incubated with 20 µl competent *E. coli* (DH5α strain) for 30 min on ice, then underwent a heat shock at 42 °C for 1.5 min followed by 5 min incubation at 5 °C. In 15 ml tube, the ligated plasmid - *E. coli* mixture was suspended in 1 ml SOC solution and incubated at 37 °C for 45 min with shaking. The bacterial solution was centrifuged at 1100 RPM for 3 min and the supernatant was decanted leaving 30 µl solution to resuspend the pellet. After suspension, the bacterial solution was smeared on 1.5% agar plate augmented with the desired antibiotic; the inoculated plasmid can resist. Agar plate was incubated overnight at 37 °C.

Small culture

On the next day, a single colony was picked up from the plate using a nuclease free pipette tip and thrown into a 50 ml tube containing 10 ml of LB medium supplemented with antibiotic (25 µg/ml kanamycin or 100 µg/ml ampicillin). Small culture was incubated overnight at 37 °C.

Glycerol stock preparation and DNA purification

Glycerol stock was prepared by mixing 700 µl of the overnight incubated small culture with 700 µl of 86% glycerol. Glycerol stocks were stored at -80 °C.

The rest of the small culture was purified using a miniprep kit (Promega, MA, USA) according to the manufacturer's recommendation. Concentration of the plasmid was detected using a NanoDrop™ 1000 spectrophotometer and plasmids were stored at -20 °C.

Preparation of the solutions used in the cloning protocol

10X PBS solution (pH 6.8): 1.37 M NaCl, 27 mM KCL, 100 mM Na₂HPO₄* 2 H₂O, 18 mM KH₂PO₄.

1X PBS solution (pH 7.4): 10X PBS diluted in dH₂O.

SOC solution: 10 mM NaCl, 2.5 mM KCL, 10 mM MgCl₂, 20 mM MgSO₄, 2% LB broth. This solution was autoclaved then cooled down before supplemented with 20 mM D-glucose. Then the solution was aliquoted into 1 ml Eppendorf tubes and be stored at -80 °C.

LB medium: 20 g LB agar dissolved in 1 liter of dH₂O. The solution is autoclaved, cooled down then stored at +4 °C.

LB agar solution: 20 g LB broth + 16 g micro agar in 1 liter of dH₂O. The solution is autoclaved, cooled down then stored at +4 °C.

Agar plate: LB agar solution was melt in microwave and poured while still hot into 50 ml tube. The solution was cooled then augmented with antibiotic (25 µg/ml kanamycin or 100 µg/ml ampicillin). 12.5 ml of the LB agar-antibiotic solution was poured into sterile plate. After solidifying, agar plates were sealed with parafilm and stored upside down at +4 °C.

DH5α competent cells: In a 50 ml tube, 20 µl of DH5α glycerol stock (stored at -80 °C) was suspended in 5 ml of cold LB medium. The suspension was shaken overnight at 37 °C, 400 RPM. On the next day, the overnight culture was inoculated into 200 ml warm LB medium and shaken at 37 °C, 210-250 RPM for at least 1.5 h or until the OD₆₀₀ of the culture reached 0.375. Then the bacterial solution was divided into four 50 ml tubes and centrifuged, 4 °C, 3000 RPM, 7 min, no brake. The supernatant was decanted, and the pellet was resuspended in 10 ml cold CaCl₂ solution [60 mM CaCl₂, 10 mM Pipes (pH 7) and 15% glycerol] and incubated on ice for 30 min.

The suspension was centrifuged, 4 °C, 2500 RPM, 5 minutes, no brake, the supernatant decanted, and the pellet dried for some minutes. The dried pellet was resuspended in a new 10 ml CaCl₂ solution, and the tubes were incubated for another 30 min on ice. Then the suspension was centrifuged; 4 °C, 2500 RPM, 5 min, no brake, and the pellet were resuspended in 2 ml CaCl₂ solution and incubated overnight at 4 °C. On the next day, the DH5α competent cells were aliquoted in cryogenic tubes (200 µl/tube) and stored at -80 °C).

Preparation of 86% glycerol: using 25 ml serological pipet, 21.5 ml glycerol was added into 50 ml and filled up to 25 ml with dH₂O. The solution is stored at 4°C.

3.2. Plasmid Construction

In all prepared constructs, the fluorescent proteins were fused to the N termini of the receptors. All plasmids were verified by sequencing.

Control plasmids

Control plasmid constructs EGFP-mCherry (GC⁺) and EGFP-TagBFP (GB) are complemented with a CGC GAT CCA CCG GTA ATG linker sequence after the sequence of EGFP. In the proline-separated TagBFP-P30-EGFP construct (B-P30-G) and EGFP-p30-mCherry (GC⁻) construct, there is a GGT CCG GTC GCC ACC CGC GAT CCA CCG GTA ATG linker before the proline spacer (30 repeats, mixed from the 4 proline codons) followed by the same short linker sequence.

Full length nuclear receptors tagged with EGFP or mCherry fluorescent proteins EGFP-NR or mCherry/NR

As a template for PCR, human cDNA, splice variant (isoform) 1, was used: RXR α , (Santa Clara, CA, USA), PPAR γ , RAR α , and VDR (DNA Resource Center, Bloomsburg, PA). PCR was carried out according to the above-mentioned protocol using the primers shown in *Table 4*.

PCR products were subcloned into the EGFP-C3 vector or mCherry-C3 vector using the restriction sites BglII/HindIII, XhoI/SalI, BglII/HindIII, and XhoI/HindIII, respectively.

Table 4. Primers used to clone NRs into pCMV-C3 vectors

Insert	Primers	
PPAR γ	FW XhoI	TATTATCTCGAGTTACCATGGTGACACAGAGATGCCATCTGG
	REV SalI	TATATACGTCGACTGCTAGTACAAGTCCTTGTAGATCTCCTGCAG
RAR α	FW BglII	AAGTACTCAGATCTCTTGCCAGCAACAGCAGCTCCTGC
	REV HindIII	ATAATTAAAGCTTCTACGGGGAGTGGGTGGCCGGGCTGCTTCTGTTGGAGCTGGGGCTGAHHCTGGGGCT
VDR	FW XhoI	TATTATCTCGAGTTGAGGCAATGGCGGCGGCCAGCAATTCCCTGCCT
	REV HindIII	TATTATAAGCTTCTAGGAGATTCTCATTGCCAAACACTTCGAGCAC
RXR α	FW BglII	TATTACTCAGATCTCTTGACACCAAACATTTC
	REV HindIII	ATAATAAAGCTTCTAAGTCATTTGGTGCGGCCCTCCAGCA T

NLS mutant receptors tagged with EGFP, EGFP-NR/*nls*m

Candidate Nuclear localization signals (NLS1) in the DBDs of the involved receptors have been defined to be between amino acids 136-141 for PPAR γ , 113-118 for RAR α , 49-54 for VDR and 160-165 for RXR α in a previous study ¹³⁴. NLS-mutant receptors were prepared by introducing a point mutation in the NLS1 into the coding sequence of EGFP-tagged receptors using site-directed mutagenesis via the overlap extension PCR method ¹³⁵. NLS mutant receptors were abbreviated throughout the text as “NR/*nls*m”. The designed primers to induce the above-mentioned mutations are shown in *Table 5*.

*Table 5. Primers used to clone NR/*nls*m into pCMV-C3 vectors.*

Insert	Primers	
PPAR γ / <i>nls</i> m	1- FW XhoI	TATTATCTCGAGTTACCATGGTGACACAGAGATGCCA TCTGG
	2- REV mutated NLS	<u>TGTCCGATTGTTCCCT</u> GGAAGAAACCCTTGCATCCTTCA *Reverse complement of the mutated NLS
	3- FW mutated NLS	<u>AGGGAACAATCGGACA</u> GAAGCTTATCTATGACAGATGT G *The mutated NLS
	4- REV SalI	TATATACGTCGACTGCTAGTACAAGTCCTTGTAGATCT CCTGCAG
RAR α / <i>nls</i> m	1- FW BglII	AAGTACTCAGATCTCTTGCCAGCAACAGCAGCTCCTG C
	2- REV mutated NLS	<u>GCCCGATGCTGCCTT</u> GGAAGCCGCCCTTGCAGCCCTCAC *Reverse complement of the mutated NLS
	3- FW mutated NLS	<u>AAGGCAGCATCGGGC</u> AGAACATGGTGTACACGTGTCAC C *The mutated NLS
	4- REV HindIII	ATAATTAAGCTTCTACGGGGAGTGGGTGGCCGGGCT GCTTCTGTTGGAGCTGGGGCTGAHHCTGGGGCT

Insert	Primers	
VDR/ <i>nls</i> m	1- FW XhoI	TATTATCTCGAGTTTGAGGCAATGGCGGCGGCCAGCAA TTCCCTGCCT
	2- REV mutated NLS	<u>TGCCCCATGCTTCCCTG</u> GAAGAAGCCTTTGCAGCC TCA * <u>Reverse complement of the mutated NLS</u>
	3- FW mutated NLS	<u>CAGGGAAGCATGGGGC</u> AGAAGGCACTATTACCTGCCC CTTC * <u>The mutated NLS</u>
	4- REV HindIII	TATTATAAGCTTCTAGGAGATTCTCATTGCCAAACACT TCGAGCAC
RXR α / <i>nls</i> m	1- FW BglII	TATTACTCAGATCTCTTGACACCAAACATTTC
	2- REV mutated NLS	<u>GGCCCACCGTCCCCTG</u> GAAGAAGCCCTTGCACCCCTCG C * <u>Reverse complement of the mutated NLS</u>
	3- FW mutated NLS	<u>CAGGGGACGGTGGGGC</u> AGGACCTGACCTACACCTGCCG C * <u>The mutated NLS</u>
	4- REV HindIII	ATAATAAAGCTTCTAAGTCATTGTTGGTGCGGCGCCTCCA GCAT

The mutagenesis workflow:

EGFP-NR constructs were used as templates and a series of PCRs were run to create the NLS mutant receptors.

4 PCRs were run as follows:

PCR 1: EGFP-NRs as template with primer 1 and primer 2 yielding **product A**.

PCR 2: EGFP-NRs as template with primer 3 and primer 4 yielding **product B**.

PCR 3: 250 ng of product A + 250 ng of product B + [dNTPs + HF buffer + fusion polymerase] for 10 cycles.

This PCR step will merge the two products yielding the NR/*nls*m template (**Product C**) which will be multiplied in the PCR 4 step.

PCR 4: product C + primer 1 + primer 4 + [dNTPs + HF buffer + fusion polymerase] yielding **product D.**

Both the product D (as an insert) and the pCMV-EGFP-C3 (as a vector) were double-digested with the restriction enzymes which have restriction sites at primer 1 and primer 4.

The sticky ends of the amplicon and the vector were ligated, and the rest of the cloning procedure was carried out as has been described in the protocol above.

Accordingly, the following point mutations were introduced: in EGFP-PPAR γ /*nls*m, R136Q, R137G, R140G, and L141Q; in EGFP-RAR α /*nls*m, R113Q, R114G, Q117G, and K118Q; in EGFP-VDR/*nls*m, R49Q, R50G, K53G, and R54Q; in EGFP-RXR α /*nls*m, K160Q, R161G, R164G, and K165Q.

TagBFP-RXR α /*nls*m was generated from EGFP-RXR α /*nls*m by replacing EGFP with TagBFP-C3 using NheI and BglII restriction enzymes.

Zinc fingers mutant RXR

The zinc finger mutant RXR, BFP-RXR α /*znm*, was prepared by mutating all 8 cysteines within the two zinc finger motifs of the DBD to alanines using the overlap extension PCR method. Accordingly, the following point mutations were introduced: C135A, C138A, C152A, C155A, C171A, C177A, C190A, and C195A. Zn finger mutant RXR is abbreviated throughout the text as “RXR α /*znm*”. The cloning was carried out as the following:

I. pCMV-C3- RXR vector:

The first step was to prepare the pCMV-C3-RXR vector; pCMV-C3 vector was cut out using PstI and BglII restriction enzymes. RXR sequence as an insert was cut out from EGFP-C3-RXR using the same restriction enzymes; PstI and BglII. The sticky ends of insert and vector were ligated and the rest of the cloning procedure was carried out as has been described in the protocol above.

II. Cloning of RXR/*znm*:

Applying the site-directed mutagenesis via the overlap extension PCR method required us to find specific restriction sites within RXR which can help to introduce the mutation to the sequence within sequential PCR series, i.e. C135 and C138 are located before BsrGI restriction site while C152 and C155 after it, C171 and C177 are located before AgeI restriction site while C190 and

C195 after it. Accordingly, the primers having the needed mutation (TGC, cysteine mutated to GCC, alanine) and the specific restriction site were designed as illustrated in *Table 6*.

Table 6. Primers used to clone RXR/nlsm into pCMV-C3 vectors.

Primer	Primer sequence
1. FW BglIII	TATTACTCAGATCTCTTGACACCAAACATTTC
2. Rev BsrGI	ATAATATGTACACTCCATAGTGCTTGCCTGAGGAGCGGTCCCCG GCGATGGCGGCGATG
ggc: the reverse complement of Alanine codon (gcc), the induced mutations C138A and C135A, respectively	
3. Rev AgeI	CTGGCACCGGTTCCGCTGCCGCTTGTC AATCAGGGCGTCCTTGT TGTCGCGGGCGGTGTAGGTCAG
ggc: the reverse complement of Alanine codon (gcc), the induced mutations C177A and C171A, respectively	
4. FW BsrGI	TATGGAGTGTACAGCGCCGAGGGGGCCAAGGGCTTCTTC
ggc: Alanine seq, the induced mutations C152A and C155A, respectively	
5. FW AgeI	CAGCGGAACCGGTGCCAGTGGCGCTACCCAGAAGGGCCTGGC CATGGGC
ggc: Alanine seq, the induced mutations C190A and C195A, respectively	
6. Rev HindIII	ATAATAAAGCTTCTAAGTCATTGCTGGCGCGCCTCCAGCAT

The mutagenesis workflow:

Step 1:

PCR 1: pCMV-C3- RXR as template with primer 1 and primer 3 yielding **product A**. product A (as an insert) and pCMV-C3- RXR (as a vector) were double-digested using **AgeI and BglIII restriction sites**. The digestion mixtures were run on 1% agarose gel and proper length bands were cut out from the gel and cleaned up.

200 ng of the insert and 50 ng of the vector were ligated overnight, cleansed on next day and named **ligation 1**. [ligation 1 has the mutations: C171 and C177]

Step 2:

PCR 2: pCMV-C3- RXR as template with primer 1 and primer 2 yielding **product B**.

product B (as an insert) and ligation 1 (as a vector) were double digested using **BglII and BsrGI restriction sites**. The digestion mixtures were run on 1% agarose gel and proper length bands were cut out from the gel and cleaned up.

200 ng of the insert and 50 ng of the vector were ligated overnight, cleansed on next day and named **ligation 2**. [ligation 2 has the mutations: C171, C177, C135A and C138A]

Step 3:

PCR 3: pCMV-C3- RXR as template with primer 4 and primer 6 yielding **product C**. product C (as an insert) and ligation 2 (as a vector) were double digested using **BsrGI and HindIII restriction sites**. The digestion mixtures were run on 1% agarose gel and proper length bands were cut out from the gel and cleaned up.

200 ng of the insert and 50 ng of the vector were ligated overnight, cleansed on next day and named **ligation 3**. [ligation 3 has the mutations: C171, C177, C135A, C138A, C152A and C155A]

Step 4:

PCR 4: pCMV-C3- RXR as template with primer 5 and primer 6 yielding **product D**. product C (as an insert) and ligation 3 (as a vector) were double digested using **AgeI and HindIII restriction sites**. The digestion mixtures were run on 1% agarose gel and proper length bands were cut out from the gel and cleaned up.

200 ng of the insert and 50 ng of the vector were ligated overnight, cleansed on next day and named **ligation 4**. [ligation 4 has all the mutations: C171, C177, C135A, C138A, C152A, C155A, C190A and C195A]

Step 5: amplifying of pCMV-C3-RXR/*znm*

Ligation 4, RXR/*znm*, (as an insert) and pCMV-C3-RXR (as a vector) were double-digested using **BglII and HindIII restriction sites**. The digestion mixtures were run on 1% agarose gel and proper length bands were cut out from the gel and cleaned up.

200 ng of the insert and 50 ng of the vector were ligated overnight, cleansed on next day and the rest of the cloning protocol was carried out as explained above.

III. Cloning of Tag BFP-RXR/*znm*

Tag BFP C-3 was inserted to the pCMV-C3-RXR/*znm* sequence as the following:

Tag BFP-C1 was used as a PCR template and proper primers were designed to correct for the frame shift and to include the **BglIII and XhoI restriction sites**.

Tag BFP C-3 (as an insert) and pCMV-C3-RXR /*znm* (as a vector) were both double-digested with **NheI and BglIII**. The digestion mixtures were run on 1% agarose gel and proper length bands were cut out from the gel and cleaned up. 200 ng of the insert and 50 ng of the vector were ligated overnight, cleansed on next day and the rest of the cloning protocol was carried out as explained above.

Table 7 summarizes the mutation we induce in NRs and *Fig. 8* shows a schematic representation of the DNA binding domain of RXR α as an example of NRs and the mutation localization we introduced.

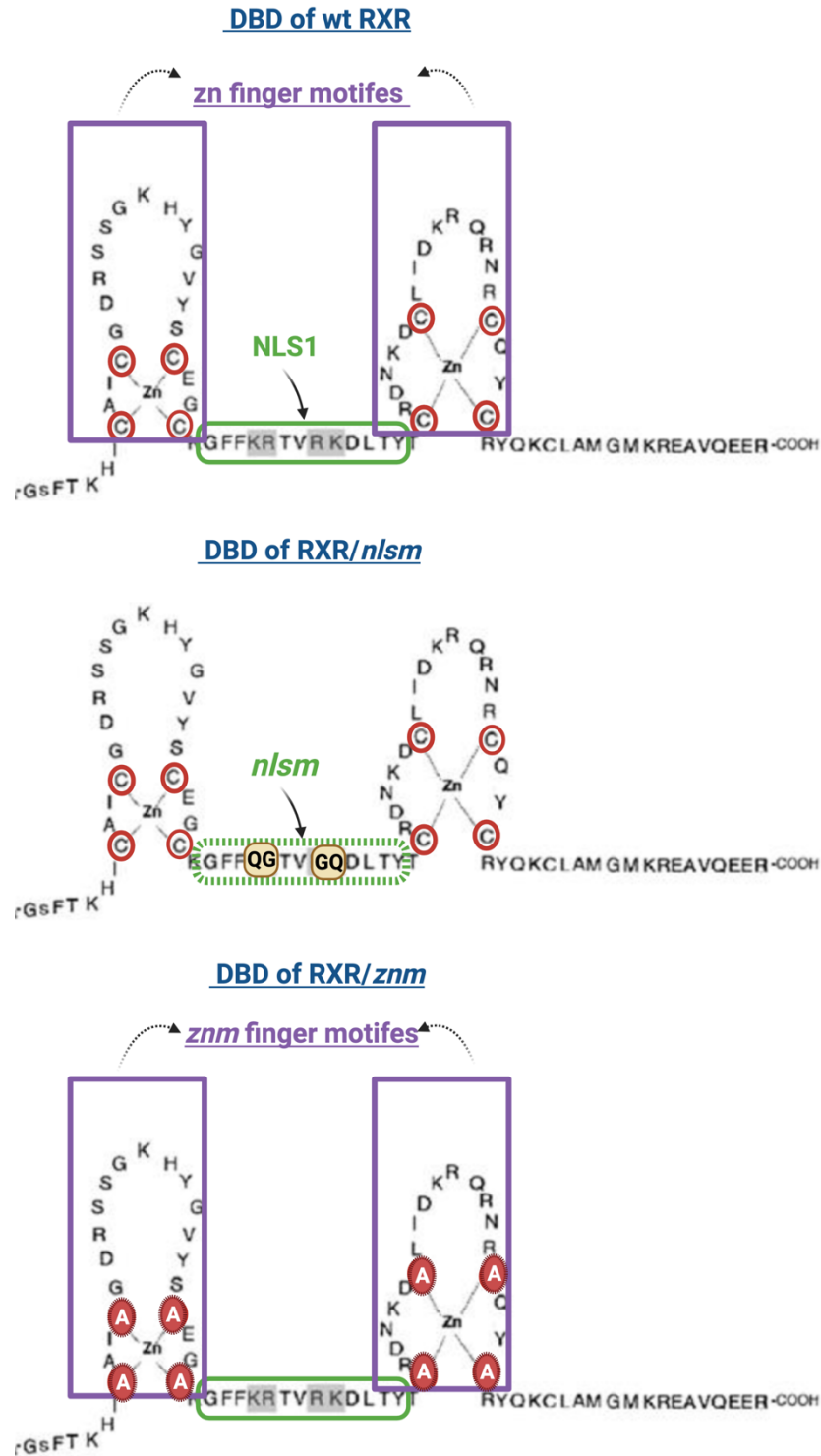


Figure 8. Schematic representation of the RXR α DNA binding domain.

(A) wild type RXR α , (B) nuclear localization mutated RXR α (RXR α /nlsm), (C) zinc finger mutated RXR α (RXR α /znm). The schematic representation of the DBD is adopted from Prufer, K. 2002¹⁰⁹ and modified using BioRender.com website to show the induced mutations.

Table 7. Summary of the mutations induced in NRs.

Receptor	Mutated amino acids	Mutated receptor
PPAR γ	Arginine at position 136 is replaced with glutamine Arginine at position 137 is replaced with glycine Arginine at position 140 is replaced with glycine Lysine at position 141 is replaced with glutamine	PPAR γ / <i>nls</i> m
RAR α	Arginine at position 113 is replaced with glutamine Arginine at position 114 is replaced with glycine Glutamine at position 117 is replaced with glycine Lysine at position 118 is replaced with glutamine	RAR α / <i>nls</i> m
VDR	Arginine at position 49 is replaced with glutamine Arginine at position 50 is replaced with glycine Lysine at position 53 is replaced with glycine Arginine at position 54 is replaced with glutamine	VDR/ <i>nls</i> m
RXR α	Lysine at position 160 is replaced with glutamine Arginine at position 161 is replaced with glycine Arginine at position 164 is replaced with glycine Lysine at position 165 is replaced with glutamine	RXR α / <i>nls</i> m
RXR α	Cysteine at the positions; 135, 138, 152, 155, 171, 177, 190, and 195 were all replaced with alanine.	RXR α / <i>znm</i>

Cloning of EGFP- RXRLBD and mCherry- RXRLBD

EGFP-C3 and mCherry-C3 vectors were modified by inserting a (GGGGS)₂ flexible linker after the fluorophore sequence, using BsrGI and XhoI restriction sites and the [TGTACAAGGGTGGCGGAGGTAGTGGCGGTGGTGGGAAGTCTCGAG] duplex oligos. The LBD for RXR (RXR²²⁵⁻⁴⁶²) were generated using PCR and the primers in [Table 8](#) then subcloned into the newly modified vector using XhoI and HindIII restriction site.

Table 8. Primers used to clone RXRLBD into pCMV-C3 vectors.

Insert	Primers	
RXRLBD	FW XhoI	TTTATTTTCTCGAGAGCGCCAACGAGGACATG
	REV HindIII	TTTATTTTAAAGCTTCAAGTCATTTGGTGCGGCGC

4.3 Translocation assay (competition assay)

In this study, we intended to understand how the promiscuous RXR molecule chooses its interaction partner in the presence of several potential heterodimeric partners and agonists. We evaluated competition between these NRs for their common partner, RXR α , by using a translocation assay in a three-color model imaging system as illustrated in *Fig. 9*.

RXR α was tagged with TagBFP and stably expressed in HEK293 cells, HEK293^{BFP-RXR α} . NR1, called the “studied partner,” was labeled with EGFP and NR2, or the “competing partner,” with mCherry. Applying a translocation assay required a version of the studied partner present in both the cytoplasm and the nucleus when not interacting with RXR α and getting enriched in the nucleus when interacting with RXR α . Inducing a mutation in the NLS1 of PPAR γ and RAR α fulfilled these criteria, whereas VDR was more appropriate in its wt form.

A pilot study confirmed the homogeneous localization of EGFP-PPAR γ /*nls*m, EGFP-RAR α /*nls*m, and EGFP-VDR in wt HEK293 cells and their nuclear accumulation in HEK293^{BFP-RXR α} . We call this homogeneous form of the receptor the studied partner and refer to it as NR1.

Applying the competition assay also required having another version of the receptor tagged with another fluorescent protein. Therefore, we cloned wt NRs into the mCherry vector. We called this form of the receptor the competing partner and we refer to it as NR2.

Next, competition between RXR α partners for binding to RXR α was evaluated by detecting changes in heterodimerization between RXR α and the studied partner, NR1, in the presence of the other competing partner, NR2. Competition between any two selected NRs was tested in two complementary experiments, *e.g.* to study competition between RAR α and PPAR γ for binding to RXR α , we traced the distribution changes of both EGFP-PPAR γ /*nls*m in the presence of mCherry-RAR α and that of EGFP-RAR α /*nls*m in the presence of mCherry-PPAR γ in HEK293^{BFP-RXR α} cells. The role of specific agonists in governing the competition was assessed by treating the samples with the specific agonists of the involved receptors individually or in combination.

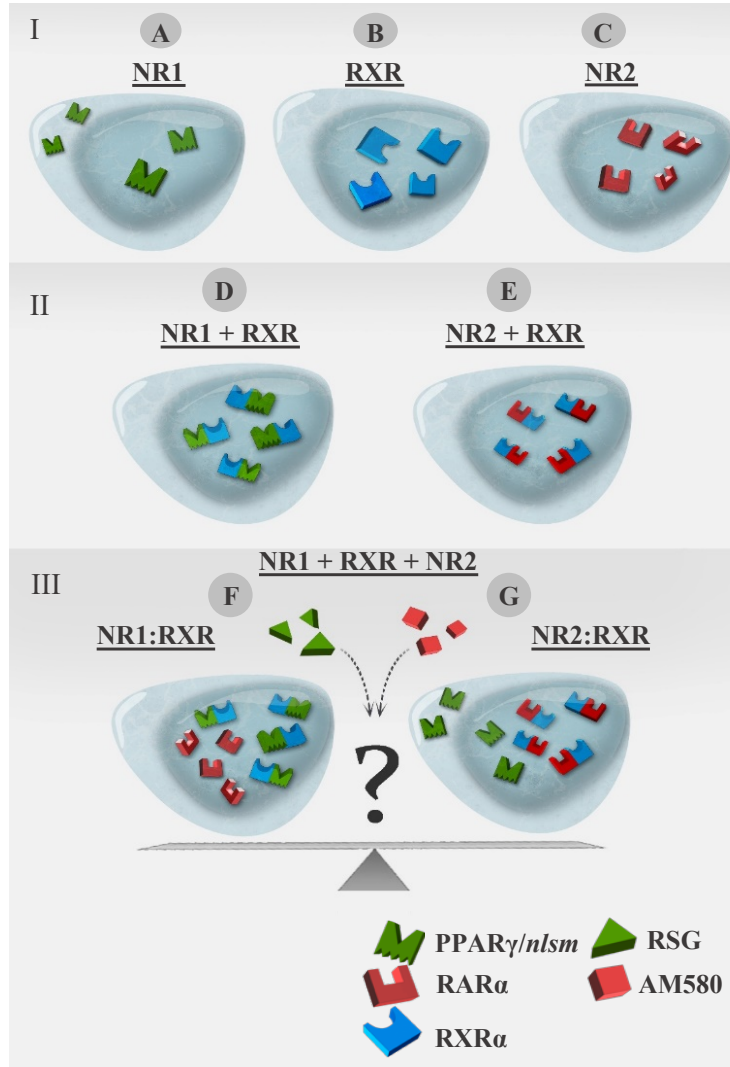


Figure 9. Schematic representation of the translocation assay in a three-color imaging model system.

I. Single expression of NRs; distribution of NR1, RXRα and NR2 expressed alone in wt HEK293 cells. (A) PPARγ/nlsm (NLS mutant form) as an example of NR1 having a homogeneous, nucleocytoplasmic distribution, (B) wt RXRα having nuclear localization, (C) wt RARα as an example of NR2 having nuclear localization. II. Double expression; NR1 or NR2 expressed in HEK293^{BFP-RXRα}. (D) Nuclear re-distribution of NR1 in HEK293^{BFP-RXRα}, (E) nuclear distribution of NR2 in HEK293^{BFP-RXRα}. III. Triple expression of NR1 + RXRα + NR2 to detect the competition between NR1 and NR2 for heterodimerization with RXRα, in the absence or presence of specific ligands of NR1 and/or NR2. (F) NR1 is expected to translocate to the nucleus if NR1 rather than NR2 is the preferred heterodimerization partner of RXRα. (G) NR1 is expected to be re-distributed homogeneously if NR2 is the preferred heterodimerization partner of RXRα. RSG: rosiglitazone, PPARγ agonist; AM580: RARα agonist.

4.3.1. Generation of TagBFP-RXR α stable cell line

The adherent version of human embryonic kidney, HEK293, cell line stably expressing TagBFP-RXR α , HEK293^{BFP-RXR α} , was prepared using viral transduction. Virus particles harboring the TagBFP-RXR α gene were purchased from VectorBuilder (Santa Clara, CA, USA).

Experimental detection of MOI in HEK293 cells

Multiplicity of infection, MOI, which is the number of virus particles needed to transduce one cell¹³⁶, was optimized experimentally for HEK293 cells. Using a control virus cells expressing EGFP-mCherry with a known concentration 10⁸/ml, 100 million virus particle per 1 ml, the multiplicity of infection (MOI) was detected experimentally.

On day 0, cells were plated in 24 plates, 60,000 cells/well. On day 1, cells were infected with a gradient dose of virus particles giving a MOI between 0 and 14 as shown in *Table 9*. The medium was changed the next day, and cells started to express EGFP-mCherry from day 3. On day 5, cells were passaged into a new plate (the content of one well went into two wells). On day 6, cells were collected into sorting tubes (washed with PBS, de-attached with warm TE, washed twice with cold PBS, suspended in 200 μ l PBS), and examined with a NovoCyte 3000 RYB flow cytometer (ACEA Biosciences, Inc., San Diego, CA) to detect the percentage of transduced cells at each MOI.

Table 9. Experimental detection of MOI in HEK293 cells.

MOI	Number of virus particle (60,000 * MOI)	Volume of virus	% Positively transduced cells (Expressing EGFP-mCherry)
0	0	0 µl	0
4	240,000 particles	2.4 µl	54.81 %
5	300,000 particles	3 µl	60.13 %
6	360,000 particles	3.6 µl	53.13 %
7	420,000 particles	4.2 µl	57.59 %
8	480,000 particles	4.8 µl	61.23 %
9	540,000 particles	5.4 µl	64.44%
10	600,000 particles	6 µl	68.61 %
11	660,000 particles	6.6 µl	66.64 %
12	720,000 particles	7.2 µl	70.32 %
13	780,000 particles	7.8 µl	70.5%
14	840,000 particles	8.4 µl	70.6%

HEK293 stably expressing TagBFP-RXR, HEK293^{BFP-RXRα}

Using the control virus particles, a MOI of 12 was detected to give ~70% transduction efficiency and to keep the cells in good viability conditions; thus, it was chosen to transduce the cells.

In a 6-well plate, 500,000 cells were seeded per well. Two wells were considered as a control (no virus particle treatment) while the four other wells were infected at MOI=12 with virus particles harboring the TagBFP-RXR α gene. Two days later, the cells started to express TagBFP-RXR and were passaged into a small flask.

Second, Geneticin antibiotic, G418, as a selection marker was applied in a dose of 500 µg/ml to get rid of non-transduced cells.

Third, cells were further sorted with a FACS Aria III (BD Bioscience, San Jose, CA, USA) cell sorter to collect a cell population expressing TagBFP-RXR α within an expression range with a coefficient of variation (CV) of 50%.

4.3.2. Cell culture

Both HEK293 and HEK293^{BFP-RXR α} cells were maintained in DMEM, supplemented with phenol red, 10% fetal calf serum (Sigma-Aldrich, Saint Louis, MO), 1 \times GlutaMAX (Fisher Scientific, Tokyo, Japan), and 50 mg/l gentamycin (KARA, Novo Mesto, Slovenia). Cells were passaged twice a week and used between the 3rd and the 8th passages.

4.3.3. Immunofluorescence labelling and flow cytometry

wt HEK293 or HEK293^{B-RXR α} cells were fixed with 4% formaldehyde (FA) in PBS (10 min, 4°C). After fixation, cells were incubated in 25 mM glycine in PBS (20 min) to quench the free aldehyde groups in FA, then permeabilized with 90% methanol in PBS, washed three times with TTBS, blocked with milk solution (5% milk powder (Santacruz) / 0.2% Tween-20 (Promega) / PBS, 20 min, 24°C), incubated (overnight, 4°C) with rabbit polyclonal anti-RXR polyclonal antibody (RXR α / β / γ antibody (Δ N 197): sc-774, Santa Cruz Biotechnology, Dallas, TX), washed three times with TTBS, incubated with Alexa Fluor 647 goat anti-rabbit polyclonal antibody (Invitrogen, Oregon, USA) in milk powder solution (1 h, 24°C), washed three times with TTBS and resuspended in 200 μ l TTBS. Cells were examined with a NovoCyte 3000 RYB flow cytometer (ACEA Biosciences, Inc., San Diego, CA), fluorescence was excited at 640 nm and detected through a 660/20 nm filter. Data were analyzed using FCS express 6 (De Novo software Inc). Geometric mean of fluorescence intensities was calculated and corrected for non-specific labeling and autofluorescence by subtracting the mean intensity of samples treated with the secondary antibody only.

4.3.4. Western Blot

10⁶ cells were lysed in 100 μ l RIPA lysis buffer supplemented with 1 \times protease inhibitor cocktail and 1 mM PMSF according to the manufacturer's instructions (sc-24948, Santa Cruz Biotechnology, Dallas, TX). Then total cellular protein (20 μ l) was separated on a 10% SDS–polyacrylamide gel and electroblotted onto a 0.45 μ m pore size PVDF membrane. The blot was saturated with milk blocking buffer (5% low-fat milk powder / 0.2% Tween-20 / PBS) for 1 h and then RXR and β -actin were labeled by rabbit polyclonal anti-RXR (RXR α / β / γ antibody (Δ N 197): sc-774, Santa Cruz) and mouse monoclonal anti-actin (sc-8432, IgG1, Santa Cruz), respectively,

as primary antibodies. Both were applied at a final concentration of 2 µg/ml in milk blocking buffer and incubated overnight at 4°C.

After washing with 0.2% Tween-20/PBS for 6×5 min, the membrane was incubated with both goat-anti-rabbit and goat-anti-mouse IgG secondary antibodies conjugated with horseradish peroxidase at a final concentration of 2 µg/ml in milk blocking buffer for 1.5 h at room temperature. After washing with 0.2% Tween20/PBS for 6×5 min, the bands were visualized with SuperSignal™ West Pico PLUS Chemiluminescent Substrate (Thermo Fisher Scientific, Waltham, MA).

The signal was detected by chemiluminescence using the FluorChem Q gel documentation system (Alpha Innotech Corp., San Leandro, CA). Immunoreactive bands were quantified with densitometry using the Image J software.

4.3.5. Transfection

For microscopy experiments, wt HEK293 or HEK293^{BFP-RXRα} cells were sub-cultured in 8-well chambered coverslips (ibidi, Munich, Germany) and maintained in phenol red-free DMEM due to the potential estrogenic effect of phenol red ¹³⁷, and supplemented with 10% charcoal-stripped fetal calf serum (PAN-Biotech, Aidenbach Germany) to get rid of the endogenous NR ligands.

24 h after seeding, cells reached 50–60% confluency and were transiently transfected with 75–80 ng of either one RXR partner (NR1) or two competing partners (NR1 + NR2) using FuGENE® HD transfection reagent (Promega, MA, USA) as suggested by the manufacturer. Cells were used for microscopy within 48 h after transient transfection.

4.3.6. Limiting pool of RXR and RXR overexpression conditions

In our triple co-expression experiments, the combined expression of NR1 and NR2 was greater than that of RXR, (NR1+NR2)>RXRα, to ensure a limiting pool of RXRα; thus, competition for RXR could be observed. Experiments were also carried out at RXR overexpression conditions; cells were transfected with half the amount of DNA for NR1 and NR2 as that used previously, and microscopy was done 24 h after transfection rather than 48 h to obtain lower expression levels. These increased the pool of RXR relative to NR1 and NR2; (NR1+NR2)<RXRα. See *Fig. 10*.

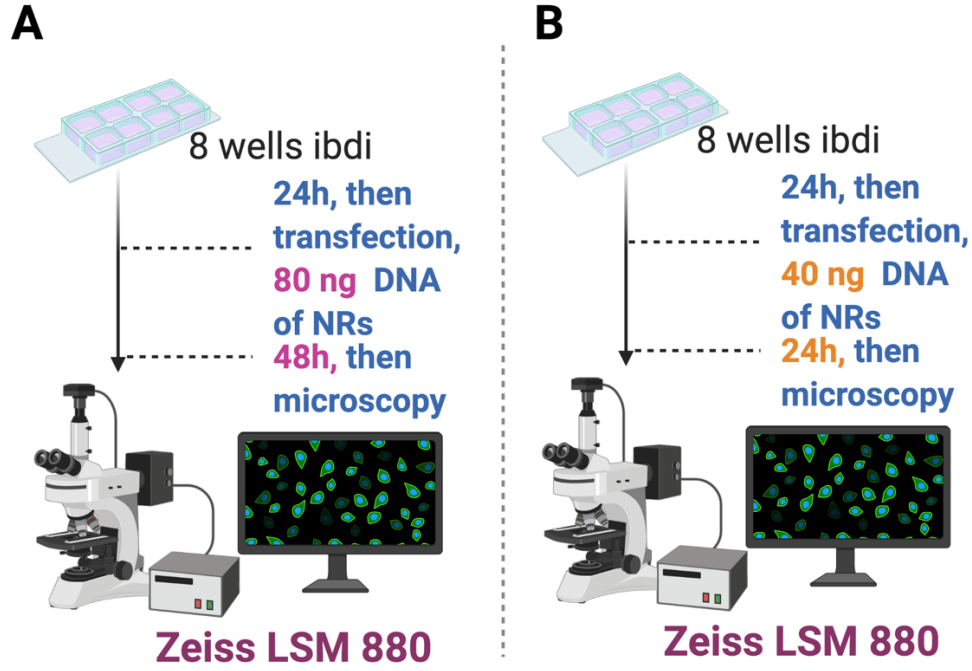


Figure 10. Schematic representation of the transfection conditions yielding either
 (A) limiting pool of RXR; $(NR1+NR2) > RXR\alpha$, or (B) overexpression of RXR; $(NR1+NR2) < RXR\alpha$.

Created with BioRender.com

Relative expression levels of the fluorescently tagged NRs were assessed as follows:

The intensity of BFP-RXR in the blue channel and that of EGFP-NR1 in the green channel were measured, and the ratio of these signals, I_G/I_B , was calculated. Similar I_G/I_B ratios from TagBFP-P30-EGFP (and EGFP-TagBFP) fusion proteins expressing the two fluorophores at a 1:1 ratio were determined and averaged, serving as a standard value, Q_1 .

The molecular expression ratio N_G/N_B of the NRs was then calculated as:

$$N_G/N_B = (I_G/I_B)/Q_1 \quad (\text{eq. 2})$$

For determining the relative expression ratio of G-NR1 to C-NR2, N_G/N_C , we used the EGFP-mCherry fusion protein as a standard in a similar fashion to calculate, Q_2 :

$$N_G/N_C = (I_G/I_C)/Q_2 \quad (\text{eq. 3})$$

whereas the relative expression ratio of C-NR2 to B-RXR α (N_G/N_B) was calculated as:

$$N_C/N_B = (N_G/N_B)/(N_G/N_C) \quad (\text{eq. 4})$$

4.3.7. Ligand treatment

Stock solutions of ligands were prepared in DMSO. For daily use, ligand aliquots were prepared in 1:1 DMSO–ethanol solvent to avoid repetitive freezing and thawing. All ligand solutions were stored at -20 °C. Ligands, shown in *Table 10*, were applied to the transfected cells 30–60 min before imaging at 37 °C, 5% CO₂. The percentage of the ligand solution in the medium was 0.1%.

Table 10. NRs ligands used in the study

Ligand	Targeted receptor	Final Concentration	Company
RSG, rosiglitazone	PPAR γ specific agonist	1 μ M	BioVision (Milpitas, CA, USA)
Cal, calcitriol	VDR specific agonist	100 nM	
AM580	RAR α specific agonist	100 nM	
LG268	RXR α specific agonist	100 nM	
GW9662	PPAR γ antagonist	1 μ M	Promega, MA, USA

4.3.8. Microscopy

Confocal images were recorded by a Zeiss LSM 880 (Carl Zeiss, Jena, Germany) confocal microscope using a 40 \times , 1.2 NA water immersion objective. A 405-nm laser was used to excite the blue fluorescence signal of TagBFP detected between 429 and 481 nm, the 488-nm line of an argon-ion laser for the green signal of EGFP detected between 499 and 562 nm, and a 543-nm. HeNe laser for the red signal of mCherry measured between 561 and 735 nm. An incubator built around the microscope maintained the temperature at 37 °C during the measurements.

4.3.9. Analysis of microscopy data

The average intensity per pixel was measured in two separately, manually selected regions of interest, (ROIs), one contouring the entire cytoplasm and another contouring the entire nucleus, excluding the nucleoli, as illustrated in *Fig. 11*. The values were corrected for background by subtracting the mean intensity calculated for non-transfected HEK293 cells. The nuclear-to-cytoplasmic ratio (NCR) was calculated as:

$$NCR = \frac{\langle I_{Nuc} \rangle - \langle I_{BG} \rangle}{\langle I_{Cyt} \rangle - \langle I_{BG} \rangle} \quad (\text{eq. 5})$$

The intensities were determined using the open-source FIJI distribution of ImageJ (version 2.0.0-rc-69/1.52i).

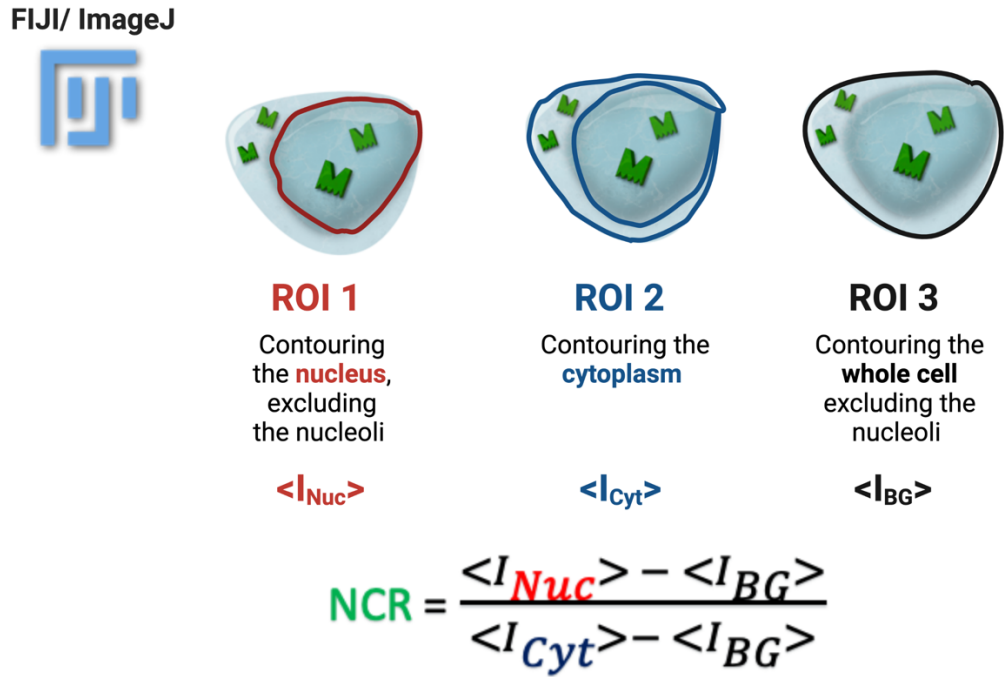


Figure 11. Schematic representation of image analysis and NCR calculation.

4.3.10. Statistics

Data were presented as a ratio of nuclear-to-cytoplasmic fluorescence intensities (NCR), displayed as box-and-whiskers plots depicting the 10th, 25th, 50th, 75th, and 90th percentiles and the arithmetic means for at least 30 cells.

Analysis of variance was used to compare the differences between the groups, and Student's t-test for pairwise comparisons. Prism 8.4.0 was used for statistical analysis and graphs.

4.4. SPIM-FRET-ALEX-FCCS

The first single plane illumination (SPIM) FCS/FCCS was developed by Jörg Langowski's group in DKFZ, Heidelberg. The single plane illumination microscope creates a 2.5 μm thick light sheet in the sample, and the fluorescence is collected perpendicular to this light sheet by a water immersion objective then detected by an EMCCD camera. The two dyes are illuminated by alternative laser excitation and detected without cross talk in separate channels. Images are acquired with a time resolution of 1 ms. Next, autocorrelation functions characterizing the mobility of the green and the red dye, and their cross-correlation function characterizing their co-mobility are calculated. Alternative excitation introduced by our lab in collaboration with the group in Heidelberg made it also possible to calculate FRET efficiency reporting about molecular proximity.

To detect the co-mobility of two different molecules we can label them with spectrally distinct dyes. If they diffuse in a complex, their fluctuations in the two detection channels will be parallel. The cross-correlation function will have a positive amplitude. From the ratio of the crosscorrelation amplitude and the autocorrelation amplitude we can assess the fraction of associated molecules with the $rCCF$ parameter.

4.4.1. Samples preparation

To prevent cell movement during measurements, cover slips were poly-L-lysinated using 0.01% poly-L-lysine solution (Sigma Aldrich) for 5 minutes, followed by washing with sterile water.

HeLa cells were maintained in phenol-red free DMEM medium supplemented with 10% fetal calf serum and 200 mM L-glutamine. Cells were passaged every 3 days and held in a humidified atmosphere at 37 °C and 5% CO₂. 48 hours prior to measurements, 120,000 cells were plated into 35 mm² petri dishes containing 3 pre-treated cover slips (10 mm diameter, thickness 2 from Thermo Fisher Scientific, Waltham, MA). After incubation for 24 h the medium was changed to phenol-red free DMEM supplemented with 2% FBS and 200 mM L-glutamine. Transient transfection was then carried out according to the user manual of the Fugene HD transfection reagent (Promega, Mannheim, Germany). Per dish 200 or 400 ng (controls and RXR-LBD) DNA and 3 μl Fugene HD were used. Cell measurements took place approximately 24 h afterwards.

SPIM measurements were carried out in FluoroBrite DMEM medium (Thermo Fisher) at room temperature. In ligand-treatment experiments the appropriate ligands were added to FluoroBrite

medium before the measurement. The cover slips with the cells were inserted into 8 ml buffer also containing the ligands if needed.

4.4.2. Microscopy setup

Single Plane Illumination Microscopy (SPIM) is a method widely applied in 3D-imaging of larger samples, although it may, depending on the setup, feature resolution sufficient for investigating intracellular processes¹³⁸.

The detailed description of the setup can be found in Krieger et al (<https://pubmed.ncbi.nlm.nih.gov/26540588/>). On the detection side, fluorescence was collected by a 60x water immersion objective (CFI Apo-WNIR 60x/1.0W, Nikon, Tokyo, Japan). Images were spectrally split to two color channels (500-550 nm, >593 nm) to detect EGFP and mCherry emission by an iXon X3 860 EMCCD camera (Andor Technology) at a frame time of 530 μ s, and an EM gain of 300 for F(C)CS. A 51 μ m \times 8 μ m (128 \times 20 pixel) rectangular region out of the 512 \times 512 pixel total area was imaged to increase speed. In SPIM, a \sim 1.3 μ m thin slice within the detection focal plane is illuminated by overlapping 488 and 561nm light sheets produced by a cylindrical lens. For FCCS two different data acquisition schemes were used: first, continuous (and simultaneous) excitation by both lasers, and secondly, alternating laser excitation (ALEX) by the two lasers.

4.4.3. Fluorescence (Cross-)Correlation Spectroscopy, F(C)CS

FCS is a technique used to detect molecular mobility. Fluorescence intensity fluctuations due molecular diffusion are detected from a diffraction limited, small (\sim 1 μ m³) volume element.

From the time-dependence of the fluorescence intensity, the autocorrelation function $G(\tau)$ can be calculated, then the parameters determining the autocorrelation function can be derived; the average number of molecules in the detection volume (N), and the diffusion correlation time τ_D , which is inversely proportional to the diffusion coefficient D .

FCCS is used to detect the co-mobility of two fluorescent molecules. To this end, two different molecules are labeled with spectrally distinct dyes. If they diffuse in a complex, their fluctuations in the two detection channels will be parallel, and the cross-correlation function will have a positive amplitude. From the ratio of the amplitudes of the cross-correlation and the autocorrelation functions we can assess the fraction of associated molecules with the $rCCF$ parameter.

Analysis: By time-correlating the images acquired at a high frame rate (1-2 kHz), autocorrelation curves were derived at each pixel thus yielding spatially resolved FCS (mobility) data. Cross-correlating the two color channels corresponding to EGFP and mCherry/mRFP emission allowed 2D mapping of co-mobility. Correlation functions were calculated and analyzed using the QuickFit 3.0 (QF3) software (https://github.com/lukl/QuickFit3_rot). Frames were first background-, baseline- and bleaching-corrected¹³⁹⁻¹⁴¹. Fluctuations were then correlated, yielding the ACF0, ACF1 autocorrelation and CCF cross-correlation curves. Cells showing drift artefacts and pixels having below-threshold intensity or irregular correlation functions were excluded from analysis. A two-component diffusion model was used to fit the two ACFs and the CCF of the control samples (GC⁺, GC⁻, G/C), whereas for the RXR-LBD, a one-component model was used¹⁴². Fits yielded diffusion coefficients and proportions of the diffusing species. To measure the degree of co-mobility (apparent “dimer fraction”), the relative CCF was used, which is defined pixelwise by the ratio of the amplitudes of the CCF (CCF(τ_{\min})) and the smaller one of the two ACF amplitudes (ACF0(τ_{\min}) or ACF1(τ_{\min})):

$$rCCF = \frac{CCF(\tau_{\min})}{\min(ACF(\tau_{\min}), ACF1(\tau_{\min}))} \quad (\text{eq. 6})$$

To reduce noise, for ALEX the first 8 time-points (as “ τ_{\min} ”) of the correlation functions were averaged for evaluating this expression, whereas for continuous excitation, to get comparable time intervals, the first 16 time points. To correct for day-to-day variances of the optical alignment, the *rCCFs* of samples were normalized to the GC⁻ sample each day. *rCCFs* from pixelwise CFs and from cellular averages gave similar results as presented for selected cells. *rCCFs* and other diffusion parameters were determined pixelwise; the distributions of cellular medians are shown as box-and-whiskers plots or as mean \pm SEM values.

4.4.4. Förster resonance energy transfer, FRET

FRET is a technique used to study the proximity between two molecules. The first molecule serves as a “donor”, which transmits its excitation energy to another molecule serving as an “acceptor”. This energy transfer can occur only if the molecules are in molecular proximity, within 10 nm distance and have proper relative orientation.

Analysis: Preview images were taken directly before the FCCS measurement with a frame time of 200 ms and an EM gain of 50 with 488, then 561 nm excitation. These settings were optimized

for FRET and differed from those used for FCCS imaging. FRET data were evaluated on a pixel-by-pixel basis.

Matlab (Mathworks, Natick, MA) scripts were used to determine average background intensity values, crosstalk factors, the α factor and FRET efficiencies. Images were collected in three channels: a donor and a transfer image (I_1 , I_2) arising from excitation at 488 nm in the green and red detection channels, and an acceptor image (I_3) from 561 nm excitation detected in the red channel. Their respective intensities can be expressed as:

$$I_1(488, 500 - 550) = I_D(1 - E) \quad (\text{eq. 7})$$

$$I_2(488, > 600) = I_D(1 - E)S_1 + I_A S_2 + I_D E \alpha \quad (\text{eq. 8})$$

$$I_3(561, > 600) = I_A \quad (\text{eq. 9})$$

where I_D , I_A are the unquenched donor and acceptor intensities in channel 1 and 3 respectively, whereas E is the FRET efficiency. Pixels outside the cell boundaries were masked and excluded. Average background intensities were calculated using non-transfected HeLa cells. Signals $I_1 - I_3$ were background corrected using these values. 2D intensity dot-plots (I_2 vs I_1 and I_2 vs I_3) were made to exclude too bright and too dim pixels from the analyses. Spectral crosstalk factors S_1 and S_2 were calculated using cells transfected with either EGFP-only or mCherry-only samples, respectively, as:

$$S_1 = \frac{I_2}{I_1} \quad (\text{eq. 10})$$

$$S_2 = \frac{I_2}{I_3} \quad (\text{eq. 11})$$

The factor α is the ratio of the signal arising from an excited mCherry molecule detected in channel 2, to the signal from an excited EGFP molecule detected in channel 1. The α factor was determined using the EGFP-mCherry fusion protein (GC⁺) containing the two fluorophores at a 1:1 ratio. α can be written as:

$$\alpha = \frac{I_A S_2}{I_D} \frac{\varepsilon_{488}^D}{\varepsilon_{488}^A} \quad (\text{eq. 12})$$

$\frac{\varepsilon_{488}^D}{\varepsilon_{488}^A}$ is the ratio of extinction coefficients of EGFP and mCherry at 488 nm. Using the measured intensities I_1 - I_3 from the GC⁺ sample the α factor can be expressed as:

$$\alpha = \frac{I_1 S_1 + (1 + \varepsilon) I_3 S_2 - I_2}{I_1} \quad (\text{eq. 13})$$

Where $\varepsilon = \frac{\varepsilon_{488}^D}{\varepsilon_{488}^A}$.

FRET efficiencies were calculated using the following formula:

$$E = \frac{S_2(I_2 - I_1 S_1 - I_3 S_2)}{\alpha(I_1 S_2) + S_2(I_2 - I_1 S_1 - I_3 S_2)} \quad (\text{eq. 14})$$

4.5. Chromatin immunoprecipitation (ChIP)

4.5.1. ChIP Protocol

The experiment was carried out according to the following protocol. For a schematic illustration see *Fig. 12*.

I. Cross-linking (all processes carried out at RT)

20 million cells (derived from two 150 cm² plates) were used for each ChIP. Medium was aspirated then cells were fixed in two steps; first using Disuccinimidyl glutarate (DSG) for 45 min at RT; second, with formaldehyde (FA) for 10 min at RT.

DSG (Sigma 80424-50MG-F) ampule having 50 mg DSG was freshly dissolved in 300 µl DMSO yielding a 0.5 M DSG solution. DSG was applied at a final concentration of 0.002 M by adding to each plate 10 ml PBS + 40 µl of 0.5 M DSG solution. Plates were gently swirled every 10 min.

DSG/PBS solution was completely aspirated after 45 min, then crosslinking was pursued with methanol-free ultrapure FA (Thermo Scientific prod # 28908) for 10 min at room temperature. FA was applied at a final concentration of 1%, to each plate (10 ml PBS + 625 µl of 16% FA). Quenching free aldehyde groups in FA was achieved by applying 1.5 ml of freshly prepared 1 M glycine to the FA/PBS solution (yielding an end concentration of 125 mM) for 10 min at RT. [1M glycine was prepared by dissolving 0.75 g of glycine in 10 ml PBS]. FA-Glycine-PBS solution was completely aspirated from the plates, then cell lysis was immediately initiated.

II. Cell Lysis and Chromatin Shearing (all process carried out at 4 °C)

First, 30 ml of ChIP lysis buffer was prepared for a duplicate (1% Triton X-100, 0.1% SDS, 150 mM NaCl, 1mM EDTA pH 8, 20mM Tris pH 8) and supplemented with 3 tablets of protease inhibitor (Roche complete, Mini/standard, protease inhibitor tablets free of EDTA). Cells were scraped up from the plate in 1 ml ChIP Lysis Buffer using a cell lifter or a scarper and cell lysates were transferred to 1.5 ml centrifuge tubes, centrifuged with 12,000 × g for 1 min at 4 °C. Supernatant was decanted and another 1 ml ChIP Lysis Buffer was added. Cells were homogenized by being pipetted up and down for at least 20 times, then the whole cell volume was pushed through in a 1 ml insulin syringe. Cells were centrifuged again and re-homogenized in a new 1 ml ChIP lysis buffer by pipetting up and down and pushing through a syringe with the same routine. Next, the 1 ml of resuspended nuclei was transferred into a single 15 ml conical tube (BD Falcon REF 352095). Cells were sonicated, and the chromatin was sheared randomly with ultrasound to get

fragments between 100 and 2000 bp using the Diagenode Bioruptor® Standard model, 2×5 min long cycles were used, with 30-s on and 30-s off and high-power setting.

Sheared chromatin was transferred to 1.5 ml tubes and centrifuged at $12,000 \times g$ for 10 min at 4 °C. After centrifugation, chromatin was recovered leaving 100 µl in the tube in order not to disrupt the pellet. 25 µl of the sheared chromatin was set aside as input. 375 µl of ice-cold absolute ethanol was added to the input tube and tubes were placed in -20 °C overnight. The rest of the sheared ~875 µl was transferred to a 15 ml conical tube and diluted with ChIP lysis Buffer to 8 ml.

III. Immunoprecipitation (carried out at 4 °C, using ice-cooled solutions)

6 µg of antibody was added to the diluted chromatin and the 15 ml conical tubes of diluted chromatin and antibody were incubated on a rotating tube rack at 4 °C overnight. Paramagnetic beads (Dynabeads Protein) were pre-blocked with a freshly filtered ice-cold blocking solution (0.5% BSA in PBS), using a 0.2 µm syringe filter. Beads were washed 3× with the blocking solution using a magnetic rack. Beads were incubated with the blocking buffer at 4 °C overnight using a magnetic rack.

The beads needed for the whole ChIP experiment were handled in a 15 ml conical tube considering that each ChIP required 190 µl of beads and 1 ml of blocking buffer per wash.

After overnight incubation, the 15 ml conical tubes containing antibody-chromatin complexes were centrifuged down in a pre-refrigerated centrifuge at 4 °C for 20 min at ~3500 rpm. The upper 90% of the centrifuged chromatin was used for bead binding (7.2 ml).

Using a magnetic rack, the paramagnetic beads were reconstituted to their original volume by aspirating off the blocking buffer and adding 190 µl of blocking buffer/ per one ChIP.

In a new 15 ml conical tube, the 190 µl of pre-blocked paramagnetic beads were added first, then the 90% of the centrifuged chromatin (7.2 ml). The tubes containing the antibody-chromatin-bead complexes were incubated on a magnetic rack at 4 °C for 6 h. Meanwhile, the washing buffers 1, 2 and 3 were prepared as indicated in [Table 11](#) and supplemented with Protease Inhibitor Tablets (1 tablet is added to 20 ml buffer). After 6 h incubation, the tubes were incubated on a magnetic rack for 2 min or until the liquid appeared clear, the supernatant was aspirated, and a similar volume of IP wash buffer (8 ml) was added. Washing has been accomplished once using IP wash Buffer 1, twice with IP wash Buffer 2 and once with IP wash Buffer 3. After the last wash, all the traces of the IP wash Buffer were carefully aspirated. Then, the antibody-chromatin-bead

complexes were resuspended in 200 μ l TE buffer [TE: 100 nM EDTA (pH 8) + 200nM Tris (pH 8)] and transferred to a low-binding 1.5 microcentrifuge tube. The 15 ml tube was washed again with another 200 μ l TE buffer and transferred to the same microcentrifuge tube. The microcentrifuge tubes containing the antibody-chromatin-bead complexes were placed on a magnetic rack, the supernatant was removed using a pipette tip. Another 1 ml of TE buffer was added to wash the beads, then carefully removed by a 1 ml pipette tip.

Table 11. Recipe for washing buffers used in ChIP.

IP Wash buffer 1	IP Wash buffer 2	IP Wash buffer 3
1% Triton X-100.	1% Triton X-100.	0.25 M LiCl.
0.1% SDS.	0.1% SDS.	0.5% NP-40.
150 mM NaCl.	500 mM NaCl.	1 mM EDTA, pH 8.
1 mM EDTA, pH 8.	1 mM EDTA, pH 8.	20 mM Tris, pH 8.
20 mM Tris, pH 8.	20 mM Tris, pH 8.	0.5 % sodium deoxycholate.
0.1% sodium deoxycholate.	0.1% sodium deoxycholate.	
Washing times, 1X	Washing times, 2X	Washing times, 1X

IV. Bead Elution, De-crosslinking (carried out at RT)

Elution buffer was prepared and maintained at RT, as it contains SDS, which crystalizes on ice. [Elution Buffer: 1 M NaHCO_3 + 20% SDS + NFW].

Elution was carried out in two steps; first 200 μ l of bead elution buffer was added to each tube, vortexed at moderate speed for seconds. Then, the tubes were placed on a thermomixer for 15 min, shaken at 1000 rpm. The tubes were placed back into a magnetic rack and the supernatant was collected into clean LoBind tubes. Second, the same elution step was repeated, and the supernatant was collected to the same LoBind tubes. After the second elution step, to the 400 μ l eluted solution 16 μ l of 5 M NaCl was added and samples were incubated overnight at 65 °C to de-crosslink the immunoprecipitated chromatin.

On the following day, 2 μ l of 10 μ g/ μ l RNase A was added to each sample and samples were incubated for 30 min at 37 °C. Then, 16 μ l of 1 M Tris–HCl pH 7.0, 8 μ l of 0.5 M EDTA pH 8.0, and 2 μ l of Proteinase K (20 μ g/ μ l) were added and samples were incubated for at least 2 h at 45 °C on a thermomixer at 1,000 rpm.

V. DNA Purification

The immunoprecipitated DNA (total volume = 444 μ l) was purified using a PCR clean-up kit (MN, Germany) according to the manufacturer's recommendation.

VI. DNA concentration measurement

DNA concentration was measured using a Qubit fluorimeter (Invitrogen).

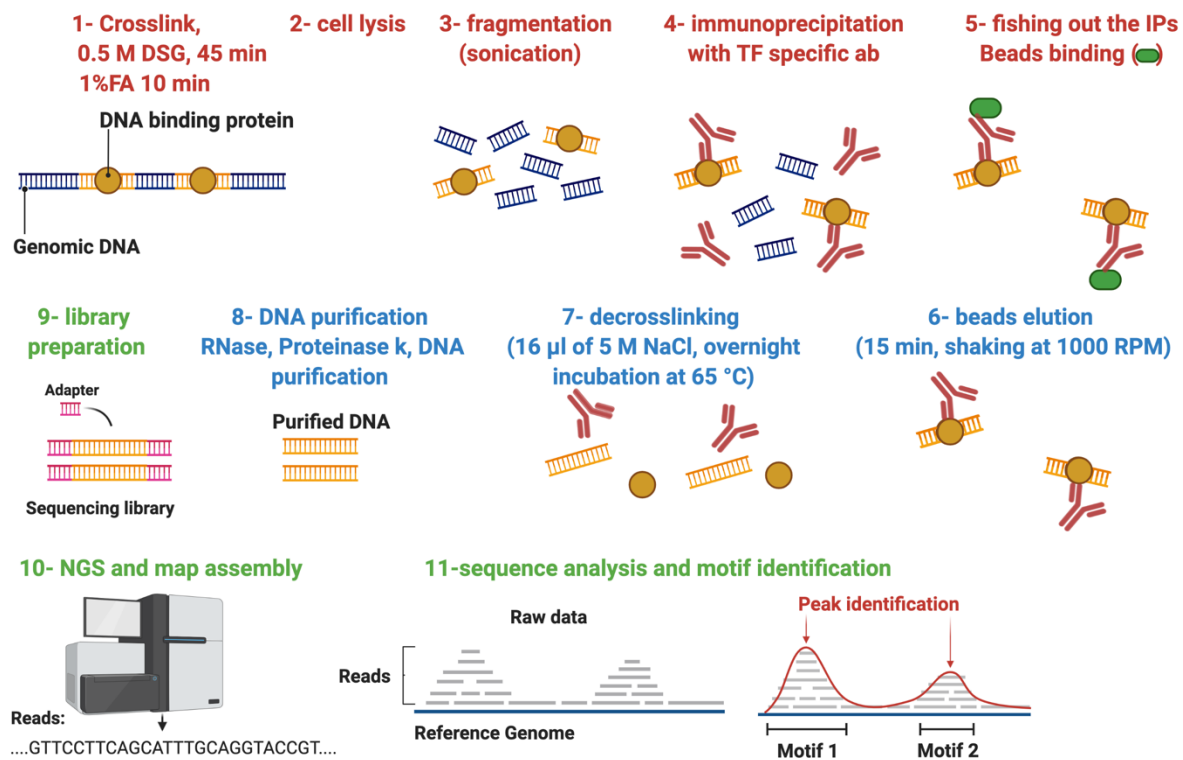


Figure 12. Schematic representation of the ChIP-seq experiment workflow.

Created with BioRender.com

4.5.2. VDR ChIP in THP1 cells

4.5.2.1. Cell culture and ligand treatment

The human monocytic cell line THP-1 was maintained in Roswell Park Memorial Institute medium (RPMI) supplemented with 10% fetal calf serum (Sigma-Aldrich, Saint Louis, MO), 1× GlutaMAX, (Fisher Scientific, Tokyo, Japan), 50 mg/l gentamycin (KARA, Novo Mesto, Slovenia). 12 h prior to the experiment, the medium was supplemented with 10 µmol/ml PMA (phorbol-12-myristate-13-acetate). PMA helped the cells to differentiate to macrophages and to become adherent. 60 min prior to ChIP assay, THP-1 cells were maintained in phenol red-free RPMI supplemented with 10% charcoal-stripped fetal calf serum and treated with either vehicle, 1:1 DMSO:ethanol, or 100 nM calcitriol.

6 µg of mouse monoclonal anti-VDR antibody was applied (sc-13133, Santa Cruz Biotechnology). TruSeq ChIP library systems (Illumina) were used for library preparation according to the manufacturer's instructions.

4.5.2.5. ChIP-seq data analysis and peak prediction

Raw ChIP-seq reads were aligned to the hg19 reference genome assembly with default parameters by using the BWA tool (v0.7.17), and BAM files were generated with *SAMtools* (v1.7) ^{143,144}. Peaks were predicted with the *findPeaks* program of the HOMER toolkit, and their widths were fixed to 200 bp relative to their summits ¹⁴⁵. Artifacts were removed according to the blacklisted genomic regions of ENCODE ¹⁴⁶. Then, peaks that were present in both replicates (separately for control and calcitriol-treated samples) and reached a minimum of 3 units (normalized tag densities as determined within +/-25 bp relative to peak summits by HOMER's *annotatePeaks*; $n=8401$ for the control and $n=10927$ for the calcitriol-treated samples) were merged ($n=13915$) and considered in the further analyses. Genome coverage (bedgraph) files were generated by HOMER's *makeUCSCfile* program.

Classification and characterization of peaks

Peaks were divided into three groups based on the presence or absence of VDRE or NR half-site. For this, VDRE and NR half-site motif matrices were downloaded from the HOMER Motif Database. Tag density of the central 50-bp region of the 13915 peaks was determined for each sample with HOMER's *annotatePeaks* (-hist 50 and -ghist options). Tag density values were then

normalized with the per-sample upper decile value and were averaged per condition. For heat maps, the three peak groups (with VDRE, NR half, or None) were further divided by k-means clustering ($k=2$), applying the centered correlation similarity metric using the Cluster 3.0 (v1.59) software. For histograms, average tag densities were generated with HOMER's *annotatePeaks* (-hist 10) and were normalized with the previously determined decile values. Genomic distribution and annotation of the peak groups were defined also by HOMER's *annotatePeaks*. The pathway terms were predicted using the KEGG database ¹⁴⁷.

Motif analysis and mapping

De novo motif enrichment analyses were carried out by HOMER's *findMotifsGenome* and were performed on the central 200-bp regions of the peaks. The targeted motif lengths were 10, 12, 14, and 16 bp. P-values were calculated by comparing the enrichment within the target regions and that of a random set of regions (background) generated by HOMER. For motif distribution plots, matrices of the enriched motifs were mapped following the order of regions in the tag density heat maps by using the *-mbed* parameter of HOMER's *annotatePeaks* in 20-bp windows within 2-kb frames relative to the peak centers.

Visualization

Heat maps were visualized by Java TreeView (v1.1.6r4) ¹⁴⁸. Histograms and bar charts were plotted by using GraphPad Prism (v8). Area-proportional Venn diagram was generated by BioVenn ¹⁴⁹. Genome coverage (bedgraph) files were visualized by Integrative Genomics Viewer (v2.4.16) ¹⁵⁰.

4.5.2.8. Data availability

ChIP-seq data have been submitted to Sequence Read Archive and Gene Expression Omnibus databases under accession numbers PRJNA632899 and GSE150652, respectively.

4.6. Fluorescence recovery after photobleaching, FRAP

The FRAP technique is used to study the diffusion and binding kinetics of fluorescently labeled molecules in live cells.

The method relies on perturbing the steady-state fluorescence distribution of the fluorescently labelled molecule in the sample by bleaching its fluorescence at a selected region of interest (ROI) using a high laser power for a very short time. After this perturbation, the relaxation of fluorescence distribution toward the steady state can be detected. Images are recorded before and after bleaching using a very low laser power. (Fig. 13)

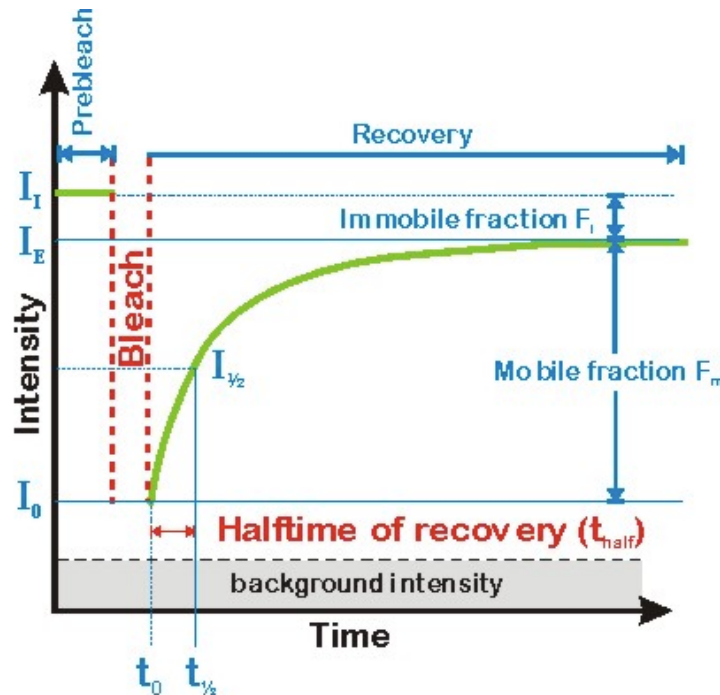


Figure 13. An idealized plot of a FRAP recovery curve.

(Adopted from https://www.embl.de/eamnet/frap/html/recovery_dynamics.html)

I_I : initial intensity

I_0 : intensity at time point t_0 (first postbleach intensity)

$I_{1/2}$: half recovered intensity ($I_{1/2} = (I_E - I_0) / 2$)

I_E : end value of the recovered intensity

t_{half} : Half-time of recovery corresponding to $I_{1/2}$ ($t_{1/2} - t_0$)

Mobile fraction $F_m = (I_E - I_0) / (I_I - I_0)$

Immobile fraction $F_i = 1 - F_m$

4.6.1. Cell culture and transfection

HeLa cells stably expressing EGFP-RAR α , HeLa^{EGFP-RAR α} , were prepared as described previously¹⁰⁵.

Both HeLa and HeLa^{EGFP-RAR α} were maintained in RPMI supplemented with phenol red, 10% fetal calf serum (Sigma-Aldrich, Saint Louis, MO), 1 \times GlutaMAX (Fisher Scientific, Tokyo, Japan), and 50 mg/l gentamycin (KARA, Novo Mesto, Slovenia).

For microscopy experiments, HeLa or HeLa^{EGFP-RAR α} cells were subcultured in 8-well chambered coverslips (ibidi, Munich, Germany) 48 h before the measurement and maintained in phenol red-free RPMI supplemented with 10% charcoal-stripped fetal calf serum (PAN-Biotech, Aidenbach, Germany).

24 h after seeding, HeLa cells reached 50–60% confluency and were transiently transfected with 80 ng of EGFP dimer using FuGENE® HD transfection reagent (Promega, MA, USA) as suggested by the manufacturer.

4.6.2. Applied treatment

Doxorubicin (Promega) treatment was applied for 2 hours at 37 °C before imaging. Treatment solutions were prepared in phenol red-free RPMI at the following concentrations: 0, 1.125, 4.5, 18 μ M. Doxorubicin was applied either alone or in combination with AM580, a specific RAR α agonist. AM580 was applied to the cells at 100 nM final concentration for 30 min at 37 °C before imaging.

3.6.3. FRAP microscopy setting

FRAP measurements were performed on a Zeiss LSM 880 (Carl Zeiss, Jena, Germany) confocal microscope using a 40 \times , 1.2 NA water immersion objective. The 488-nm laser line was used to excite EGFP with a laser power of 2 μ W at the objective (10%), and emission was detected through a 493 to 529 nm band pass filter. For quantitative analysis, a 256 \times 256-pixel area was selected and scanned with an open pinhole (5.56 Airy units) and 10 \times zoom (pixel size: 0.08 μ m), with a pixel dwell time of 1.33 μ s. A 405-nm laser was used to bleach the EGFP molecules at a selected stripe-shaped region of interest (FRAP ROI) having an area of 140 \times 10 pixels, a laser power of 20 μ W at the objective, and a pixel dwell time of 8.24 μ s. Before bleaching, 10 images were collected at a repetition rate of 204.8 ms/frame followed by one bleach period at the FRAP ROI, and then

collecting 189 post-bleach images for a total time of 42 seconds. To standardize the geometry of the measurement, the scanned field was rotated to make the long axis of the selected nucleus vertically oriented in the image, and the stripe-shaped FRAP ROI (bleached area) was positioned horizontally at ca. one third of the vertical extension of the nucleus, avoiding nucleoli, *Fig. 14*.

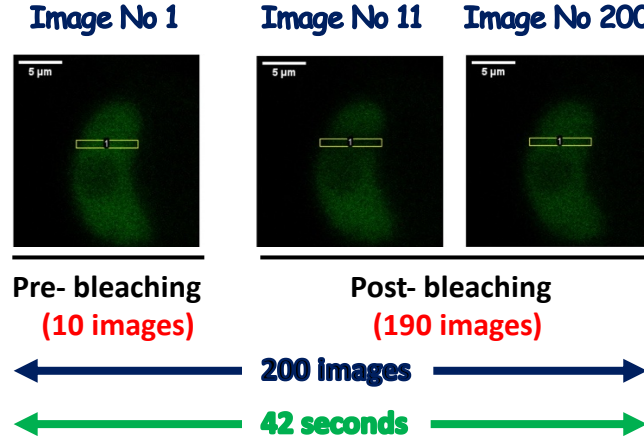


Figure 14. Representative confocal microscopic images showing the applied FRAP settings.

Cells expressing EGFP-RAR before bleaching, at bleaching point and after bleaching. In this setting: in 42 sec, 200 images were collected as follows: 10 images before bleaching and 190 images after bleaching.

4.6.4. Data analysis

Images were processed using the ZEN software (Carl Zeiss Jena) to acquire the fluorescence intensity recovery curves required for FRAP analysis. The width of the FRAP ROI was cropped to match the width of the nucleus. Another ROI contouring the whole nucleus but excluding the nucleoli was made to calculate the total fluorescence intensity of the nucleus. A third ROI outside the cell was drawn to calculate the intensity of the background. Following the double normalization method¹⁵¹, the intensity in the FRAP ROI during the recovery period was normalized to its pre-bleach value $I_{ROI}(0)$, and corrected for acquisition bleaching of the whole nucleus using the following equation:

$$I_{norm}(t) = \frac{I_{ROI}(t) - I_B}{I_{ROI}(0) - I_B} \times \frac{I_{total}(0) - I_B}{I_{total}(t) - I_B} \quad (\text{eq. 15})$$

where $I_{ROI}(t)$ is intensity of the FRAP ROI at a given time during the recovery, $I_{ROI}(0)$ is the average intensity of the ROI before bleaching, $I_{total}(t)$ is the intensity of the whole nucleus at a given time

during recovery, $I_{total}(0)$ is the average intensity of the whole nucleus before bleaching, and I_B is average intensity of the background. Using the Prism version 8.4.0 software, a two-component exponential curve (eq. 2) was fitted to the normalized recovery curve of the EGFP-RAR α while a one-component exponential to the EGFP dimer:

$$I_{norm}(t) = (I_{min} - I_{\infty}) \times \left(r_{fast} \exp\left(-\frac{t}{\tau_{fast}}\right) + r_{slow} \exp\left(-\frac{t}{\tau_{slow}}\right) \right) + I_{\infty} \quad (\text{eq. 16})$$

The fit yielded the τ_{fast} and τ_{slow} recovery times of the fast and the slow components, their fractions r_{fast} and r_{slow} adding up to 1, the plateau I_{∞} at infinite time and the fitted intensity value right after bleaching I_{min} . The mobile fraction was determined as:

$$r_{mobile} = (I_{\infty} - I_{min}) / (I_{\infty} - I_{min}) \quad (\text{eq. 17})$$

The average recovery time was calculated as a weighted average of the fast and slow components:

$$\tau_{average} = r_{fast}\tau_{fast} + r_{slow}\tau_{slow} \quad (\text{eq. 18})$$

5. RESULTS

5.1 RXR dependent nuclear accumulation of NRs as a pre-requisite step to apply our three-color imaging model system

We hypothesized that competition for heterodimerization with RXR is dictated, by the availability of the partner-specific agonist. To examine this hypothesis, we developed a robust system relying on a nuclear-translocation assay applied in a three-color imaging model system by detecting changes in heterodimerization between RXR α and one of its partners (NR1), in the presence of another competing partner (NR2). To this end, NR1 was present in a form showing homogeneous distribution when expressed alone and translocating into the nucleus when interacting with RXR α . The model system is explained in detail in the material and method section; “page 48” and illustrated in *Fig.9*.

First, we needed to minimize the impact of endogenously expressed NRs on the observed results. Thus, we needed a cell line that expresses the NRs involved in our study at low levels as compared to the transfected ones.

We analyzed published RNA-seq data from wt HEK-293T cells ¹⁵², and plotted the average gene expression values of the studied NRs. As shown in *Fig.15*, wt HEK-293T cells express the NRs involved in our study at low/medium levels, which made it appropriate for our investigations.

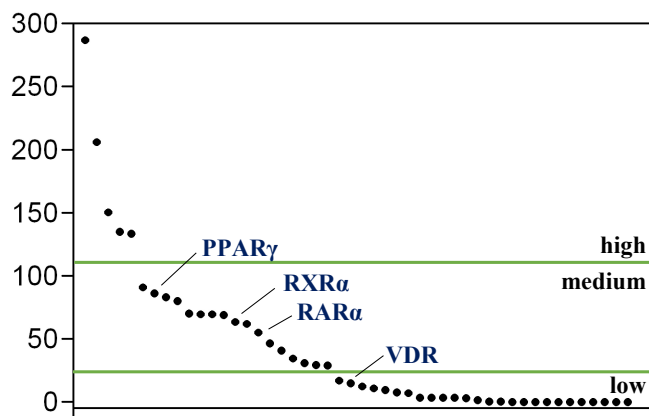


Figure 15. Gene expression level of NRs in HEK293 T cell line.

RNA seq results showing the expression level of the studied NRs in HEK-293T cells. The average CPM (count per million) values of the two replicates are depicted. Data sets from Gene Expression Omnibus GSM3889081 and GSM3889082.

We generated a stable cell line, HEK293^{BFP-RXR α} , overexpressing TagBFP-RXR α . According to our immunofluorescence and Western-blot analyses, the endogenous RXR expression level in wt HEK293 was \sim one-fourth of the level in HEK^{BFP-RXR α} *Fig. 16*.

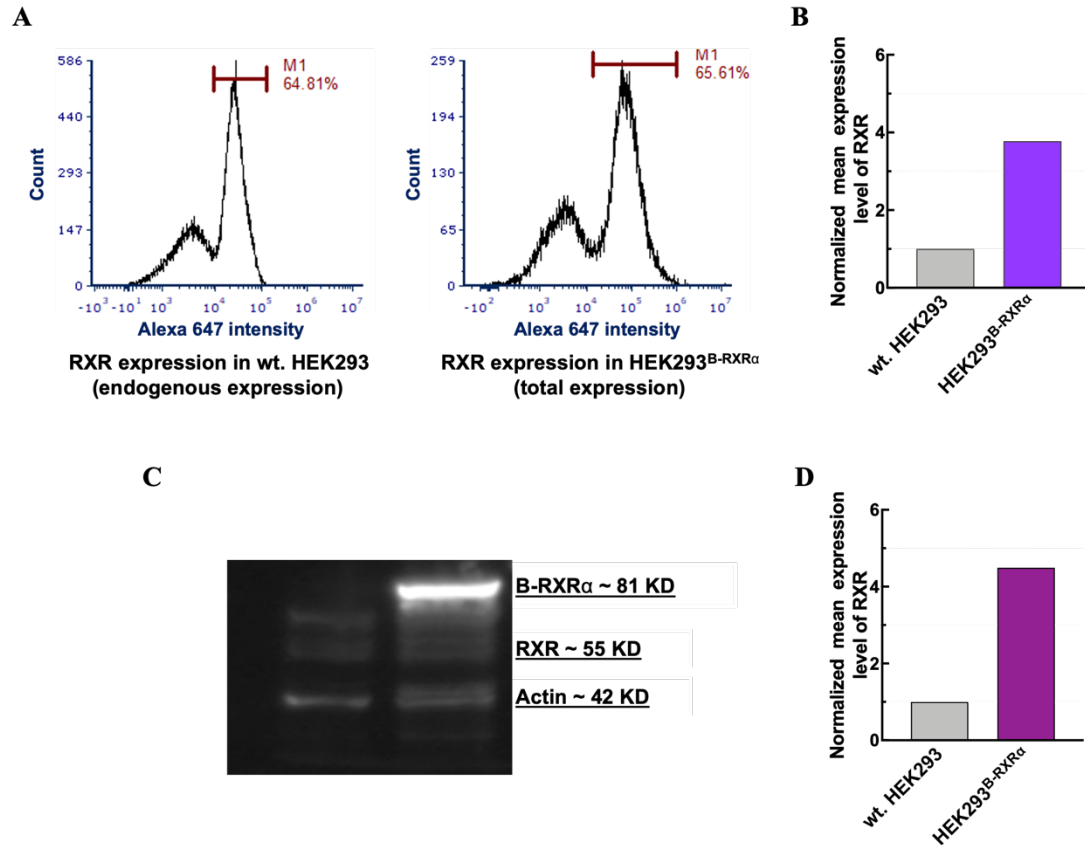


Figure 16. Endogenous expression of the RXR in cells involved in the study.

(A) Flow cytometric histogram of RXR in wt HEK293 (left) and of RXR and B-RXR α in HEK293^{B-RXR α} (right) using polyclonal anti-RXR and Alexa 647-tagged GARIG. Cells expressing RXR were gated. (B) Normalized average fluorescence intensities of the RXR-expressing gated subpopulations. (C) Western-blot analysis of RXR expression levels in wt HEK293 and HEK293^{B-RXR α} cells. (D) Intensities of bands were normalized to actin, and the endogenous level was set to 1. G: EGFP, B: BFP

First, we expressed NRs tagged with EGFP and studied their changes of localization in response to the addition of ligands and co-expression of RXR α . We transfected both wt HEK293 and HEK293^{BFP-RXR α} cell lines with EGFP-NRs. EGFP-PPAR γ and EGFP-RAR α were localized mainly in the nucleus (*Fig. 17A*) even in the absence of exogenously added RXR α or agonist. To impede the nuclear transport of these NRs in the absence of RXR α , we induced a mutation in the nuclear localization signal localized in their DBD between the two zinc finger motifs, NLS1. This mutation is denoted throughout the text as (*/nlsm*).

Then, we observed the subcellular distribution of these NLS mutant receptors (EGFP-PPAR γ /*nlsm*, EGFP-RAR α /*nlsm*) in wt HEK293 cells and studied the effect of specific agonist treatment (RSG and AM580, respectively) on their localization. As shown in *Fig. 17C*, the nuclear-to-cytoplasmic ratio (NCR) for EGFP-PPAR γ /*nlsm* and EGFP-RAR α /*nlsm* were ~ 1 irrespective of ligand treatment.

Next, we transfected the NLS mutant receptors into HEK293^{BFP-RXR α} cells to see the effect of dimerization with RXR α on their localization (*Fig. 17B, C*). We detected a 6-fold enrichment in the nucleus for EGFP-PPAR γ /*nlsm* and 5-fold for EGFP-RAR α /*nlsm*. Specific agonist treatment caused a further increase in the nuclear accumulation of these receptors.

Contrary to both EGFP-P-PPAR γ and EGFP-RAR α , EGFP-VDR (expressed alone in wt HEK293 cells in the absence of agonist) was distributed in the cells with an NCR of ~ 2 (*Fig. 17C*). Treatment with a specific agonist, calcitriol, or co-expression of RXR α (using HEK293^{BFP-RXR α} cells) enhanced the translocation of EGFP-VDR to the nucleus, resulting in an NCR value of ~ 3 . Expressing EGFP-VDR in HEK293^{BFP-RXR α} combined with calcitriol treatment led to an even higher NCR value of ~ 6 . (*Fig. 17B, C*). Because wt VDR showed an increased localization in the nucleus in the presence of RXR α , we could use it in its wt form to detect heterodimerization with RXR α .

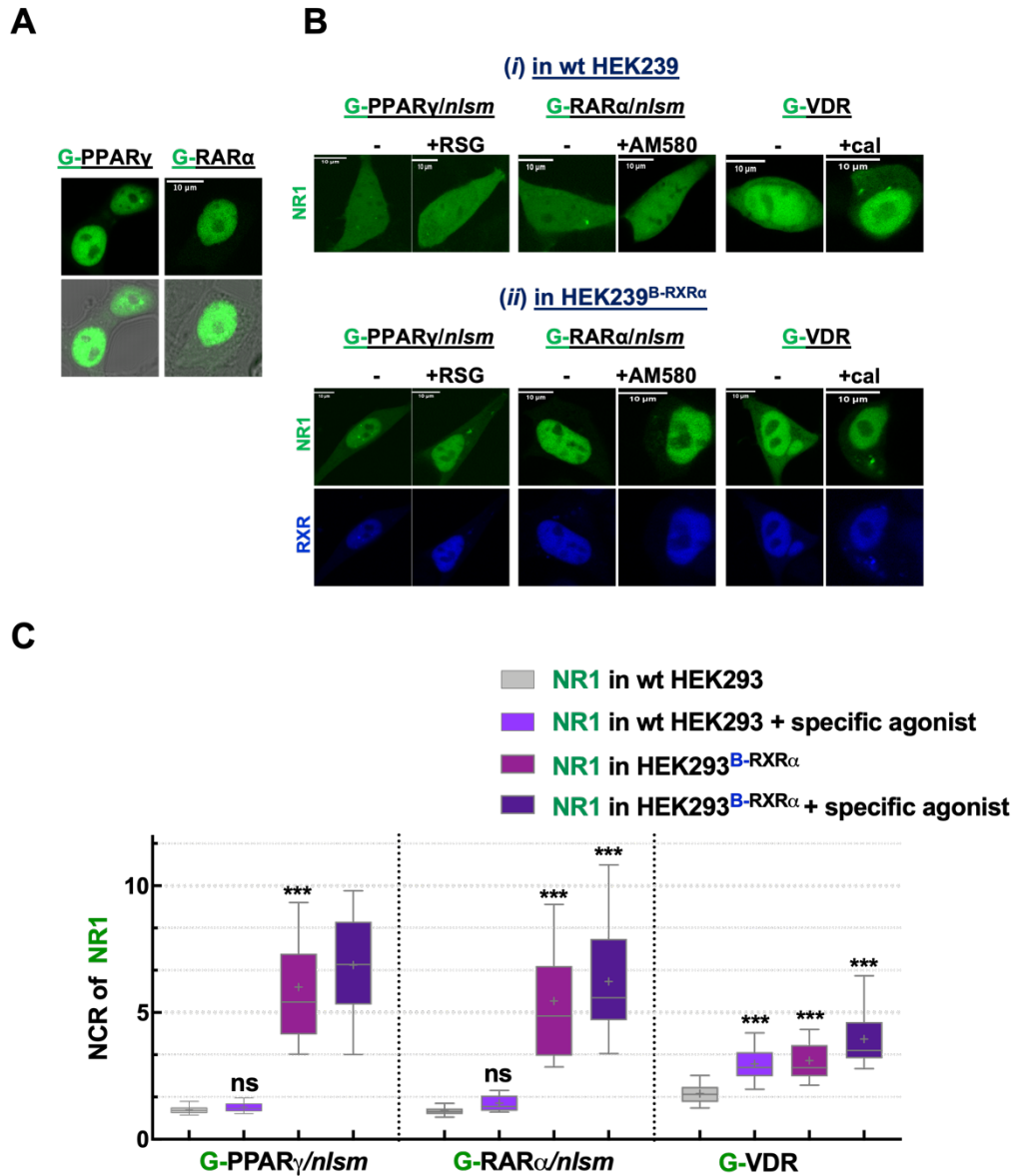


Figure 17. Subcellular distribution of NRs involved in this study.

(A) Representative confocal images show the nuclear localization of G-PPAR γ and G-RAR α in wt HEK293 cells. (B) Representative confocal images of NR1s; the NLS mutants G-PPAR γ /nlsm, G-RAR α /nlsm and wt G-VDR transiently transfected into wt. HEK293 (top) or HEK293^{B-RXR α} cells, stably expressing B-RXR α , (bottom), in the absence or presence of specific NR1 agonists (10^{-6} M RSG, 10^{-7} M AM580 and 10^{-7} M calcitriol (cal)). (C) Nuclear-to-cytoplasmic fluorescence intensity/pixel ratios (NCR) of NR1; ***: $p < 0.0001$ in comparison with NR1 distribution in wt HEK293. Box-and-whiskers plots represent 10th, 25th, 50th, 75th and 90th percentiles, (+) indicates the mean value. G: EGFP; B: TagBFP; C: mCherry. Scale bar: 10 μ m, ***: $p < 0.0001$.

The next question was whether RXR α -dependent nuclear enrichment of NR1 is mediated by the DNA-binding of RXR α or it depends merely on heterodimerization. To address this question, a similar experiment was carried out in which RXR α was expressed either as a zinc finger mutant, RXR α /*znm*, or as an NLS mutant, RXR α /*nls*m.

While RXR α /*znm* lack the direct DNA binding capability, which is mediated by the four zinc finger motifs in the DNA binding domain, the mutation in the NLS of RXR affects its nuclear localization. As shown in *Fig. 18A, B*, RXR α /*znm* had a nuclear localization similar to that of wt RXR α whereas RXR α /*nls*m distributed homogeneously in the cell.

Interestingly, RXR α /*znm* augmented the translocation of NR1 into the nucleus as effectively as wt RXR α did, whereas RXR α /*nls*m failed to do so (*Fig. 18D*). Thus, nuclear enrichment of NR1 in the presence of RXR α is due to heterodimerization rather than binding to DNA.

Calcitriol treatment could not only cause nuclear enrichment of its cognate receptor, VDR, (*Fig. 18D*), but also when VDR was co-expressed with RXR α /*nls*m, both of these homogeneously distributed receptors got enriched in the nucleus upon calcitriol treatment (*Fig. 18C*).

To conclude, the mutation in NLS1 abolished the spontaneous nuclear accumulation of RAR α and PPAR γ but conserved their ability to heterodimerize with RXR α and to bind their ligands efficiently.

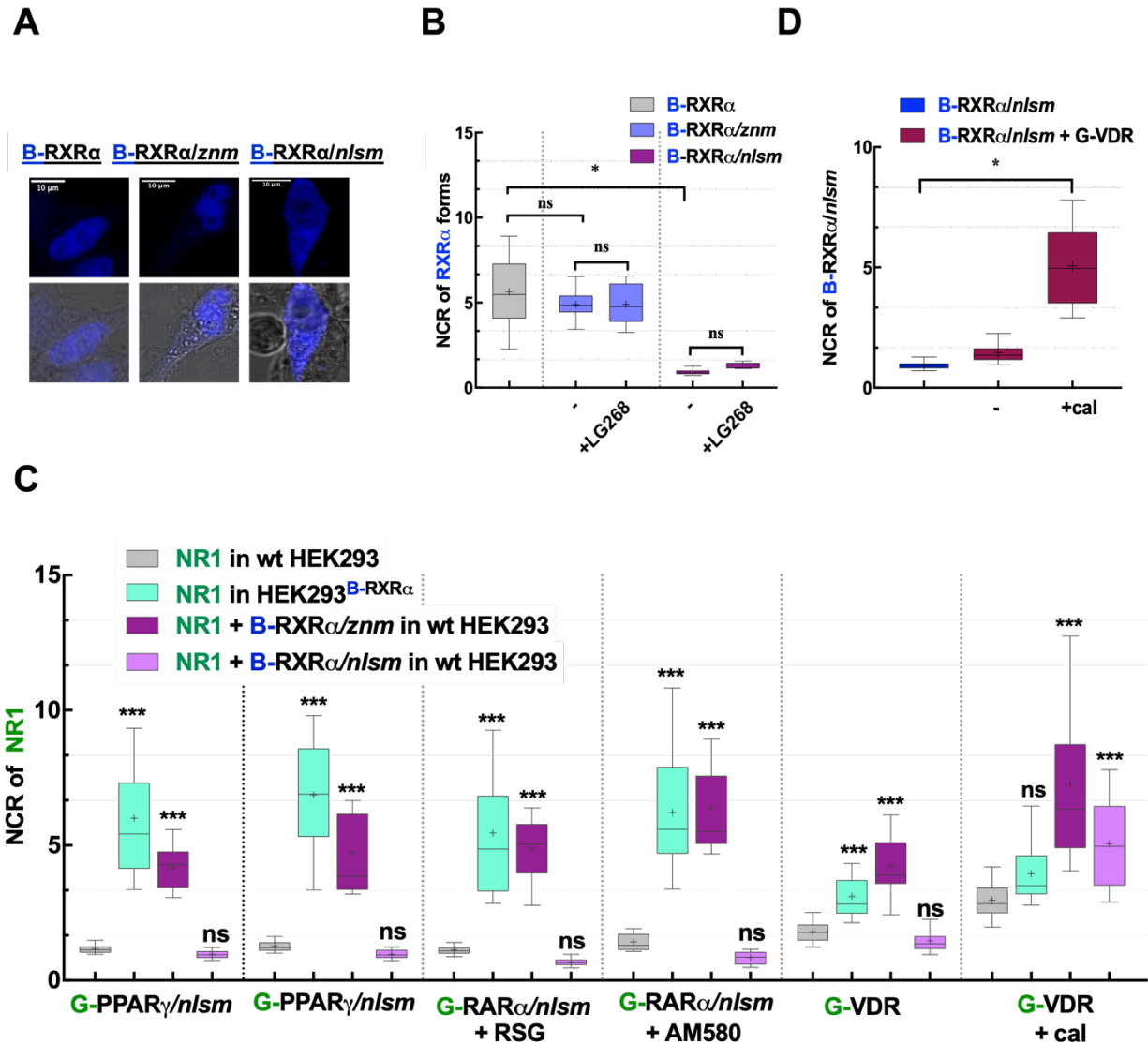


Figure 18. RXR-dependent nuclear enrichment of NR1 is mediated by heterodimerization.

(A) Representative confocal images show the nuclear localization of B-RXR α forms; B-RXR α and the zinc finger mutants B-RXR α /znm and B-RXR α /nlsm in wt HEK293. (B) NCR of B-RXR α forms. (C) Effect of calcitriol on governing the nuclear localization of B-RXR α /nlsm cotransfected with G-VDR. (D) Nuclear-to-cytoplasmic fluorescence intensity/pixel ratios (NCR) of NR1 when either transfected alone (grey box), with wt RXR (green box), with RXR α /znm (purple box) or with RXR α /nlsm (pink box). Box-and-whiskers plots represent 10th, 25th, 50th, 75th and 90th percentiles, (+) indicates the mean value. G: EGFP; B: TagBFP; C: mCherry. Scale bar: 10 μ m, ***: $p < 0.0001$.

5.2 Competition between RXR partners revealed by three-color imaging model system

Because EGFP-PPAR γ /*nls*m, EGFP-RAR α /*nls*m and wt EGFP-VDR had homogeneous distribution when expressed alone and translocated into the nucleus when heterodimerizing with RXR α irrespective of the presence or absence of ligand, they could serve as a suitable model system in our study (we refer to them always as NR1). NR1 nuclear shuttle can be explained by a piggy-back mechanism¹⁵³; the NR1-RXR α heterodimeric complex translocated into the nucleus depending on the NLS of RXR α .

In all the competition experiments, the combined expression levels of NR1 and NR2 were higher than that of RXR α , (NR1+NR2) > RXR α , resulting in a limiting pool of RXR α . This was assessed by comparing the relative fluorescence intensities of the fluorescent protein labels of the NRs to those of EGFP-mCherry and EGFP-TagBFP fusion proteins expressing the fluorescent proteins at a 1:1 ratio. More details about the experiment setting can be found in the material and method section, page 53.

5.2.1. Competition between PPAR γ and RAR α

Competition between PPAR γ and RAR α for binding to RXR α was assessed by detecting the distribution changes of EGFP-PPAR γ /*nls*m (NR1) in HEK293^{BFP-RXR α} in the presence of mCherry-RAR α (NR2) and cognate agonists. As can be seen in [Fig. 19A, B](#), the nuclear accumulation of EGFP-PPAR γ /*nls*m in HEK293^{BFP-RXR α} was dramatically reduced when cells were additionally co-transfected with mCherry-RAR α ; EGFP-PPAR γ /*nls*m became homogeneously distributed with an NCR value of ~ 1 , similar to the case when EGFP-PPAR γ /*nls*m was expressed alone in wt HEK293. Treatment with RSG caused a 4-fold nuclear enrichment of EGFP-PPAR γ /*nls*m, whereas AM580 or LG268 (RXR agonist) treatment kept EGFP-PPAR γ /*nls*m homogeneously distributed.

The challenge was to prove that dominance of RAR α over PPAR γ in competing for RXR α was not due to expressing mutant PPAR γ and intact RAR α ; therefore, a complementary experiment was also carried out. Here, EGFP-RAR α /*nls*m served as NR1 and the changes in its nuclear localization were detected in HEK293^{BFP-RXR α} in the presence of mCherry-PPAR γ as NR2.

Results were consistent with our previous observation; mCherry-PPAR γ failed to inhibit binding of EGFP-RAR α /*nls*m to BFP-RXR α . EGFP-RAR α /*nls*m was still dominantly located in the nucleus with an NCR of ~ 5.5 and this was further enhanced by AM580 treatment. On the other

hand, RSG treatment recovered the binding of mCherry-PPAR γ to RXR α and led to a homogeneous redistribution of EGFP-RAR α /nls in this triply transfected cell (Fig. 19C, D).

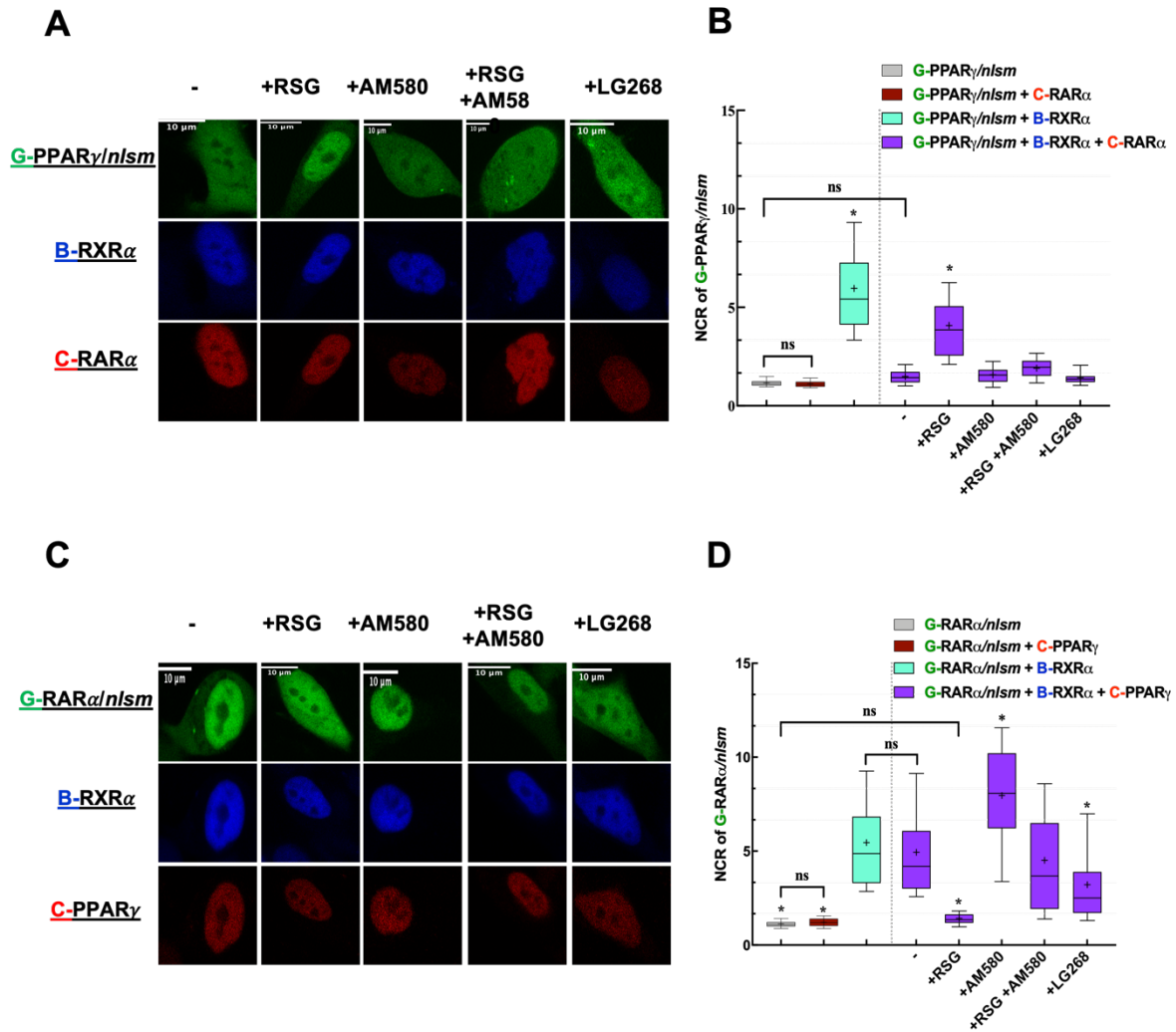


Figure 19. Competition between PPAR γ and RAR α : RXR α is more prone to heterodimerize with RAR α than with PPAR γ unless PPAR γ gets liganded.

(A) and (C) Representative confocal images show NR1 in green, RXR α in blue and NR2 in red. Scale bar: 10 μ m. (A) Changes in the distribution of G-PPAR γ /nls in HEK293^{B-RXR α} co-transfected with C-RAR α were assessed in the absence or presence of agonists (10⁻⁶ M RSG, 10⁻⁷ M AM580 or 10⁻⁷ M LG268). (C) Analogously, changes in the distribution of G-RAR α /nls were assessed in HEK293^{B-RXR α} cotransfected with C-PPAR γ . (B, D) Nuclear-to-cytoplasmic fluorescence intensity/pixel ratios (NCR) of NR1. ***: $p < 0.0001$ in comparison with NR1 distribution in HEK293^{B-RXR α} cotransfected with NR2 (the green box). Box-and-whiskers plots represent 10th, 25th, 50th, 75th and 90th percentiles, (+) indicates the mean value. G: EGFP; B: TagBFP; C: mCherry. Scale bar: 10 μ m.

We were also interested in how the affinities of liganded RAR α and liganded PPAR γ towards RXR α compare. To answer this question, we first treated our samples with saturating doses of RSG and AM580 simultaneously. EGFP-RAR α /nls m and EGFP-PPAR γ /nls m responded to the double treatment similar to AM580 treatment alone; i.e., EGFP-RAR α /nls m became nuclear-localized, whereas EGFP-PPAR γ /nls m remained homogeneous (Fig. 19C, D). This implies that liganded RAR α has a higher affinity toward RXR α than liganded PPAR γ . Then, we co-treated the cells with RSG, the agonist of the weak partner, at its saturating dose (1 μ M) and titrated AM580, the ligand of the dominant partner, from 0 to saturation, 100 nM. RSG dependent nuclear enrichment of EGFP-PPAR γ /nls m in HEK293^{BFP-RXR α} cotransfected with mCherry-RAR α was abolished gradually with increasing doses of AM580 (Fig. 20).

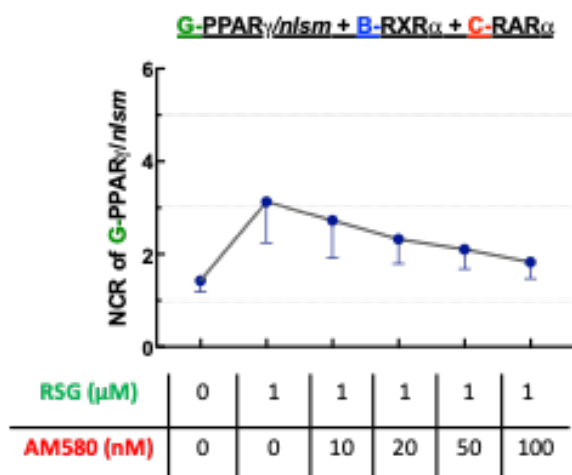


Figure 20. RXR α partner selection is dose dependent.

The dose-response curve shows the nuclear-to-cytoplasmic ratio (NCR) of EGFP-RAR α /nls m under different cotreatment doses; EGFP-RAR α /nls m and EGFP-PPAR γ /nls m were cotransfected in HEK293^{BFP-RXR α} cells and treated with RSG, the ligand of the weak partner at its saturating dose, 1 μ M and AM580, the ligand of the dominant partner was titrated from 0 to saturation. G: EGFP; B: TagBFP; C: mCherry.

To conclude, in the absence of an agonist, RAR α has a higher binding affinity to RXR α than PPAR γ while treatment with specific PPAR γ agonist, RSG, tips the scale in favor of PPAR γ . We can say that RXR partner selection is mediated by the availability of the specific ligand and in a dose dependent manner.

5.2.2. Competition between RAR α and VDR

We also examined the competition between VDR and RAR α for the limiting pool of RXR α in HEK293^{BFP-RXR α} cells. In a similar manner, we expressed EGFP-RAR α /*nls*m (as NR1) and mCherry-VDR (as NR2) in HEK293^{BFP-RXR α} cells. There was a slight decrease in the enrichment of EGFP-RAR α /*nls*m in the nucleus of HEK293^{BFP-RXR α} from 5.5 to 3.8 as shown in *Fig. 21B*. While the nuclear accumulation of EGFP-RAR α /*nls*m was augmented by AM580 treatment, it was abolished by calcitriol treatment after which EGFP-RAR α /*nls*m was distributed more homogeneously in HEK293^{BFP-RXR α} just as in wt HEK293 *Fig. 21B*. Interestingly, simultaneous treatment with AM580 and calcitriol increased the NCR value to ~6, even higher than AM580 alone. LG268 treatment had no impact on this competition (*Fig. 21A, B*).

Associated changes in the localization of mCherry-VDR are shown in *Fig. 21C*; treatment with AM580 kept mCherry-VDR in the cytoplasm, whereas calcitriol induced its nuclear translocation with an NCR of ~5. Interestingly, double treatment with AM580 and calcitriol increased the NCR value to ~6.6.

The complementary experiment was also carried out: changes of EGFP-VDR localization in HEK293^{BFP-RXR α} were followed in the presence of the competing partner, mCherry-RAR α (*Fig. 21D, E*). EGFP-VDR failed to maintain its nuclear accumulation in HEK293^{BFP-RXR α} when cells were co-transfected with mCherry-RAR α and redistributed homogeneously with a similar NCR value as in wt HEK293. As shown in *Fig. 21E*, calcitriol treatment abolished the dominance of mCherry-RAR α over EGFP-VDR in competing for RXR α and boosted the nuclear accumulation of VDR resulting in an NCR value of ~5, whereas calcitriol treatment in combination with AM580 resulted in an NCR of ~4.

To conclude, RXR α is more likely to heterodimerize with RAR α than with VDR unless VDR gets liganded with its specific agonist, calcitriol.

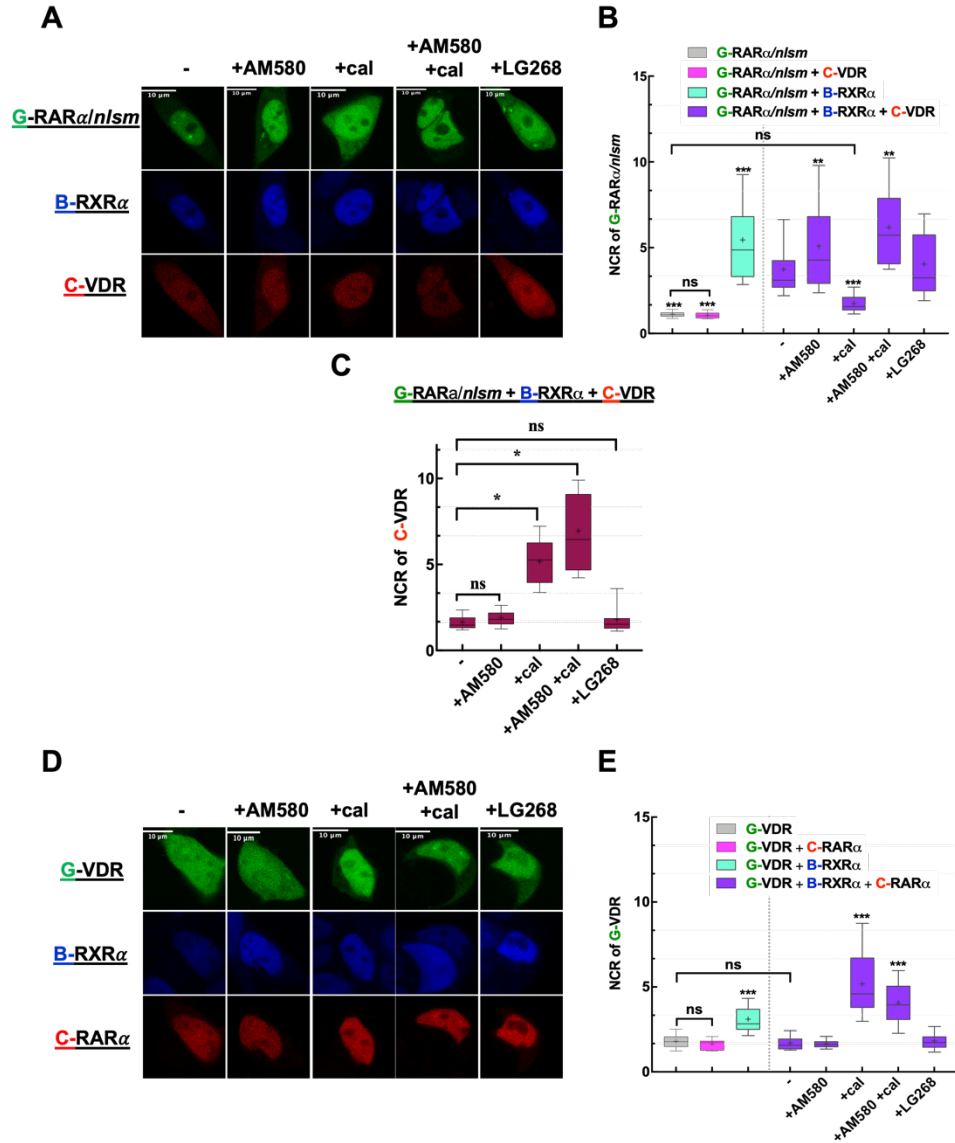


Figure 21. Competition between RARα and VDR: RXRα is more prone to heterodimerize with RARα than with VDR unless VDR gets liganded.

(A) and (D) Representative confocal images show NR1 in green, RXRα in blue and NR2 in red. Scale bar: 10 μm. (A) Changes in the distribution of G-RARα/nls-m in HEK293^{B-RXRα} co-transfected with C-VDR were assessed in the absence or presence of treatment with agonists (10⁻⁷ M AM580, 10⁻⁷ M calcitriol (cal) or 10⁻⁷ M LG268). (D) Analogously, changes in the distribution of G-VDR were assessed in HEK293^{B-RXRα} cotransfected with C-RARα. (B, E) Nuclear-to-cytoplasmic fluorescence intensity/pixel ratios (NCR) of NR1. ***: $p < 0.0001$, **: $p < 0.01$ in comparison with NR1 distribution in HEK293^{B-RXRα} cotransfected with NR2 (non-treated sample marked with "-"). (C) NCR values of NR2, C-VDR in HEK293^{B-RXRα} co-transfected with G-RARα/nls-m. Box-and-whiskers plots represent 10th, 25th, 50th, 75th and 90th percentiles, (+) indicates the mean value. G: EGFP; B: TagBFP; C: mCherry.

5.2.4. Competition between PPAR γ and VDR

In a similar fashion, competition between PPAR γ and VDR was also investigated. We first detected changes of the NCR of EGFP-PPAR γ /*nls*m in HEK293^{BFP-RXR α} ensuing in the presence of mCherry-VDR and specific agonists.

As shown in *Fig. 22A, B*, in the absence of ligand treatment, the nuclear accumulation of EGFP-PPAR γ /*nls*m was diminished in cells co-expressing mCherry-VDR (the NCR decreased from 6 to 3.7), though to a lesser extent than due to mCherry-RAR α (*Fig. 22B*). Agonist treatment shifted the competition between NRs in favor of the liganded partner: RSG treatment induced EGFP-PPAR γ /*nls*m enrichment in the nucleus of triply transfected cells, whereas calcitriol redistributed EGFP-PPAR γ /*nls*m within HEK293^{BFP-RXR α} cells with an NCR value equaling that measured in wt HEK293 cells. Double treatment with RSG and calcitriol increased the NCR value of EGFP-PPAR γ /*nls*m to ~ 4.4 favoring again the binding of RXR α to EGFP-PPAR γ /*nls*m and abolishing the effect of calcitriol. LG268 did not affect the competition; EGFP-PPAR γ /*nls*m remained nuclear-localized. Associated changes in the localization of mCherry-VDR are shown in *Fig. 22C*. In these triply transfected cells, mCherry-VDR was homogeneously distributed in the absence of ligand and also upon RSG or LG268 treatment, whereas its NCR value increased to ~ 5 after treatment with calcitriol alone and to ~ 4.4 upon combined treatment with calcitriol and RSG.

In the complementary experiment, we traced localization changes of EGFP-VDR (as NR1) in HEK293^{BFP-RXR α} cells cotransfected with mCherry-PPAR γ (as NR2) at the same agonist treatment conditions (*Fig. 22D, E*).

Without agonist treatment, the NCR of EGFP-VDR was around 2, similar to its value in wt HEK293. Both RSG and LG268 treatment kept the NCR of VDR low indicating impediment of the interaction between VDR and RXR α , while calcitriol boosted the NCR of EGFP-VDR to around 4.8 when applied alone and to ~ 4 when applied in combination with RSG.

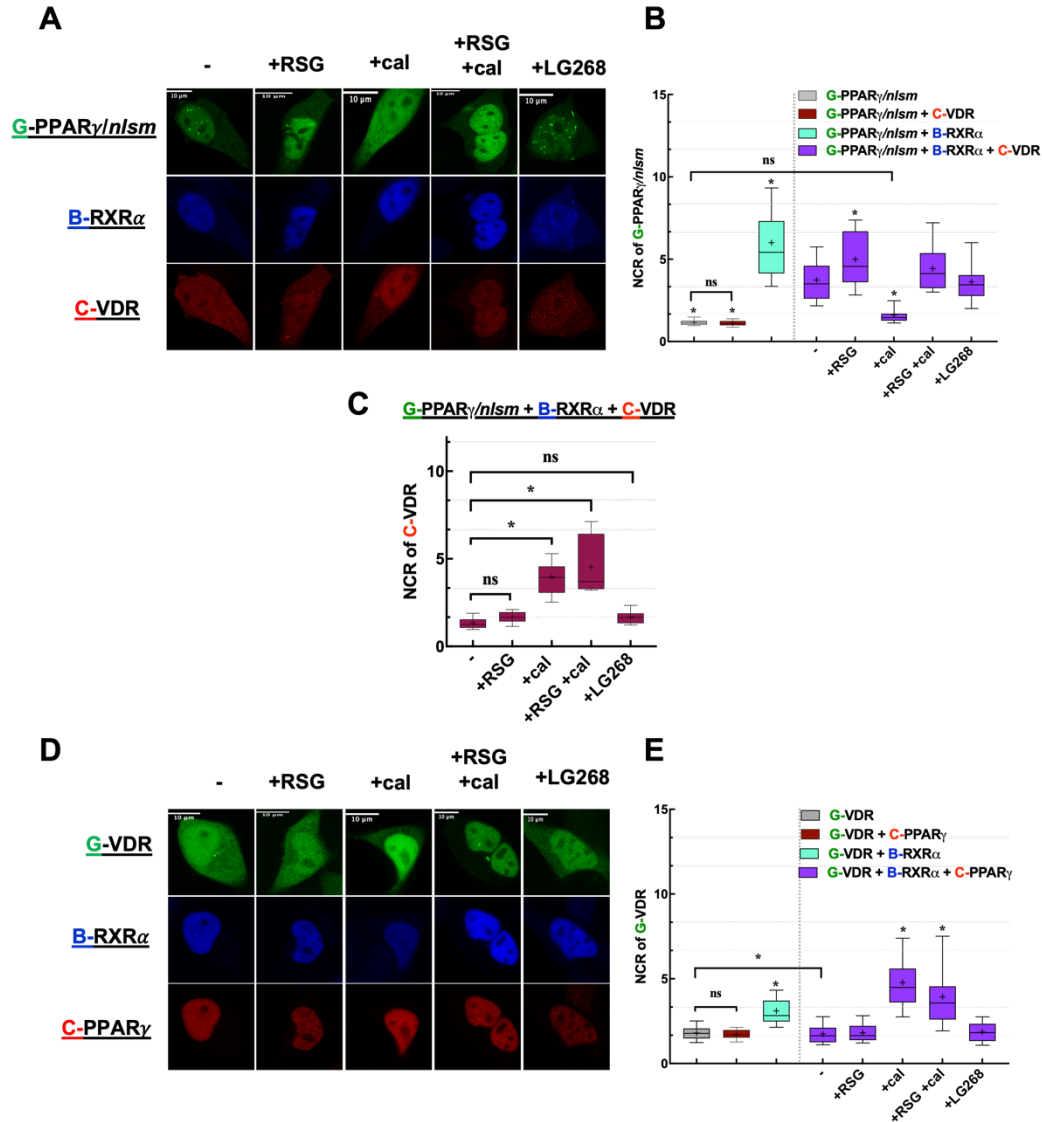


Figure 22. Competition between PPAR γ and VDR: RXR α is more likely to heterodimerize with PPAR γ than with VDR unless VDR gets liganded.

(A) and (D) Representative confocal images show NR1 in green, RXR α in blue and NR2 in red. Scale bar: 10 μ m. (A) Changes in the distribution of G-PPAR γ /nlsm in HEK293^{B-RXR α} co-transfected with C-VDR were assessed in the absence or presence of treatment with agonists (10^{-6} M RSG, 10^{-7} M calcitriol (cal) or 10^{-7} M LG268). (D) Analogously, changes in the distribution of G-VDR were assessed in HEK293^{B-RXR α} cotransfected with C-PPAR γ . (B, E) Nuclear-to-cytoplasmic fluorescence intensity/pixel ratios (NCR) of NR1; ***, $p < 0.0001$ in comparison with NR1 distribution in HEK293^{B-RXR α} cotransfected with NR2 (non-treated sample marked with "-"). (C) NCR values of NR2, C-VDR in HEK293^{B-RXR α} co-transfected with G-PPAR γ /nlsm. Box-and-whiskers plots represent 10th, 25th, 50th, 75th and 90th percentiles, (+) indicates the mean value. G: EGFP; B: TagBFP; C: mCherry.

To exclude the effect of endogenously produced PPAR γ ligands on our results, we also used a PPAR γ antagonist (GW9662). This antagonist enhances co-repressor binding and stabilizes PPAR γ in its *apo* conformation¹⁵⁴. Thus, it could displace the bounded endogenous ligands.

The dominance of PPAR γ over VDR was retained even when GW9662 was present (*Fig. 23*) suggesting that this dominance was not due to binding endogenous agonists.

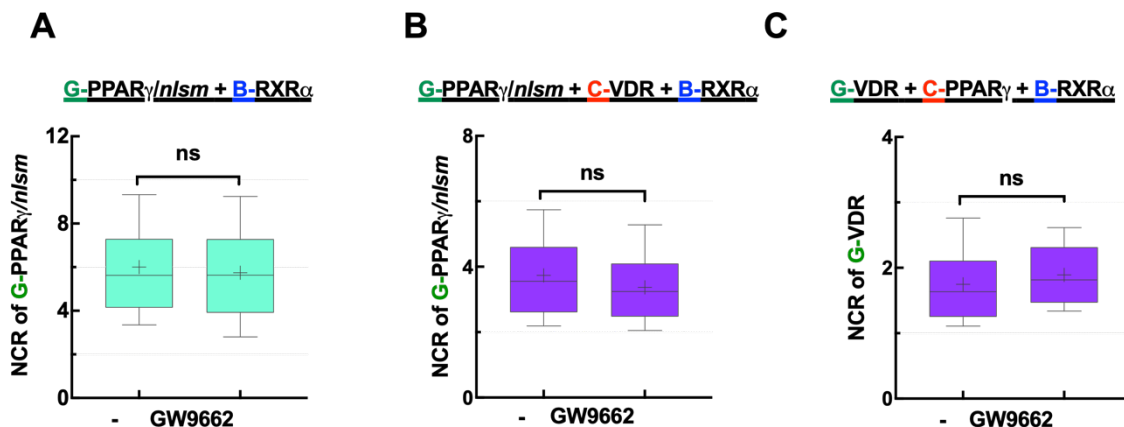


Figure 23. Endogenous ligand does not contribute to the competition in our model system.

PPAR γ antagonist GW9662 (10^{-6} M) did not change the NCR of NR1 (compared to non-treated samples).

Box-and-whiskers plots represent 10th, 25th, 50th, 75th and 90th percentiles, (+) indicates the mean value.

G: EGFP; B: TagBFP; C: mCherry.

To conclude, RSG treatment favors RXR α heterodimerization with PPAR γ and calcitriol augments VDR binding to RXR α , whereas without agonists RXR α binds to PPAR γ with a higher affinity.

We could also highlight that in our model system, in HEK293 cells treated with charcoal stripped FBS, endogenous ligands did not contribute to the reported results.

5.2.5. Competition of VDR/*nls*m, as NR1, with RAR α or PPAR γ

The mutation in NLS1 of VDR rendered EGFP-VDR/*nls*m to be cytoplasmic in wt HEK293 cells (NCR~0.6) and this remained so even in HEK293^{BFP-RXR α} cells (Fig. 24A, B). Interestingly, it was RXR α that followed EGFP-VDR/*nls*m to the cytoplasm (Fig. 24A, C) indicating that EGFP-VDR/*nls*m was competent to heterodimerize with RXR α but the heterodimeric complex failed to translocate to the nucleus. Therefore, we also traced changes in the localization of BFP-RXR α to detect the presence or absence of heterodimerization between EGFP-VDR/*nls*m and RXR α (Fig. 24C).

Specific agonist treatment had an interesting effect, in wt HEK293 the NCR of EGFP-VDR/*nls*m was doubled upon treatment with calcitriol reaching a value of ~1.3 (Fig. 24B). Moreover, both EGFP-VDR/*nls*m and RXR α became enriched in the nucleus of HEK293^{BFP-RXR α} cells upon calcitriol treatment; the NCR of EGFP-VDR/*nls*m increased to ~3.3 (Fig. 24B), and the NCR of BFP-RXR α was restored to ~5, close to its normal value (Fig. 24C).

In competition experiments between EGFP-VDR/*nls*m and mCherry-RAR α in HEK293^{BFP-RXR α} cells, RXR α was enriched in the nucleus together with PPAR γ rather than being sequestered in the cytoplasm with VDR/*nls*m suggesting the preference of RXR α for RAR α over VDR (Fig. 24D).

Similarly, when EGFP-VDR/*nls*m and mCherry-PPAR γ were cotransfected in HEK293^{BFP-RXR α} cells, RXR α was trapped in the nucleus where PPAR γ resided rather than colocalizing with VDR/*nls*m in the cytoplasm. This also indicated the dominance of PPAR γ over VDR (Fig. 24E).

In both experiments, EGFP-VDR/*nls*m became slightly enriched in the nucleus of HEK293^{BFP-RXR α} after treatment with calcitriol (Fig. 24D, E).

To conclude, our results on VDR/*nls*m without ligand treatment are in accordance with those gained with wt VDR indicating the dominance of both RAR α and PPAR γ over VDR. The role of calcitriol in the competition was more obvious when we used wt VDR than in the case of VDR/*nls*m.

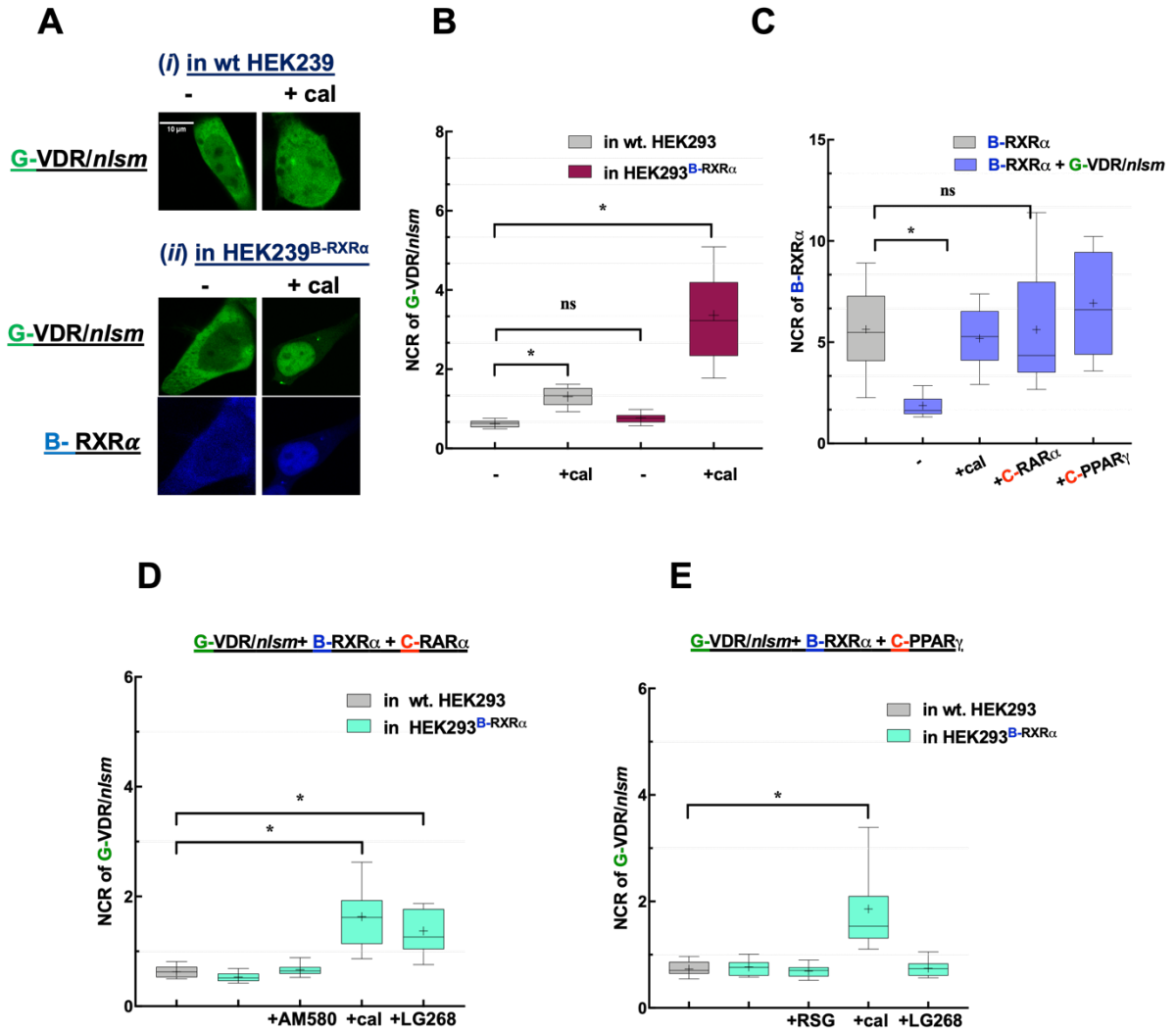


Figure 24. EGFP-VDR/nlsm as NR1 in competition with RARα and PPARγ.

Both RARα and PPARγ dominate over VDR/nlsm in competing for dimerization with RXRα. (A) Representative confocal images of G-VDR/nlsm transiently transfected into wt HEK293 (left) or HEK293^{B-RXRα} cells (right) in the absence (top) or presence (bottom) of specific NR1 agonists (10^{-7} M calcitriol (cal)). Scale bar: 10 μm. (B) Nuclear-to-cytoplasmic fluorescence intensity/pixel ratios (NCR) of G-VDR/nlsm. (C) NCR values of B-RXRα. (D) NCR of G-VDR/nlsm in HEK293^{B-RXRα} co-transfected with C-RARα were assessed in the absence or presence of agonists (10^{-7} M AM580, 10^{-7} M cal or 10^{-7} M LG268). (E) Changes in the distribution of G-VDR/nlsm in HEK293^{B-RXRα} co-transfected with C-PPARγ were assessed in the absence or presence of agonists (10^{-6} M RSG, 10^{-7} M cal or 10^{-7} M LG268). Box-and-whiskers plots represent 10th, 25th, 50th, 75th and 90th percentiles, (+) indicates the mean value, *: $p < 0.05$, ***: $p < 0.0001$. G: EGFP; B: TagBFP; C: mCherry.

5.2.6. Overexpression of RXR α abrogates competition between its potential heterodimerization partners

We have shown that NRs compete for RXR α and revealed differences in the binding affinities between RXR α and its partners. Competition was observed in a situation where the combined expression levels of NR1 and NR2 were larger than that of RXR α alone; therefore, RXR α was limiting. More details about the experiment setting can be found in the Materials and methods section, page 53.

To assess whether the competition for RXR α is the primary cause for our observed results, experiments were repeated in cells expressing less NR1 and NR2. Thus, HEK293^{BFP-RXR α} cells were transfected with half the amount of the plasmids of NR1 and NR2 as compared to the amounts used previously, and experiments were carried out 24h rather than 48h after transfection.

In the new model system, RXR α is not limiting anymore; RXR α > (NR1+NR2). The dominance of RAR α over PPAR γ was abolished because RXR α became sufficient for both partners (*Fig. 25A*): EGFP-PPAR γ /*nls*m in HEK293^{BFP-RXR α} was enriched in the nucleus with an NCR of ~5, very close to the case where mCherry-RAR α was absent. This supports our previous conclusions; the homogeneous distribution of EGFP-PPAR γ /*nls*m in HEK293^{BFP-RXR α} co-transfected with mCherry-RAR α is due to monopolizing of RXR α by the dominant partner, RAR α , when RXR α is limiting.

In the same manner, we showed how the reduced amount of heterodimerization partners relative to RXR α abolished the dominance of RAR α (*Fig. 25B*) and PPAR γ (*Fig. 25C*) over VDR; EGFP-VDR maintained its RXR-dependent nuclear localization in contrast to the previous situation where RXR was limiting and was monopolized by the dominant partner.

To conclude, in cells where there is a limiting or sequestered pool of RXR combined with the expression of several RXR heterodimerization partner NRs, a competition between NRs for their common partner RXR is most likely to occur.

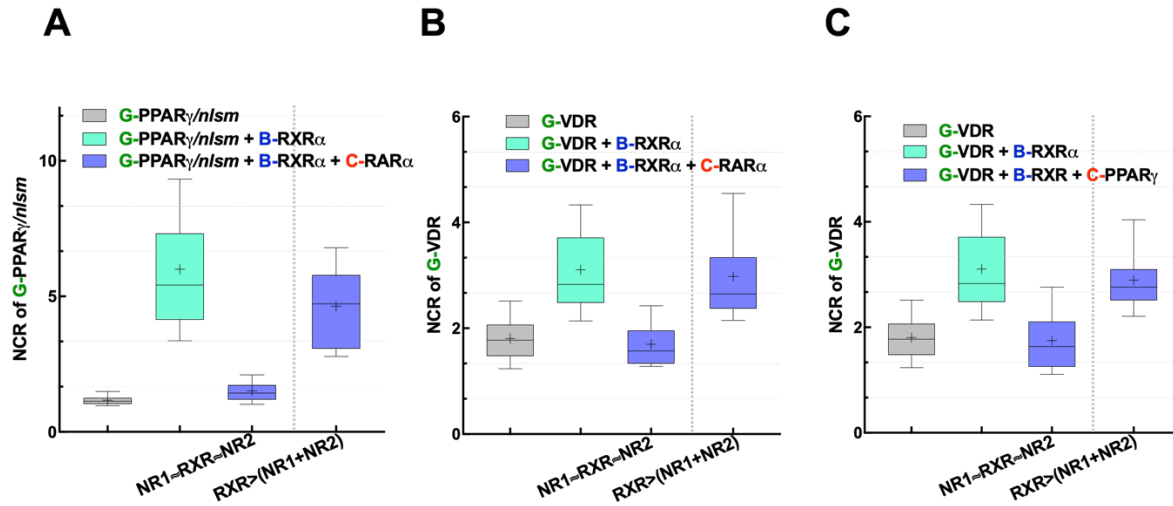


Figure 25. Increased availability of RXR α abolishes the competition between NRs for RXR α heterodimerization.

Distribution of NR1 in wt HEK293 is shown in grey, in HEK293^{B-RXR α} cells in light green, in HEK293^{B-RXR α} cells co-transfected with NR2 in blue. In the first blue box, HEK293^{B-RXR α} cells were transfected with 80 ng of each of NR1 and NR2 and experiments were carried out 48h after transfection; these conditions result in a limiting pool of RXR α ; (NR1+NR2)>RXR α . In the second blue box, HEK293^{B-RXR α} cells were transfected with 40 ng of each of NR1 and NR2; experiments were carried out 24h after transfection, resulting in a larger RXR α pool relative to NR1 and NR2; RXR α >(NR1+NR2). Box-and-whiskers plots represent 10th, 25th, 50th, 75th and 90th percentiles, (+) indicates the mean value. G: EGFP; B: TagBFP; C: mCherry.




5.3. The effect of specific agonist treatment on RXR homodimerization revealed by SPIM-ALEX-FRET-FCCS

Quantitative mapping of molecular (co-)mobility by fluorescence (cross-)correlation spectroscopy (F(C)CS) in a Single Plane Illumination Microscope (SPIM) has been introduced to reveal molecular diffusion and binding. A complementary aspect of interactions is proximity, which can be studied by Förster resonance energy transfer (FRET). Here, we extend SPIM-FCCS by alternating laser excitation, which reduces false positive cross-correlation, and facilitates co-mapping of FRET. Thus, different aspects of interacting systems can be studied simultaneously, and molecular subpopulations can be discriminated by multiparameter analysis.

In FCCS acquisition, continuous (and simultaneous) excitation by the two lasers introduces unwanted contributions in the red channel: donor crosstalk, sensitized emission due to FRET, and direct excitation of the red dye at 488 nm. To avoid these artifacts and allow FRET and FCCS analysis from the same images, we implemented alternating laser excitation (ALEX) for subsequent frames. Excitation at 488 nm produces a donor and a transfer signal, while excitation at 561 nm generates a pure acceptor signal for FRET. The donor and acceptor signals, time-shifted by 1 frame time (0.53 ms), can be used for FCCS analysis.

To validate this concept, we acquired FRET and FCCS data with continuous excitation (cont. exc.) and with ALEX on dedicated control samples shown in *Table (12)*.

Table 12. Control samples used in SPIM-ALEX-FRET-FCCS experiments.

Control samples		in FRET	in FCCS
	GC⁺ : fusion protein where EGFP (G) is linked to mCherry (C) via 6 AAs.	Positive	Positive
	GC⁻ : fusion protein where EGFP (G) is linked to mCherry (C) via a long rigid linker; 5 AAs then a polyproline spacer (30 repeats).	Negative	Positive
	G/C : EGFP and mCherry constructs are cotransfected.	Negative	Negative

As can be seen in *Fig. 26*, the GC⁺ dimer showed high FRET and crosscorrelation, while the GC⁻ sample had similar cross-correlation but low FRET. Due to the short donor-acceptor distance, a high median E (32.9% from cont. exc. and 21.4% from ALEX) can be measured on GC⁺. The higher E from preview images is probably due to the shorter illumination, thus less (acceptor) bleaching. In contrast, for GC⁻ we got very low values (0.8% and -2.5% with cont. exc. and ALEX). Because in the G/C sample the molecules diffuse separately, no FRET or cross-correlation were obtained. Crosstalk correction decreases *rCCF* in every sample as expected. However, the dynamic range, defined by the difference between values for GC⁻ and G/C, increases by ~30%. ALEX further increases the dynamic range (by 45%); and the near-zero value for the negative control makes quantification of dimerization more reliable and increases sensitivity.

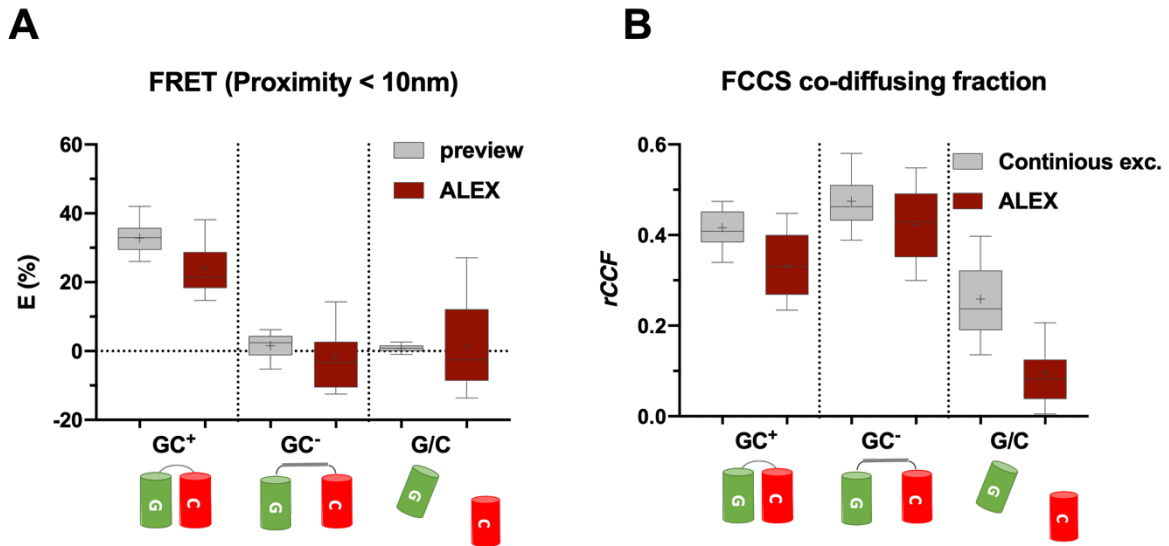


Figure 26. Validation of the SPIM-ALEX-FRET-FCCS method with control samples.

Box plots of cellular medians of E , calculated from preview images or from ALEX data; (B) $rCCF$ values of the same cells calculated from continuous excitation FCCS data and from ALEX data where crosstalk is eliminated.

Previous FCCS studies in the lab showed that RXR expressed alone, diffuse freely or in small complexes constituting a fast population and agonist binding induces transition to a slow, chromatin-bound state^{105,106}. In another study, Chen et al. have shown the increase of dimerization between the LBDs of RAR and RXR upon treatment with RXR agonist¹⁵⁵. Here we aimed to address the impact of specific agonist treatment, LG268, on RXR homodimerization applying this novel SPIM-ALEX-FRET-FCCS technique on constructs expressing only the LBD of RXR tagged N-terminally with EGFP or mCherry. These RXR-LBDs should have the capacity to heterodimerize but do not bind to DNA.

We cotransfected Hela cells with EGF-RXR LBD and mCherry-RXR LBD and applied LG268. We characterized the dimerization and the chromatin binding of these LBDs via FRET and FCCS in reference to our validated control samples GC⁺, GC⁻, and G/C and we used preview images for FRET calculations because of the low FRET efficiencies. A summary of all the measured and calculated values and their indications can be seen in [Table. 13](#) for an ease follow up with the results.

Table 13. Parameters determined from SPIM-ALEX-FRET-FCCS and their meaning.

Parameter	Full name	Meaning	Calculated in
E	FRET efficiency	Characterizing proximity	FRET
rCCF	Relative cross correlation amplitude	Characterizing the dimerized fraction	FCCS
r ₁	Fast fraction	Freely diffusing fraction	FCS
r ₂	Slow fraction	DNA bound fraction	FCS
D ₁	Diffusion coefficient of the fast component	Mobility of the fast component	FCS
D ₂	Diffusion coefficient of the slow component	Mobility of the DNA-bound component	FCS

We could detect a median E value of ~3.4% in untreated cells, which increased to 5.4% upon LG268 treatment. *rCCF* increased from 0.42 to 0.61 upon LG268 treatment confirming homodimerization and its ligand-induced increase (*Fig. 27*). This result agrees with earlier photon counting histogram analysis indicating an increase of molecular brightness of RXRLBD upon LG268 treatment¹²¹. We observed a difference between the r₂ values calculated from the green and red ACFs which is evidently an artifact resulting from more extensive bleaching of mCherry than EGFP, especially for the slow component having a longer dwell time in the laser beam.

In conclusion, these results revealed ligand dependent homodimerization of RXR and demonstrate the advantage of SPIM-ALEX-FRET-FCCS again: the extent of dimerization may have been underestimated if applying FRET alone.

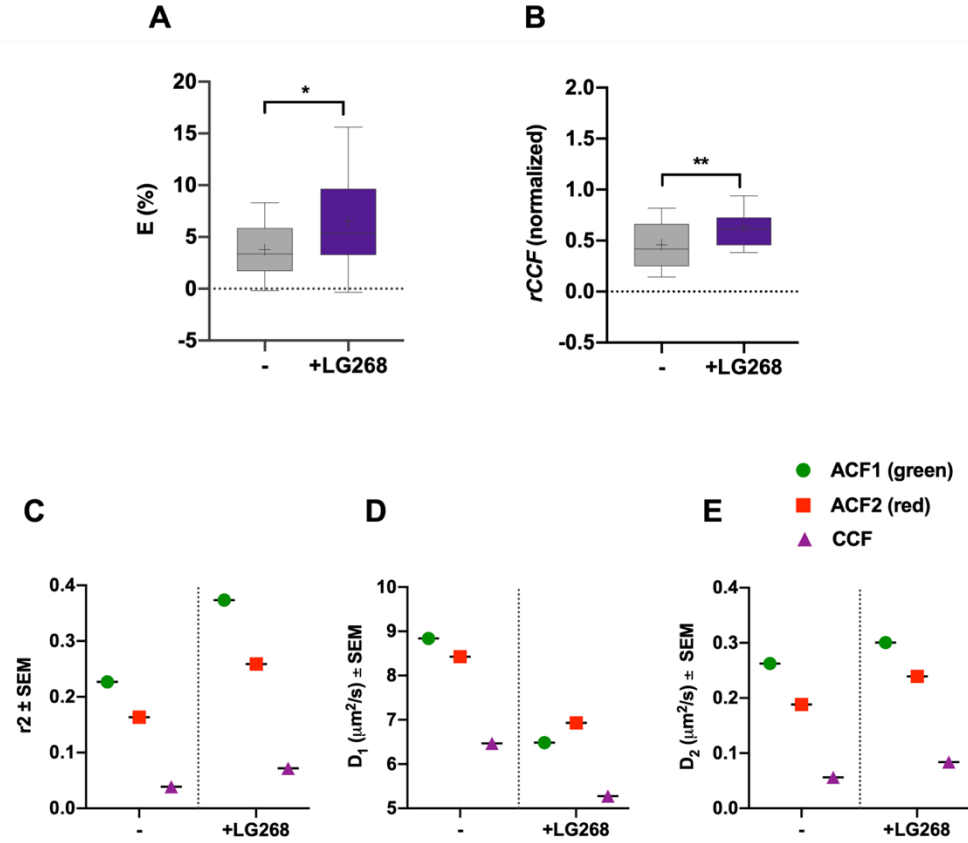


Figure 27. SPIM-ALEX-FRET-FCCS measurement reveal ligand dependent homodimerization of RXR.

(A) FRET efficiencies for the G-RXRLBD/C-RXRLBD homodimer (right, $n = 37$ and 36 for control and LG268-treated cells) determined from preview images recorded immediately before the FCCS measurements. The box plot represents the distributions of cellular medians of pixelwise E values. Cells were treated with 10^{-7} M LG268, specific agonists of RAR and RXR. (B) Co-mobility as assessed by the $rCCF$ ratio of the amplitudes of the cross- and autocorrelation functions using the minimum of the ACF0 and ACF1 (green and red channel) amplitudes, measured with ALEX. (C) Average proportion r_2 of the slow component from fits to a two-component free diffusion model assuming a fast, freely diffusing and a slow, chromatin-bound species. RXRLBD is unable to bind directly to chromatin. (D, E) Average diffusion coefficients \pm SEM of all cell medians for the ACFs and the CCF. D_1 and D_2 characterize the fast and slow component, respectively. G: EGFP; C: mCherry.

5.4. Chromatin binding of NRs is dynamically regulated by specific agonist treatment

Our finding that specific agonist binding increases the affinity of the studied NRs toward RXR raises the question if it also affects their chromatin binding properties.

We investigated this possibility in the case of VDR. The Genomic binding sites (GBSs) of VDR were detected by ChIP-seq in THP-1 macrophages. We were able to divide the total GBSs ($n=13915$) into three groups: *i*) $n_1=1866$, GBSs containing a full Vitamin D response element (a direct repeat of the AGGTCA or similar sequence with a 3-nucleotide spacer, DR3) denoted as “VDRE”. *ii*) $n_2=1572$ less specific GBSs having a single AGGTCA sequences denoted as “NR half-site”. *iii*) $n_3=10477$ GBSs where neither a VDRE nor an NR half-site sequence could be mapped, denoted as “None”. Upon calcitriol activation, VDRE-containing GBSs showed considerably higher occupancies on average than in the control, untreated sample. A similar induction, but to a much lesser extent, was detected for the NR half-site-containing regions. In contrast, the “None” GBSs did not show any induction upon calcitriol (*Fig. 28*).

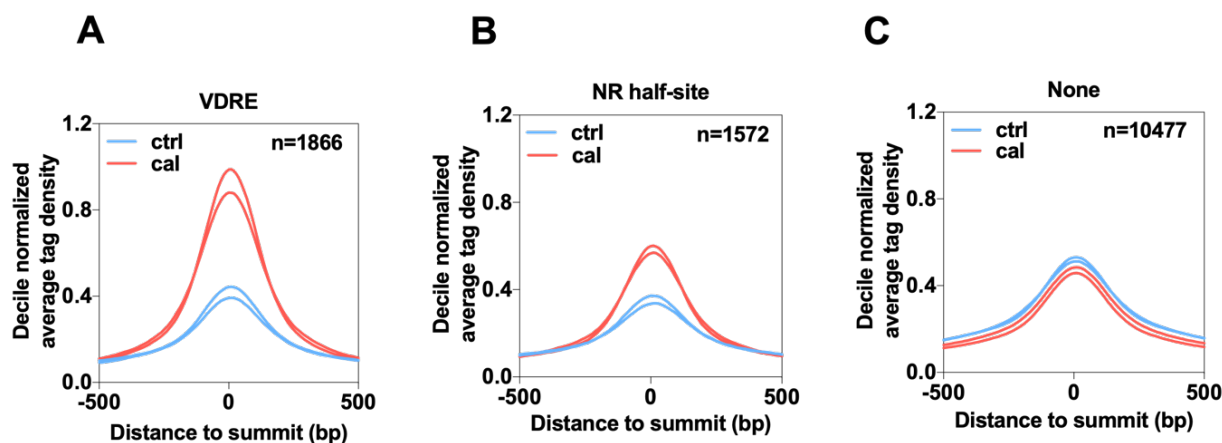


Figure 28. Genomic binding sites of VDR classified into three groups.

Histograms showing the decile-normalized average tag density of the VDR binding sites that contain (A) VDRE GBSs ($n=1866$), (B) NR half-site GBSs ($n=1572$), (C) none GBSs ($n=10477$) in the presence of calcitriol (cal) or vehicle (ctrl) in THP-1 macrophages.

To reveal more details of the stimulatory/inhibitory effect of calcitriol on VDR binding, we clustered the VDR GBSs in each group according to their tag densities and response types. We found that in the “None” group, a significant proportion ($n=6361$) of the GBSs displayed a negative response, i.e., a decrease of tag densities upon calcitriol treatment, whereas only a few VDRE- ($n=213$) and NR half-site-containing ($n=321$) GBSs behaved this way. The clusters responding negatively to calcitriol treatment were denoted by “II” whereas those responding positively by “I”. (Fig. 29).

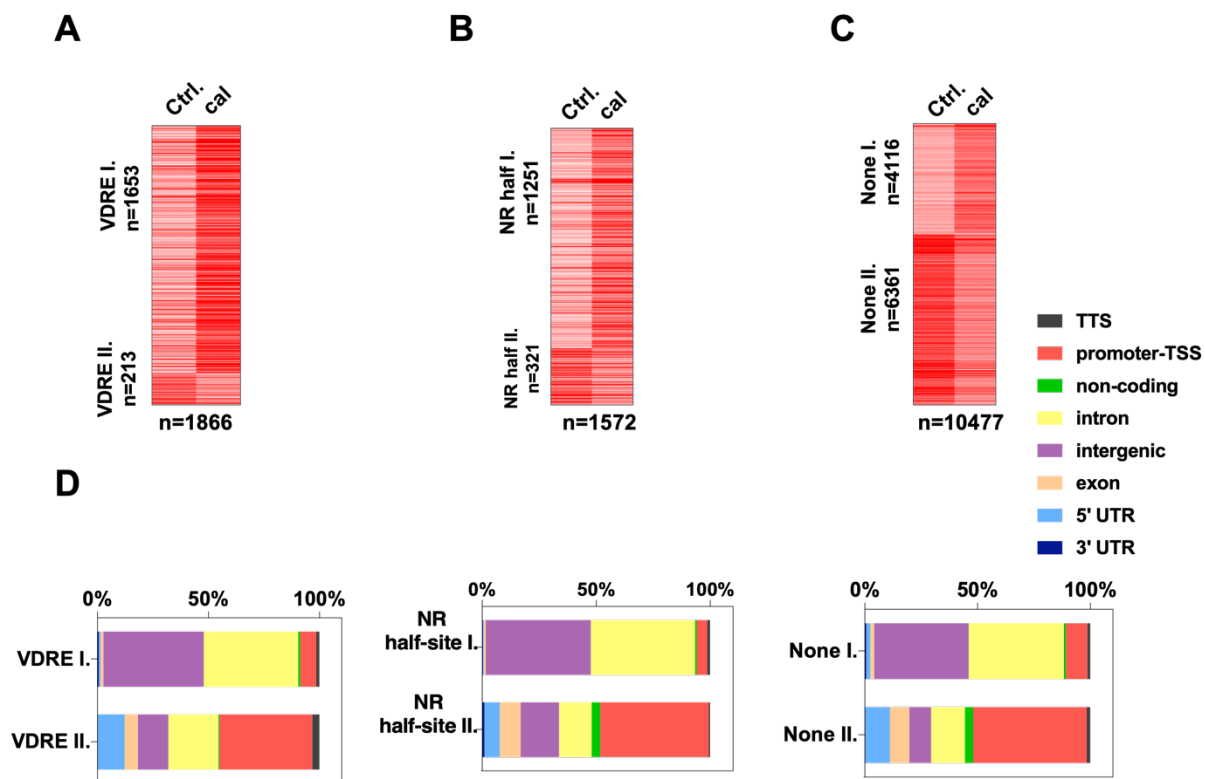


Figure 29. Clustering the genomic binding sites (GBSs) according to their tag densities and response to calcitriol treatment revealed two clusters within each GBS group.

Cluster I (top cluster), Cluster II (bottom cluster, in the vehicle, ctrl, treatment (left) or calcitriol (cal) treatment (right). (A), clusters of “VDRE”, (B) clusters of “NR half-site” (C) clusters of “none”, (D), Bar charts showing the genomic distribution of VDR binding sites separately for the two clusters (I. and II.) of the three GBS groups in THP-1 macrophages.

To better understand the factors that are responsible for this pattern, we applied *de novo* motif enrichment analysis within each group. Besides the expected motifs, the VDRE- and NR half-site-

containing GBSs mostly showed the presence of the well-known PU.1, C/EBP (enhancer-specific pioneering factors Purine-rich box 1 and CCAAT enhancer-binding protein) and AP-1 (Activator protein 1) motifs, which occurred mainly in intergenic or intronic regions while in the “None” group, the promoter specific YY1 (Yin Yang 1 transcriptional repressor protein) motif was significantly enriched (*Fig. 30*).

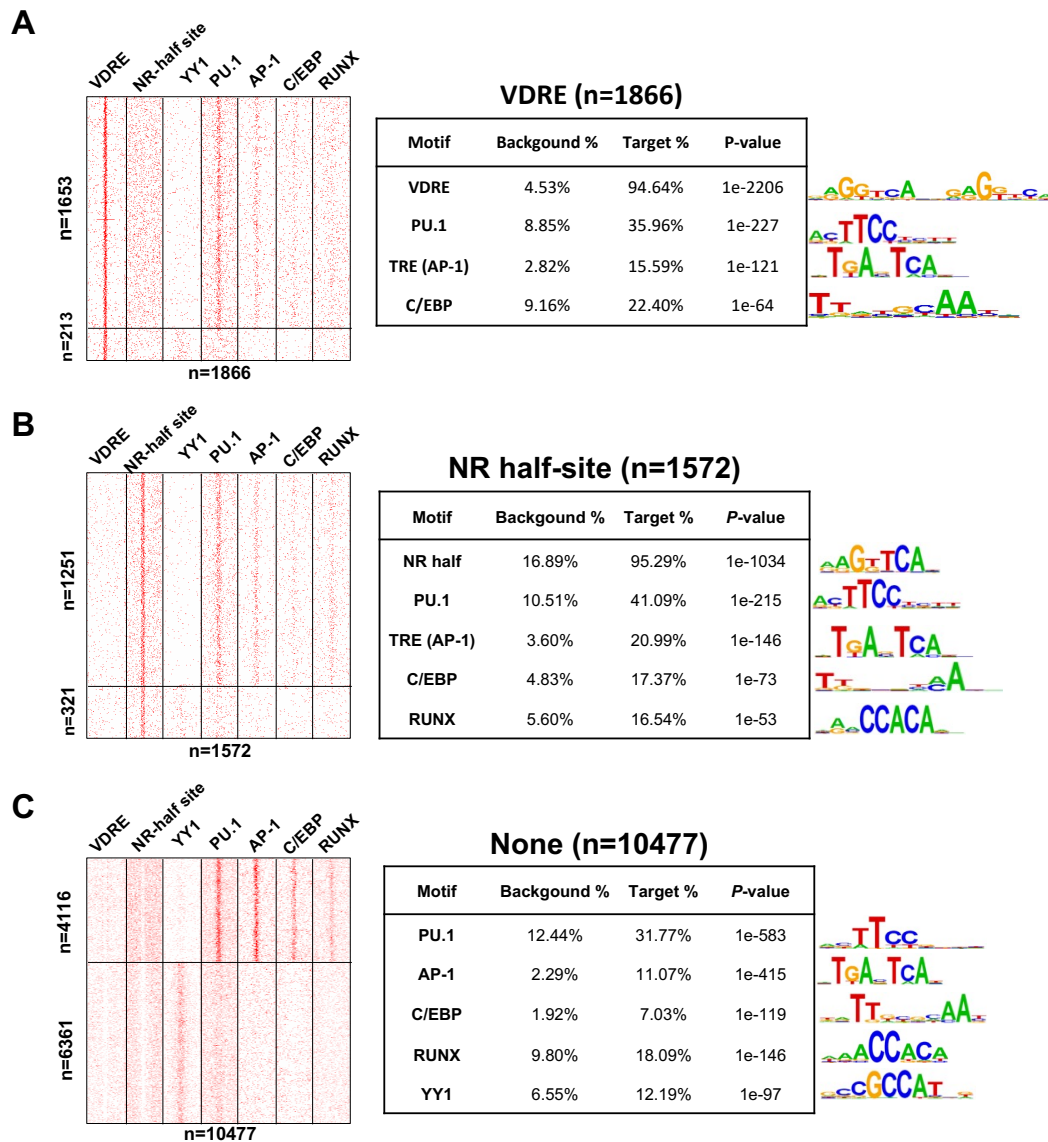


Figure 30. De novo motif enrichment analysis of VDR genomic binding sites.

The enriched motifs within the target regions containing VDRE (A), NR half-site (B), or none (C). The P-values, target, and background percentages are included for each motif (left). Motif distribution heat maps showing the presence of VDRE, NR half-site, YY1, PU.1, AP-1, C/EBP, and RUNX motifs in 2-kb frames around the center of the binding sites depicted in Fig. 29 (right).

The enrichment of PU.1, C/EBP, and AP-1 suggests that GBSs in cluster I may be enhancers and the enrichment of the YY1 motif in cluster II of each GBS proves the promoter nature of these sites as many of them were indeed located within promoter-TSS regions (*Fig. 29D, 30*).

Fig. 31A demonstrates the effect of calcitriol treatment on VDR accumulation at enhancer or promoter regions of some target genes. There is an overlap between these two sets: in the case of 507 genes binding both to the enhancer and the promoter of the same gene was found suggesting chromatin looping (*Fig. 31B*). The bar plot depicted in *Fig. 31C* shows the top 15 biological pathways in which these 507 genes play a role.

Taken all together, we can conclude that direct DNA binding (to VDREs or NR half-sites) is enhanced by calcitriol, which together with our microscopy data suggests that heterodimerization with RXR and direct DNA binding are correlated events.

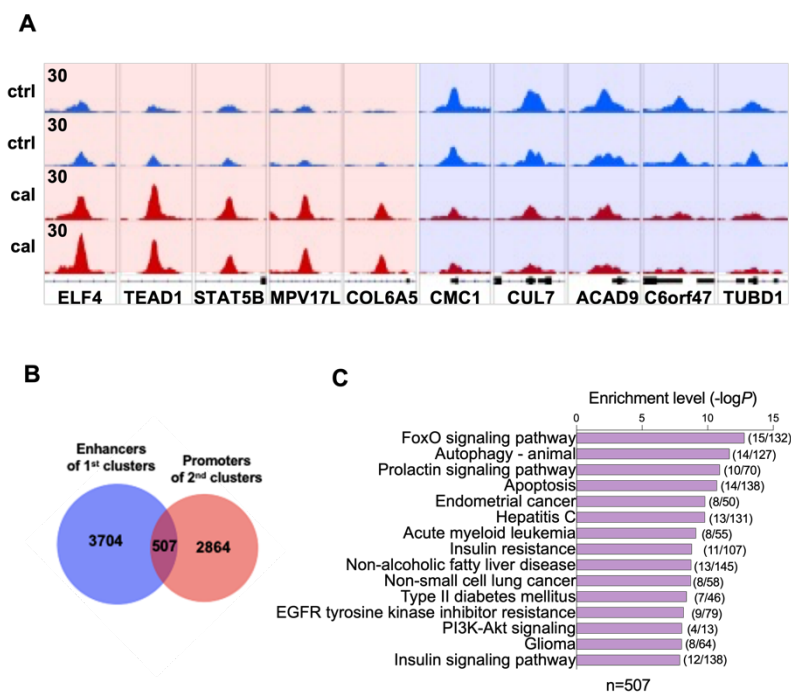


Figure 31. Calcitriol regulated genes in Enhancer and promoter regions.

(A) An Integrative Genomics Viewer (IGV) snapshot of VDR coverage representing ten VDR binding sites in control (ctrl) or calcitriol (cal) treated THP-1 macrophages from clusters I (left) and II (right). The interval scale is 30 in all cases. (B) Venn diagram illustrating the overlap between the genes annotated to putative enhancers of the I. clusters and promoters of the II. clusters, (C) bar plot showing the top 15 biological pathways in which the 507 genes defined in panel C play a role. The numbers after the bars denote the number of genes found in the overlap and the total number of known genes assigned to the given pathway.

5.5. Doxorubicin effect on the mobility of RAR α

5.5.1 Doxorubicin affects the binding of EGFP-RAR α to DNA

Doxorubicin (Dox) is a potent anti-cancer chemotherapeutic drug intercalating between DNA base pairs. Its action involves relaxation of torsional strain of supercoiled DNA and histone eviction¹³¹, which may affect the binding of nuclear proteins recognizing specific response elements like nuclear receptors. Dox inhibits the ligation of DNA breaks by topoisomerase II, which causes cell death in replicating cells. This is also the basis of its most serious side effect, Dox-induced cardiomyopathy (DIC). RAR binds downstream of the promoter in the Top II gene thereby inhibiting Top II expression; thus, treatment with RAR ligands was reported to ameliorate DIC. With this background we asked how Dox affects the DNA binding of RAR α .

To address this question, we carried out FRAP experiments to track changes in RAR mobility in the nucleus of HeLa cells stably expressing EGFP-RAR α , HeLa^{EGFP-RAR α} at different doses of Dox, in the absence or presence of specific RAR α agonist (0.1 μ M AM580).

FRAP recovery curves of EGFP-RAR α could be fitted by a two-component exponential model suggesting the presence of 2 diffusion components (*Fig. 32*): a fast one likely due to receptors not bound to or transiently bound to DNA with shorter dwell times, and a slow one corresponding to receptors bound more stably.

Our data showed that with an increasing concentration of Dox the overall mobility of RAR α increased. This is indicated by the detected reduction in the average recovery time of EGFP-RAR α (*Fig. 33A*). There was only a slight reduction detected in the binding of both the slow and fast components of EGFP-RAR α when Dox was applied at 1.25 μ M. At 4.5 μ M, the binding of EGFP-RAR α was reduced by almost 50%; the slow component decreased from \sim 4 s to \sim 2 s, while that of the fast component from 0.4 s to 0.25 s. A further 50% reduction was detected as the Dox concentration increased to 18 μ M; the recovery times of the slow component decreased further to 1.4 s, while that of the fast component to 0.2 s (*Fig. 33B & C*). At the same time, the mobile fraction decreased from 98-100% to \sim 93% (*Fig. 33D*).

The impact of RAR α specific agonist was also tested: 0.1 μ M AM580 was applied along with all the tested doxorubicin concentrations. AM580 ameliorated the Dox effect up to 4.5 μ M.

To conclude, doxorubicin treatment can affect the DNA binding of RAR α , and specific agonist treatment can ameliorate this effect. This could help design better treatment strategies, which could encounter some side effects caused by Dox in different tissues.

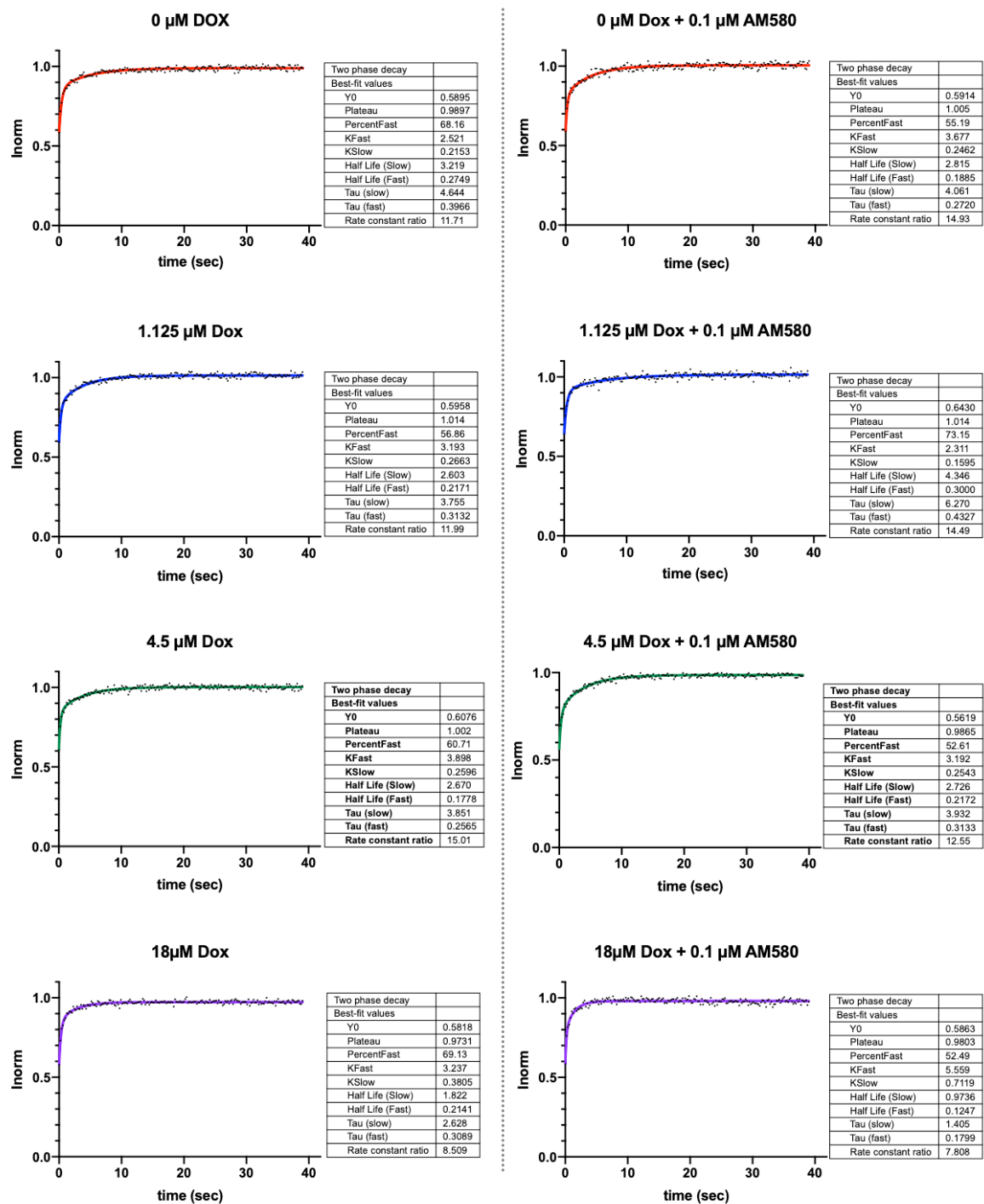


Figure 32. Representative two-component exponential fits of EGFP-RAR α normalized intensities
 EGFP-RAR α normalized intensities at different concentrations of Dox, (0, 1.125, 4.5, 18 μM) in the presence or absence of RAR specific agonist treatment, 0.1 μM AM580. Graphs and fits were created by using GraphPad Prism version 8.4.0.

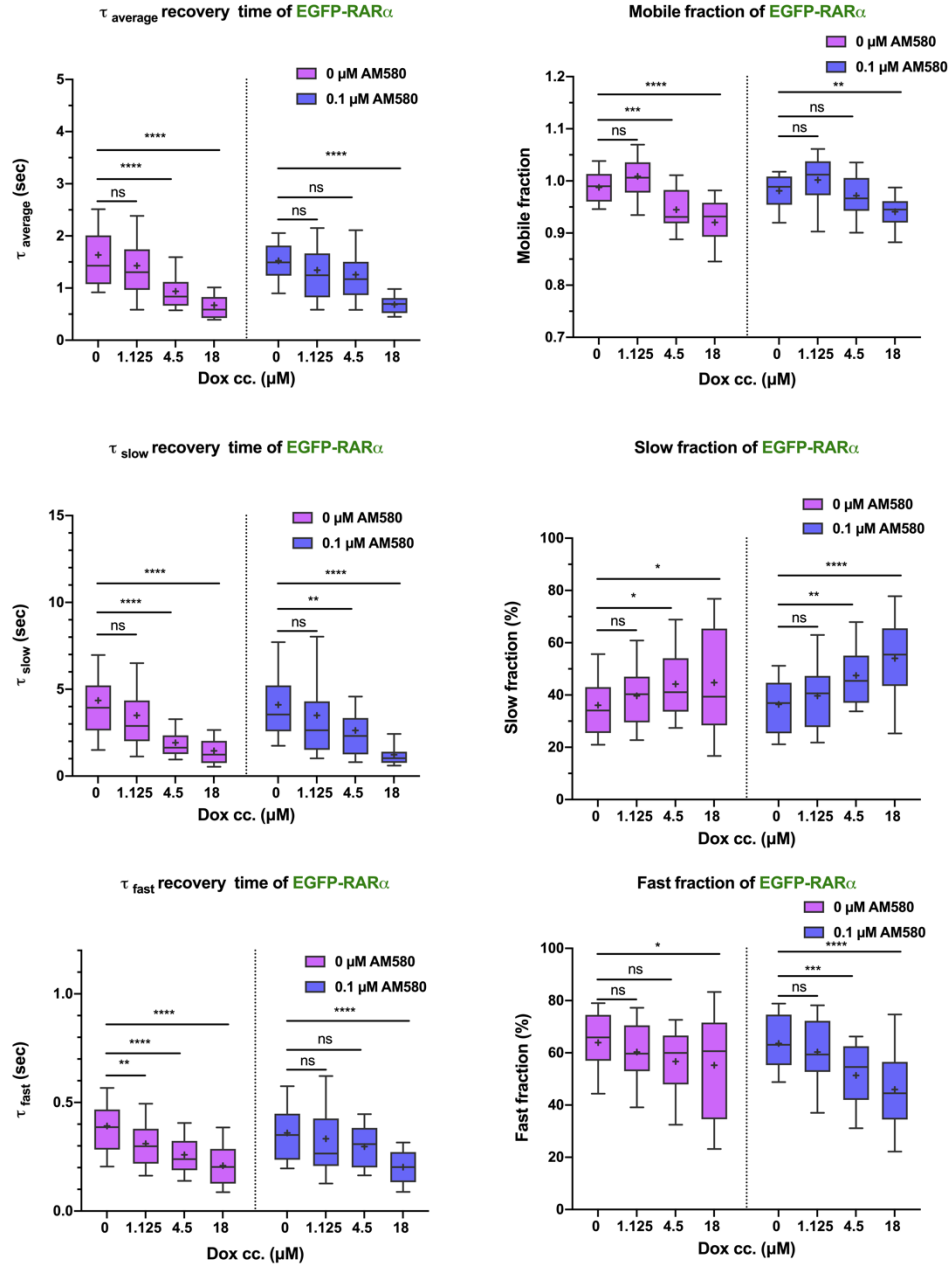


Figure 33. Doxorubicin (Dox) reduces RARα binding to DNA in vivo.

Strip FRAP recovery parameters of EGFP-RARα in cells treated with different concentrations of Dox (0, 1.125, 4.5, 18 μM) in the presence or absence of the RARα specific agonist, AM580 (0.1 μM). (a) Average recovery times. (b) Recovery times of the slow component. (c) Recovery times of the fast component. (d) Mobile fraction. (e) Percentage of the slow component. (f) Percentage of the fast component. Box-and-whiskers plots represent 10th, 25th, 50th, 75th, and 90th percentiles; +, mean value, two-way ANOVA with Tukey's multiple comparison test was used to calculate significance of changes **p* < 0.05, ***p* < 0.01, ****p* < 0.001, *****p* < 0.0001. Data were analyzed using GraphPad Prism 8.01.

5.5.2. Doxorubicin had no effect on EGFP dimer diffusion

Previous studies have shown that Dox can alter the overall chromatin structure through core histone eviction and histone aggregation^{156,157}. Such a change may affect the microviscosity of the nucleus and the rate of macromolecular diffusion. To assess if the reduced recovery times observed for EGFP-RAR α reflect reduced binding or increased diffusibility, we measured the effect of Dox on the diffusion of an inert protein having no known binding sites on the chromatin, the EGFP dimer. HeLa cells were transiently transfected with EGFP dimers and FRAP was applied to track the changes in EGFP dimer diffusion in the nucleus at the same conditions as described above. Recovery curves were fitted with a model having a single diffusion component *Fig. 34A*. As can be seen in *Fig. 34B*, Dox treatment had no impact on the recovery time of the EGFP dimer. To conclude, Dox treatment does not alter the microviscosity in the nucleus to an extent that would influence the diffusion of proteins of this size (EGFP dimer: ~54 kDa, EGFP-RAR α : 78 kDa). Thus, the reduced recovery time in the case of RAR α does indeed reflect reduced DNA-binding.

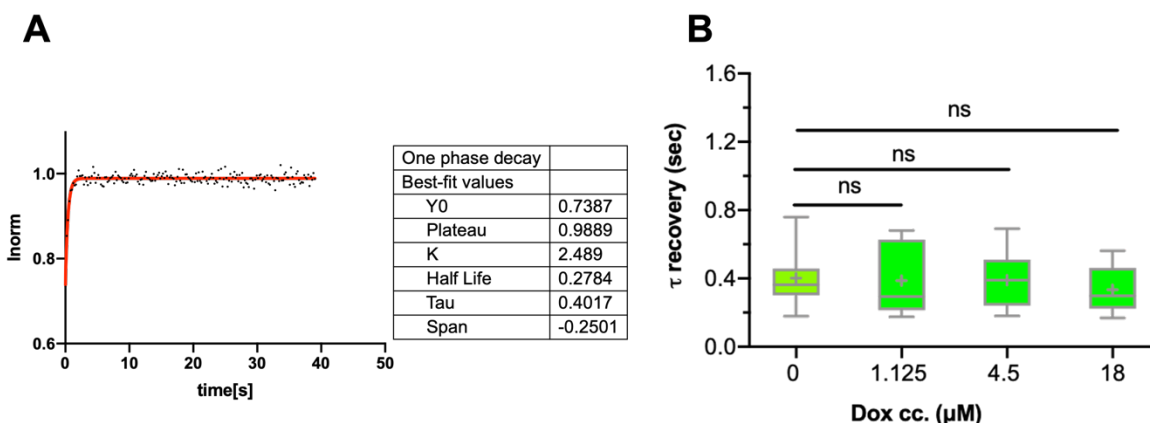


Figure 34. Nuclear mobility of EGFP dimer is unaffected by Dox treatment.

Recovery time of an inert protein, EGFP dimer as a control for FRAP experiments. **(A)** Representative one-component exponential decay fit of the normalized intensity of the EGFP dimer using GraphPad Prism version 8.4.0. **(B)** $\tau_{average}$ recovery times for the EGFP dimer at different concentrations of Dox (0, 1.125, 4.5, 18 μ M). Box-and-whiskers plots represent 10th, 25th, 50th, 75th, and 90th percentiles; +, mean value, one-way ANOVA with post hoc Dunnett's test was used to calculate significance of differences ($p < 0.05$ was considered significant).

6. DISCUSSION

Nuclear receptors are widely used targets for drug intervention in many diseases. However, in recent trials, unexpected side effects have been observed despite the high specificity of the drug-NR interaction.

Numerous fluorescence microscopy studies have analyzed the molecular mechanism of NR activation by observing protein-protein and protein-DNA interactions and dynamics¹⁵⁸⁻¹⁶⁵. Homodimerization of RXR-LBD is enhanced upon 9-cis-retinoic acid treatment as demonstrated by fluorescence fluctuation analysis¹²¹. Previously we have shown by fluorescence correlation spectroscopy that specific agonists increase chromatin binding of RAR α and RXR α in a coactivator dependent manner^{105,106}. We have shown by light sheet microscopy-based Förster resonance energy transfer and fluorescence cross-correlation measurements (SPIM-FRET-FCCS) that dimerization of RAR α and RXR α and chromatin binding of the dimer are enhanced upon agonist treatment¹¹².

Here we propose how activation of one NR pathway can interfere indirectly with other NR pathways through competition for their common heterodimeric partner RXR α and that competition is ligand dependent.

To study the interactions between NRs we applied a simple but robust assay; translocation assay applied in a three-color imaging model system.

We were able to show that there is a hierarchy in the affinities of NR partners toward RXR α , which is overridden by ligand binding. Our findings can help to explain the complex response observed in *in vivo* tests and may help design novel treatment strategies utilizing already FDA-approved drugs in an appropriate combination.

6.1. NLS1 mutants as a model system to study heterodimerization with RXR

The localization of NRs in the nucleus is mandatory for exerting their function as transcription factors; thus, their nuclear trafficking has been studied extensively. Like other nuclear proteins, nuclear localization of NRs is mediated through binding of carrier proteins called importins to the nuclear localization signal of the receptor¹⁶⁶, which is a specific sequence characterized by basic, positively charged amino acids. Changing these residues to uncharged, polar or non-polar amino acids abolishes receptor binding to importins and abrogates its nuclear accumulation^{167,168}. Based on our observations, we can conclude that mutation of the NLS1 of RXR partners increases their presence in the cytoplasm but retains their ability to heterodimerize with RXR and to bind their

ligands effectively. In line with our results, NLS mutants of Pregnane Xenobiotic Receptor (PXR) and Constitutive Androstane Receptor (CAR) also showed RXR-heterodimerization-dependent nuclear import¹¹¹. These findings allowed us to establish the NLS1 mutant receptors as a good model to detect the occurrence of heterodimerization with RXR by using a translocation assay.

6.2. Competition of NRs for their common partner, RXR α

In this work, we addressed the following questions *i)* whether RXR has different affinities to its heterodimerization partners in the absence of ligand and *ii)* if specific agonist treatment enhances these affinities. Our results demonstrated that in the absence of ligand, RXR α had the highest affinity toward RAR α , intermediate for PPAR γ and the lowest for VDR, whereas agonist treatment always tipped the scale in favor of the liganded partner. The dependency of RXR partner selection on the availability of the partner's specific agonist is consistent with the regulation of metabolism in which triggering a specific metabolic pathway is dictated by the availability of the endogenous substrates. E.g., LXR and PPAR α are involved in lipid metabolism (anabolism vs. catabolism, as illustrated in [Fig. 35](#)). These receptors serve as sensors for their endogenous ligands, free fatty acids (FFA) and oxysterol, respectively⁴³. In a fast state where energy production is needed, FFA accumulates in the liver reducing the expression of genes involved in fatty acid and cholesterol synthesis while activating genes promoting fatty acid catabolism. FFA increases the expression of PPAR α and evokes its transcriptional activity regulating genes involved in mitochondrial β -oxidation (FFA catabolism)^{169,170}. On the other hand, in a fed state, with a high-fat diet, the delivery of fatty acid to the liver is decreased and the oxysterol accumulates¹⁷¹. Oxysterol dependent activation of LXR eliminates the excess of cholesterol by increasing the expression of genes involved in bile acid synthesis, cholesterol absorption, transport and excretion¹⁷².

This example of regulation of metabolism by two NRs implies how the liver can avoid competition between two partners of RXR mediating two interacting signaling pathways by providing only one partner's ligand at a specific time.

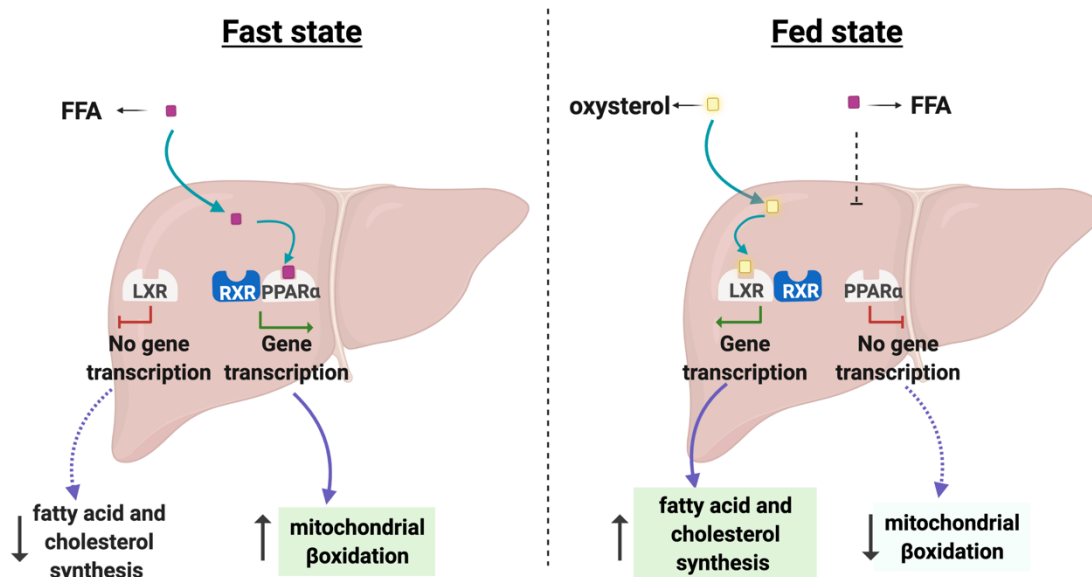


Figure 35. Schematic representation of fatty acid metabolism regulation mediated by two NRs.

(A) In fast state; catabolic pathway mediated by PPAR α . (B) In fed state; anabolic pathway mediated by LXR. Created with BioRender.com

In HEK293^{BFP-RXR α} cells, the originally nuclear localization of PPAR γ /*nls*m was dramatically reduced in the presence of RAR α , whereas RAR α /*nls*m maintained its nuclear localization even in the presence of either PPAR γ or VDR. Monopolization of RXR α by RAR α indicates competition between the two partners (due to the limiting amount of RXR α expressed by the stable cell line) with an outcome favoring RAR α . PPAR γ /*nls*m managed to maintain its nuclear localization in HEK293^{BFP-RXR α} cells co-transfected with VDR, besides, VDR was redistributed homogeneously implying a dominance of PPAR γ over VDR. The role of a potential endogenous ligand in this competition was excluded by applying a PPAR γ antagonist, GW9662, which had no impact on the distribution of the NRs. We also showed that if the RXR α pool is not limiting, competition between the heterodimerization partners is abolished; both NRs can bind to RXR α and become enriched in the nucleus. These experiments show a well-defined order of preference of RXR α for its heterodimerizing partners in the absence of agonist treatment, which is overridden by the effect of specific agonists. As illustrated in the schematic [Fig. 36](#), heterodimerization with RXR α of even

the strongest partner, RAR α /*nls*m, persisted only until its competing partners, PPAR γ or VDR, became liganded with their specific agonists, RSG or calcitriol.

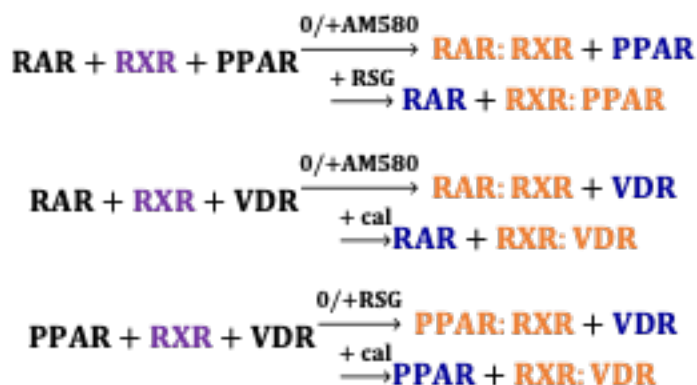


Figure 36. Summary of the results represented as chemical equations. Reactants, the two competing partners and RXR.

Products, weak partner shown in blue color, the dominant NR: RXR heterodimerization complex shown in orange color. “0”, without ligand treatment; AM580: RAR α specific agonist; RSG: rosiglitazone, PPAR γ specific agonist; cal: calcitriol, VDR specific agonist.

Previous studies showed that PPAR γ dominated the signaling pathway of both thyroid hormone receptor (TR) and VDR; it suppressed TR signaling in epiphyseal chondrocytes¹¹⁹ and it attenuated 1,25-Dihydroxyvitamin-D3-mediated transactivation of VDR¹¹⁸. In these studies, the dominance of one RXR partner over the other was abolished when RXR was overexpressed and became abundantly available for both partners simultaneously.

PPAR/RXR binding to the response element of PPAR was shown to be reduced in the presence of LXR α or β ¹⁷³. This might be the case in cells with a very large pool of sequestered RXR^{21,97,129}. Simandi, Z. *et al* have shown that retinoic acid treatment of undifferentiated mouse embryonic stem cells decreases both the expression of LXR target genes and RXR binding at LXR response elements, while inducing RXR redistribution to RAR target genes. This ligand induced switch in RXR preference from LXR to RAR is critical for proper cellular differentiation¹²².

There are other examples of ligand directed competition for a shared subunit between different protein complexes¹⁷⁴. Previously our group has also shown that interleukin-2 and -15 regulate the association of their membrane localized receptor chains in a similar mode. The β and γ_c chains of

their heterotrimeric receptors are used in common by the two cytokines, whereas the IL-2R α and IL-15R α chains are cytokine specific. The $\beta\gamma_c$ heterodimer forms a complex with the liganded receptor α chain¹⁷⁵.

6.3. Similarities and differences in the localization of NRs

Despite the similar positioning of the NLS1 of different NRs, the studied NLS-mutant NRs partitioned between the nucleus and the cytoplasm with different ratios and responded to RXR α heterodimerization with different changes in localization. PPAR γ /*nls*m and RAR α /*nls*m were distributed homogeneously in wt HEK293. Nuclear accumulation of PPAR γ /*nls*m and RAR α /*nls*m was observed in the presence of RXR α (in HEK293^{BFP-RXR α} cells). The translocation of NLS-mutant receptors into the nucleus can be explained by the piggy-back mechanism, which is mediated by protein-protein interaction with their shuttling partner RXR α . This mechanism was described previously for other NRs such as progesterone receptors¹⁵³.

Contrary to PPAR γ /*nls*m and RAR α /*nls*m, VDR/*nls*m was more cytoplasmic in wt HEK293 cells. In HEK293^{BFP-RXR α} , VDR/*nls*m not only failed to translocate into the nucleus, but it also induced a significant redistribution of RXR α . Translocation of RXR α to the cytoplasm implies that heterodimerization of RXR α with VDR/*nls*m may mask RXR's NLS1 and prevent its recognition by importins. Intriguingly, calcitriol treatment promoted the nuclear import of both VDR/*nls*m and RXR α in HEK293^{BFP-RXR α} . In accordance with these findings, when using RXR α /*nls*m, calcitriol evoked the nuclear enrichment of both VDR and RXR α /*nls*m, whereas both receptors were retained in the cytoplasm in the absence of calcitriol, similar to previous studies^{109,134}. Another study also suggested that the translocation of the VDR-RXR heterodimer into the nucleus is facilitated by the NLS of VDR¹⁷⁶. Heterodimerization of GFP-VDR and RXR-BFP in the cytoplasm has also been affirmed by FRET¹⁰⁹ and initiation of heterodimerization with RXR in the cytoplasm has been suggested for other NRs such as Xenobiotic Receptors PXR and CAR¹¹¹.

Because VDR/*nls*m did not translocate to the nucleus upon heterodimerization with RXR α in the absence of ligand, we did not rely on this mutant alone in the competition assay. Wt VDR matched our needs better; it was distributed between the nucleus and the cytoplasm evenly in wt HEK293 cells and translocated into the nucleus when treated with calcitriol. It accumulated in the nucleus of HEK293^{BFP-RXR α} cells and was further enriched there when treated with calcitriol. Thus, calcitriol increases the affinity of VDR to RXR α , which results in the accumulation of VDR in the

nucleus, in line with previous findings showing that RXR α inhibits VDR export^{109,134}. Calcitriol enhances the nuclear accumulation of VDR through increasing its affinity to importins¹⁷⁶. Nuclear enrichment of VDR/*nls*m after calcitriol treatment may be explained by the presence of a further, ligand responsive NLS in the hinge region between the DBD and the LBD^{177,178}. A similar NLS, located also in the hinge region, has been reported for other NRs like PR¹⁷⁹.

In competition experiments for dimerization with RXR α , the application of a single agonist (of NR1 or NR2) always shifted the balance toward the liganded NR. When ligands of NR1 and NR2 were both present, the outcome was different for the different pairs; RAR α dominated over PPAR γ when both NRs were liganded while in experiments involving wt VDR and another NR, both NRs were accumulated in the nucleus. In these cases, RAR α /*nls*m or PPAR γ /*nls*m probably relied on the NLS of RXR α using the piggy-back mechanism, whereas calcitriol treatment may have exposed an alternative NLS of VDR facilitating its binding to importins.

6.4. Ligand-induced chromatin binding of VDR and heterodimerization with RXR are correlated

Calcitriol treatment had a triple effect on VDR: *i*) it enhanced its nuclear localization along with *ii*) augmented heterodimerization with RXR α and *iii*) it increased its binding to its response elements; stronger to VDREs binding the heterodimer, and to a lesser extent to NR half-sites. This is in accordance with our previous finding that heterodimerization of RAR α and RXR α was also correlated with chromatin binding as measured by co-mobility¹¹².

The GBSs of VDR were primarily enhancers, where the motifs of the enhancer-specific transcription factors PU.1 and C/EBP were also enriched. On the other hand, the majority of GBSs not containing a VDRE or a half-site were localized in promoter regions and were enriched in the motif of the promoter specific YY1 transcription factor. In these regions, VDR binds indirectly. These latter GBSs became less occupied upon calcitriol treatment; thus, we can conclude that calcitriol induces a transition from promoters (and possibly from the non-DNA-bound pool of VDR) to enhancers. 507 genes were doubly assigned to an enhancer region (from the cluster of positively responding sites) as well as to a promoter region (from the negative responders) suggesting chromatin looping¹⁸⁰. A possible interpretation of the observed complex behavior is that calcitriol strengthens binding of VDR to enhancers and initiates transcription, causing the transcription machinery to move from the promoter toward the coding region of the regulated gene.

6.5. Doxorubicin effect on the DNA binding of RAR α

Doxorubicin is a widely applied anticancer drug in the course of treatment of several cancers; solid tumors and leukemias. Despite the efficacy of Dox in treating malignancies, its use has been challenged by several side effects, mainly cardiotoxicity¹⁸¹. Several studies have attributed doxorubicin induced cardiotoxicity (DIC) to topoisomerase poisoning and reactive oxygen species, ROS, production. Furthermore, the RAR ligand ATRA has been shown to induce binding of the receptor to the Top2 β promoter and down-regulate its expression levels¹⁸². ATRA also reduces ROS production through activation of the ERK2 signaling pathway¹³². These observations link Dox to RAR signaling and highlight the importance of studying the interactions between Dox and RAR.

Here we utilized FRAP to measure the mobility of EGFP-RAR α , at different concentrations of Dox and in the presence and absence of a saturating dose of AM580. Our strip-FRAP method reports on mobility on a distance scale of a few micrometres, averaged for larger areas.

First, it is important to clarify the parameters calculated in FRAP and their indications. The FRAP-detected fast and slow components refer to molecules that leave the few- μ m wide ROI during the time course of the measurement, thus, both are diffusible and even the slow component may only be transiently DNA-bound. Similar slow diffusion components were detected by other microscopic techniques for other DNA-binding proteins as well¹⁸³⁻¹⁸⁵.

Our most remarkable observation from FRAP data was the Dox-induced increase of average mobility of RAR α (*Fig. 33A*). This increase is due to shorter dwell times spent bound to DNA rather than to a change of microviscosity since the diffusion coefficient of the EGFP dimer was not affected (*Fig. 34*). On the other hand, Dox treatment slightly enhanced the immobile fraction and shifted the balance from the fast toward the slow population in a dose-dependent manner. Thus, Dox treatment may have a dual effect on the DNA-binding of RAR α : primarily, it weakens the interaction of a transiently bound population with the chromatin, while it strengthens the interaction of a smaller, more stably bound fraction.

Treatment with saturating concentrations (0.1 μ M) of AM580 partly counteracted the effect of Dox on the average mobility of RAR α : the reduction of the average FRAP recovery time was mitigated in the presence of the ligand up to 4.5 μ M Dox concentration, the order of magnitude of the therapeutic dose¹⁸⁶. At the same time, the median values of the slow fraction increased upon AM580 treatment (*Fig. 33E*), suggesting that Dox treatment did not fully impair ligand-induced

receptor dimerization and DNA-binding. However, it may decrease RAR signaling especially when the ligand is supplied at suboptimal levels, which may be a more realistic scenario *in vivo*. A possible interpretation of the effect of Dox on the DNA-binding of RAR is that monomeric RAR is competed off by Dox from HRE half-sites (single AGGTCA sequences), whereas RAR-RXR dimers, stabilized by ligand and binding to full HRE-s (AGGTCA direct repeats) with a higher affinity, resist this effect up to a higher Dox concentration. In other words, Dox may contribute to RAR signaling by shifting the balance between RXR-independent and -dependent binding. Form another point of view we can say that the reduction in DNA-binding of RAR may be due either to direct competition between Dox and RAR for the binding sites on the DNA or the drug's effect on other structural parameters of DNA. For example, Dox intercalation increases the stiffness of the DNA¹⁸⁷, which may hinder the deformability that is required for the proper binding of a nuclear receptor⁸⁶. This could differentially influence RAR α binding in the absence and presence of the ligand.

Taken all together we propose that *i*) Dox decreases the DNA-binding capacity of RAR α in general (as suggested by τ_{average} decrease) and *ii*) Dox reduces RAR binding to nonspecific sites and augments its binding at specific sites (suggested by the increase in both slow and immobile fraction despite the reduction in τ_{average} and by the partial counteracting impact of AM580 on the average mobility of RAR α induced by Dox when the latter was applied up to its therapeutic range. AM580 treatment is proven to enhance RXR-RAR heterodimerization and binding of the heterodimer complex to DNA^{104,105,112}.

In light of our results, we can understand the efficacy of the proposed cotreatment strategies (ATRA and doxorubicin)^{132,133} as ATRA treatment will preserve the DNA binding of RAR and maintain its transcriptional activities. More studies are needed to investigate the effect of doxorubicin on other NRs and to help reduce its side effects.

Summary

Tracing the dynamic distribution pattern of EGFP-VDR, EGFP-PPAR γ /nlsm and EGFP-RAR α /nlsm (homogeneous in the absence of RXR α and nuclear-enriched in response to RXR α binding) serves as a good model system for studying their competition for heterodimerization with RXR α . There is indeed dynamic competition between RXR partners, which is governed by two mechanisms. First, in the absence of agonist treatment, there is a hierarchy of affinities between RXR α and its partners in the following order: RAR α > PPAR γ > VDR. Second, in the presence of agonist treatment, RXR α partner selection is shifted towards the liganded partner.

Our results also show that RXR-NR heterodimerization and direct DNA binding are correlated events, and both are augmented by agonist treatment.

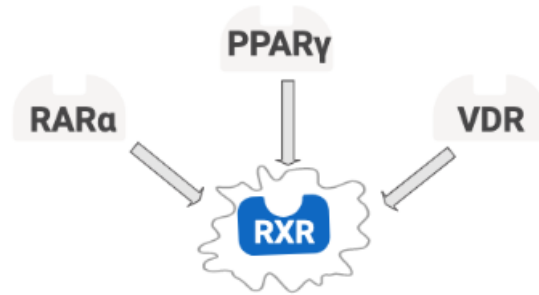
These results may explain certain side effects of drugs targeting NRs. Competition for RXR could be responsible for the symptoms of vitamin D deficiency developed in a child upon receiving systemic retinoid treatment for ichthyosis¹⁸⁸, or the antagonistic effect of co-administered vitamin A on serum calcium response to vitamin D treatment¹⁸⁹.

Our observations regarding these three RXR partners, consistently with metabolism regulation by two other RXR partners (LXR and PPAR α) and similar previous findings on membrane-localized IL-2/15 receptors encourage us to generalize the concept that specific ligand binding may often govern competition between different partners of a promiscuous receptor.

Our findings are a proof-of-concept of a hierarchy of affinities between NRs and their common partner, RXR α . These studies can be extended to a larger number of receptors to uncover the network of hierarchies, and follow-up studies will also be focusing on testing this concept in a broader and physiological context.

It is worth to mention that our or similar studies may have some limitations: i) we cannot entirely exclude the presence of endogenous ligands for the receptors; and ii) our approach may not mimic all possible physiological conditions; iii) as for the limiting nature of RXR, antibody-based approaches are at best semiquantitative to determine endogenous NR concentrations; iv) finally, we used indirect measures to assess downstream gene expression events.

RXR partners compete for heterodimerization with RXR.



Two mechanisms are governing RXR partners selection:

i) In the absence of ligand treatment: ii) Upon specific agonist treatment (■):



RXR-NR heterodimerization and site-specific DNA binding are correlated events, and both are augmented by specific agonist treatment.

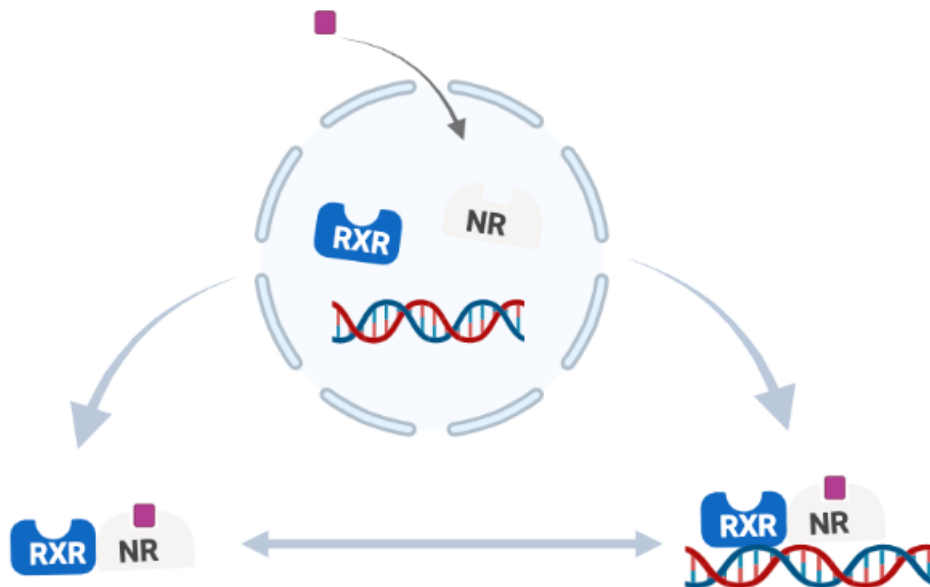


Figure 37. Schematic representation of the study results.

Possible biological consequences of the competition between NRs for a limiting pool of RXR.

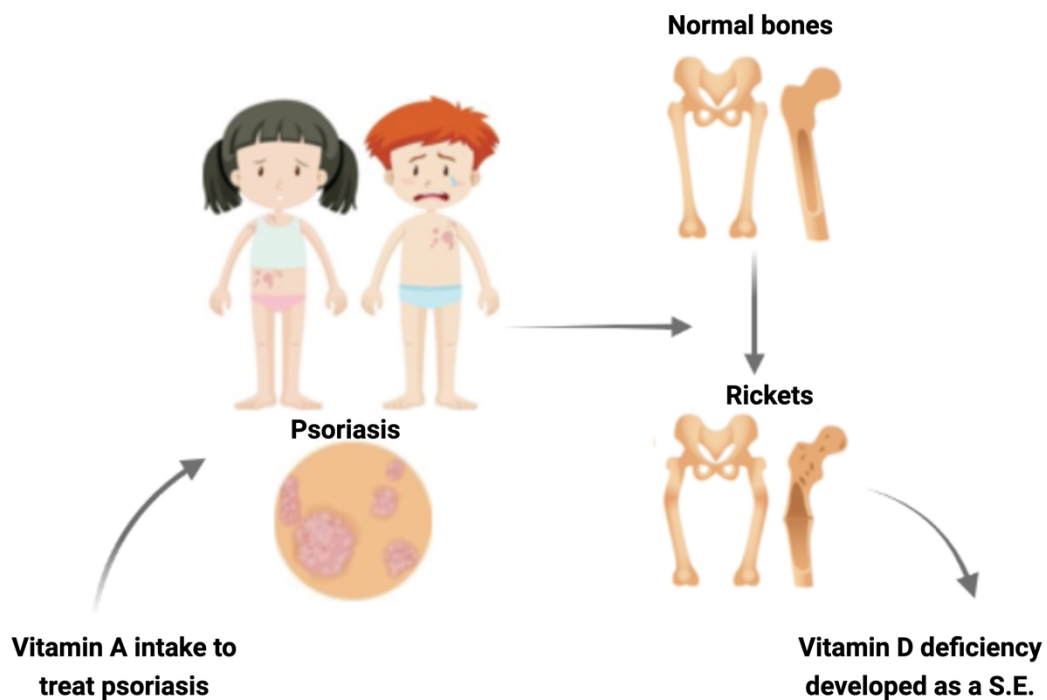
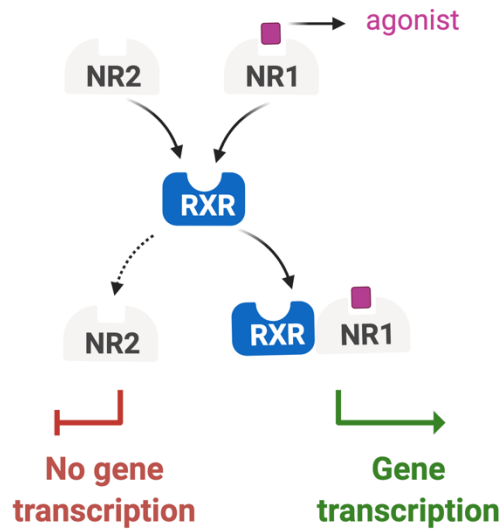


Figure 38. Schematic representation of the clinical or biological consequences of our results.

REFERENCES

- 1 Mazaira, G. I. *et al.* The Nuclear Receptor Field: A Historical Overview and Future Challenges. *Nucl Receptor Res* **5**, doi:10.11131/2018/101320 (2018).
- 2 Marrian, G. F. The chemistry of oestrin: Methods of purification. *Biochem J* **23**, 1233-1241, doi:10.1042/bj0231233 (1929).
- 3 Jensen, E. V. On the mechanism of estrogen action. *Perspect Biol Med* **6**, 47-59, doi:10.1353/pbm.1963.0005 (1962).
- 4 Hollenberg, S. M. *et al.* Primary structure and expression of a functional human glucocorticoid receptor cDNA. *Nature* **318**, 635-641, doi:10.1038/318635a0 (1985).
- 5 Green, S. *et al.* Human oestrogen receptor cDNA: sequence, expression and homology to v-erb-A. *Nature* **320**, 134-139, doi:10.1038/320134a0 (1986).
- 6 Misrahi, M. *et al.* Complete amino acid sequence of the human progesterone receptor deduced from cloned cDNA. *Biochem Biophys Res Commun* **143**, 740-748, doi:10.1016/0006-291x(87)91416-1 (1987).
- 7 Arriza, J. L. *et al.* Cloning of human mineralocorticoid receptor complementary DNA: structural and functional kinship with the glucocorticoid receptor. *Science* **237**, 268-275, doi:10.1126/science.3037703 (1987).
- 8 Chang, C. S., Kokontis, J. & Liao, S. T. Molecular cloning of human and rat complementary DNA encoding androgen receptors. *Science* **240**, 324-326, doi:10.1126/science.3353726 (1988).
- 9 Giguere, V., Yang, N., Segui, P. & Evans, R. M. Identification of a new class of steroid hormone receptors. *Nature* **331**, 91-94, doi:10.1038/331091a0 (1988).
- 10 Miyajima, N. *et al.* Identification of two novel members of erbA superfamily by molecular cloning: the gene products of the two are highly related to each other. *Nucleic Acids Res* **16**, 11057-11074, doi:10.1093/nar/16.23.11057 (1988).
- 11 Weinberger, C. *et al.* The c-erb-A gene encodes a thyroid hormone receptor. *Nature* **324**, 641-646, doi:10.1038/324641a0 (1986).
- 12 McDonnell, D. P., Mangelsdorf, D. J., Pike, J. W., Haussler, M. R. & O'Malley, B. W. Molecular cloning of complementary DNA encoding the avian receptor for vitamin D. *Science* **235**, 1214-1217, doi:10.1126/science.3029866 (1987).

- 13 Giguere, V., Ong, E. S., Segui, P. & Evans, R. M. Identification of a receptor for the morphogen retinoic acid. *Nature* **330**, 624-629, doi:10.1038/330624a0 (1987).
- 14 Evans, R. M. The steroid and thyroid hormone receptor superfamily. *Science* **240**, 889-895, doi:10.1126/science.3283939 (1988).
- 15 Mangelsdorf, D. J., Ong, E. S., Dyck, J. A. & Evans, R. M. Nuclear receptor that identifies a novel retinoic acid response pathway. *Nature* **345**, 224-229, doi:10.1038/345224a0 (1990).
- 16 Heyman, R. A. *et al.* 9-cis retinoic acid is a high affinity ligand for the retinoid X receptor. *Cell* **68**, 397-406, doi:10.1016/0092-8674(92)90479-v (1992).
- 17 Issemann, I. & Green, S. Activation of a member of the steroid hormone receptor superfamily by peroxisome proliferators. *Nature* **347**, 645-650, doi:10.1038/347645a0 (1990).
- 18 Dreyer, C. *et al.* Control of the peroxisomal beta-oxidation pathway by a novel family of nuclear hormone receptors. *Cell* **68**, 879-887, doi:10.1016/0092-8674(92)90031-7 (1992).
- 19 Keller, H. *et al.* Fatty acids and retinoids control lipid metabolism through activation of peroxisome proliferator-activated receptor-retinoid X receptor heterodimers. *Proc Natl Acad Sci U S A* **90**, 2160-2164, doi:10.1073/pnas.90.6.2160 (1993).
- 20 Evans, R. M. & Mangelsdorf, D. J. Nuclear Receptors, RXR, and the Big Bang. *Cell* **157**, 255-266, doi:10.1016/j.cell.2014.03.012 (2014).
- 21 Chan, L. S. & Wells, R. A. Cross-Talk between PPARs and the Partners of RXR: A Molecular Perspective. *PPAR Res* **2009**, 925309, doi:10.1155/2009/925309 (2009).
- 22 Baes, M. *et al.* A new orphan member of the nuclear hormone receptor superfamily that interacts with a subset of retinoic acid response elements. *Mol Cell Biol* **14**, 1544-1552, doi:10.1128/mcb.14.3.1544 (1994).
- 23 Bertilsson, G. *et al.* Identification of a human nuclear receptor defines a new signaling pathway for CYP3A induction. *Proc Natl Acad Sci U S A* **95**, 12208-12213, doi:10.1073/pnas.95.21.12208 (1998).
- 24 Blumberg, B. *et al.* SXR, a novel steroid and xenobiotic-sensing nuclear receptor. *Genes Dev* **12**, 3195-3205, doi:10.1101/gad.12.20.3195 (1998).
- 25 Kliewer, S. A. *et al.* An orphan nuclear receptor activated by pregnanes defines a novel steroid signaling pathway. *Cell* **92**, 73-82, doi:10.1016/s0092-8674(00)80900-9 (1998).

- 26 Lehmann, J. M. *et al.* The human orphan nuclear receptor PXR is activated by compounds that regulate CYP3A4 gene expression and cause drug interactions. *J Clin Invest* **102**, 1016-1023, doi:10.1172/JCI3703 (1998).
- 27 Willson, T. M. & Kliewer, S. A. PXR, CAR and drug metabolism. *Nat Rev Drug Discov* **1**, 259-266, doi:10.1038/nrd753 (2002).
- 28 Seol, W., Choi, H. S. & Moore, D. D. An orphan nuclear hormone receptor that lacks a DNA binding domain and heterodimerizes with other receptors. *Science* **272**, 1336-1339, doi:10.1126/science.272.5266.1336 (1996).
- 29 Janowski, B. A., Willy, P. J., Devi, T. R., Falck, J. R. & Mangelsdorf, D. J. An oxysterol signalling pathway mediated by the nuclear receptor LXR alpha. *Nature* **383**, 728-731, doi:10.1038/383728a0 (1996).
- 30 Wang, H., Chen, J., Hollister, K., Sowers, L. C. & Forman, B. M. Endogenous bile acids are ligands for the nuclear receptor FXR/BAR. *Mol Cell* **3**, 543-553, doi:10.1016/s1097-2765(00)80348-2 (1999).
- 31 Raghuram, S. *et al.* Identification of heme as the ligand for the orphan nuclear receptors REV-ERBalpha and REV-ERBbeta. *Nat Struct Mol Biol* **14**, 1207-1213, doi:10.1038/nsmb1344 (2007).
- 32 Iyer, A. K. & McCabe, E. R. Molecular mechanisms of DAX1 action. *Mol Genet Metab* **83**, 60-73, doi:10.1016/j.ymgme.2004.07.018 (2004).
- 33 Zhang, Y., Hagedorn, C. H. & Wang, L. Role of nuclear receptor SHP in metabolism and cancer. *Biochim Biophys Acta* **1812**, 893-908, doi:10.1016/j.bbadis.2010.10.006 (2011).
- 34 Stepien, B. K. & Huttner, W. B. Transport, Metabolism, and Function of Thyroid Hormones in the Developing Mammalian Brain. *Front Endocrinol (Lausanne)* **10**, 209, doi:10.3389/fendo.2019.00209 (2019).
- 35 Gauthier, K. *et al.* Different functions for the thyroid hormone receptors TRalpha and TRbeta in the control of thyroid hormone production and post-natal development. *EMBO J* **18**, 623-631, doi:10.1093/emboj/18.3.623 (1999).
- 36 Pagnin, M. *et al.* Role of thyroid hormones in normal and abnormal central nervous system myelination in humans and rodents. *Front Neuroendocrinol* **61**, 100901, doi:10.1016/j.yfrne.2021.100901 (2021).

- 37 Li, M. *et al.* Thyroid hormone action in postnatal heart development. *Stem Cell Res* **13**, 582-591, doi:10.1016/j.scr.2014.07.001 (2014).
- 38 Mey, J. in *Gene Regulation, Epigenetics and Hormone Signaling* 457-510, <https://doi.org/10.1002/9783527697274.ch16>, (2017).
- 39 Oliveira, L. M., Teixeira, F. M. E. & Sato, M. N. Impact of Retinoic Acid on Immune Cells and Inflammatory Diseases. *Mediators Inflamm* **2018**, 3067126, doi:10.1155/2018/3067126 (2018).
- 40 Li, B., Cai, S.-Y. & Boyer, J. L. The role of the retinoid receptor, RAR/RXR heterodimer, in liver physiology. *Biochimica et Biophysica Acta (BBA) - Molecular Basis of Disease* **1867**, 166085, doi:<https://doi.org/10.1016/j.bbadis.2021.166085> (2021).
- 41 Thompson, B. *et al.* Genetics and functions of the retinoic acid pathway, with special emphasis on the eye. *Hum Genomics* **13**, 61, doi:10.1186/s40246-019-0248-9 (2019).
- 42 Wang, Y. D., Chen, W. D., Moore, D. D. & Huang, W. FXR: a metabolic regulator and cell protector. *Cell Res* **18**, 1087-1095, doi:10.1038/cr.2008.289 (2008).
- 43 Alaynick, W. A. Nuclear receptors, mitochondria and lipid metabolism. *Mitochondrion* **8**, 329-337, doi:10.1016/j.mito.2008.02.001 (2008).
- 44 Millatt, L. J., Bocher, V., Fruchart, J. C. & Staels, B. Liver X receptors and the control of cholesterol homeostasis: potential therapeutic targets for the treatment of atherosclerosis. *Biochim Biophys Acta* **1631**, 107-118, doi:10.1016/s1388-1981(02)00366-9 (2003).
- 45 Krey, G. *et al.* Xenopus peroxisome proliferator activated receptors: genomic organization, response element recognition, heterodimer formation with retinoid X receptor and activation by fatty acids. *J Steroid Biochem Mol Biol* **47**, 65-73, doi:10.1016/0960-0760(93)90058-5 (1993).
- 46 Kojetin, D. J. & Burris, T. P. REV-ERB and ROR nuclear receptors as drug targets. *Nat Rev Drug Discov* **13**, 197-216, doi:10.1038/nrd4100 (2014).
- 47 Khammissa, R. A. G. *et al.* The Biological Activities of Vitamin D and Its Receptor in Relation to Calcium and Bone Homeostasis, Cancer, Immune and Cardiovascular Systems, Skin Biology, and Oral Health. *Biomed Res Int* **2018**, 9276380, doi:10.1155/2018/9276380 (2018).

- 48 Pike, J. W., Meyer, M. B., Lee, S. M., Onal, M. & Benkusky, N. A. The vitamin D receptor: contemporary genomic approaches reveal new basic and translational insights. *J Clin Invest* **127**, 1146-1154, doi:10.1172/JCI88887 (2017).
- 49 Yan, J., Chen, B., Lu, J. & Xie, W. Deciphering the roles of the constitutive androstane receptor in energy metabolism. *Acta Pharmacol Sin* **36**, 62-70, doi:10.1038/aps.2014.102 (2015).
- 50 Oladimeji, P. O. & Chen, T. PXR: More Than Just a Master Xenobiotic Receptor. *Mol Pharmacol* **93**, 119-127, doi:10.1124/mol.117.110155 (2018).
- 51 Walesky, C. & Apte, U. Role of hepatocyte nuclear factor 4alpha (HNF4alpha) in cell proliferation and cancer. *Gene Expr* **16**, 101-108, doi:10.3727/105221615X14181438356292 (2015).
- 52 Szanto, A. *et al.* Retinoid X receptors: X-ploring their (patho)physiological functions. *Cell Death Differ* **11 Suppl 2**, S126-143, doi:10.1038/sj.cdd.4401533 (2004).
- 53 Lin, S. J. *et al.* TR2 and TR4 Orphan Nuclear Receptors: An Overview. *Curr Top Dev Biol* **125**, 357-373, doi:10.1016/bs.ctdb.2017.02.002 (2017).
- 54 Benod, C. *et al.* The human orphan nuclear receptor tailless (TLX, NR2E1) is druggable. *PLoS One* **9**, e99440, doi:10.1371/journal.pone.0099440 (2014).
- 55 Connor, B. & Lee, Y.-S. Endogenous Ligand for Orphan Nuclear Receptor NR2E3 Forms a Light-Sensitive Retinal Transcription System. *The FASEB Journal* **31**, 616.615-616.615, doi:https://doi.org/10.1096/fasebj.31.1_supplement.616.5 (2017).
- 56 Wen, Z. *et al.* Orphan nuclear receptor PNR/NR2E3 stimulates p53 functions by enhancing p53 acetylation. *Mol Cell Biol* **32**, 26-35, doi:10.1128/MCB.05513-11 (2012).
- 57 Ktistaki, E. & Talianidis, I. Chicken ovalbumin upstream promoter transcription factors act as auxiliary cofactors for hepatocyte nuclear factor 4 and enhance hepatic gene expression. *Mol Cell Biol* **17**, 2790-2797, doi:10.1128/MCB.17.5.2790 (1997).
- 58 Polvani, S., Pepe, S., Milani, S. & Galli, A. COUP-TFII in Health and Disease. *Cells* **9**, doi:10.3390/cells9010101 (2019).
- 59 Timmermans, S., Souffriau, J. & Libert, C. A General Introduction to Glucocorticoid Biology. *Front Immunol* **10**, 1545, doi:10.3389/fimmu.2019.01545 (2019).

- 60 Lee, H. R., Kim, T. H. & Choi, K. C. Functions and physiological roles of two types of estrogen receptors, ERalpha and ERbeta, identified by estrogen receptor knockout mouse. *Lab Anim Res* **28**, 71-76, doi:10.5625/lar.2012.28.2.71 (2012).
- 61 Graham, J. D. & Clarke, C. L. Physiological action of progesterone in target tissues. *Endocr Rev* **18**, 502-519, doi:10.1210/edrv.18.4.0308 (1997).
- 62 Cable, J. K. & Grider, M. H. in *StatPearls*, doi: <http://dx.doi.org/10.20473/ovz.v10i2.2021.53-58> (2021).
- 63 Davey, R. A. & Grossmann, M. Androgen Receptor Structure, Function and Biology: From Bench to Bedside. *Clin Biochem Rev* **37**, 3-15 (2016).
- 64 Ong, G. S. & Young, M. J. Mineralocorticoid regulation of cell function: the role of rapid signalling and gene transcription pathways. *J Mol Endocrinol* **58**, R33-R57, doi:10.1530/JME-15-0318 (2017).
- 65 Casaburi, I. *et al.* Cholesterol as an Endogenous ERRalpha Agonist: A New Perspective to Cancer Treatment. *Front Endocrinol (Lausanne)* **9**, 525, doi:10.3389/fendo.2018.00525 (2018).
- 66 Tripathi, M., Yen, P. M. & Singh, B. K. Estrogen-Related Receptor Alpha: An Under-Appreciated Potential Target for the Treatment of Metabolic Diseases. *Int J Mol Sci* **21**, doi:10.3390/ijms21051645 (2020).
- 67 Xia, H., Dufour, C. R. & Giguère, V. ERRα as a Bridge Between Transcription and Function: Role in Liver Metabolism and Disease. *Frontiers in Endocrinology* **10**, doi:10.3389/fendo.2019.00206 (2019).
- 68 Bonta, P. I. *et al.* Nuclear receptors Nur77, Nurr1, and NOR-1 expressed in atherosclerotic lesion macrophages reduce lipid loading and inflammatory responses. *Arterioscler Thromb Vasc Biol* **26**, 2288-2294, doi:10.1161/01.ATV.0000238346.84458.5d (2006).
- 69 Popichak, K. A. *et al.* Compensatory Expression of Nur77 and Nurr1 Regulates NF-kappaB-Dependent Inflammatory Signaling in Astrocytes. *Mol Pharmacol* **94**, 1174-1186, doi:10.1124/mol.118.112631 (2018).
- 70 Weikum, E. R., Liu, X. & Ortlund, E. A. The nuclear receptor superfamily: A structural perspective. *Protein Sci* **27**, 1876-1892, doi:10.1002/pro.3496 (2018).
- 71 Crowder, M. K., Seacrist, C. D. & Blind, R. D. Phospholipid regulation of the nuclear receptor superfamily. *Adv Biol Regul* **63**, 6-14, doi:10.1016/j.jbior.2016.10.006 (2017).

- 72 Phan, T. S., Merk, V. M. & Brunner, T. Extra-adrenal glucocorticoid synthesis at epithelial barriers. *Genes Immun* **20**, 627-640, doi:10.1038/s41435-019-0058-z (2019).
- 73 Nadolny, C. & Dong, X. Liver receptor homolog-1 (LRH-1): a potential therapeutic target for cancer. *Cancer Biol Ther* **16**, 997-1004, doi:10.1080/15384047.2015.1045693 (2015).
- 74 Chand, A. L., Herridge, K. A., Thompson, E. W. & Clyne, C. D. The orphan nuclear receptor LRH-1 promotes breast cancer motility and invasion. *Endocr Relat Cancer* **17**, 965-975, doi:10.1677/ERC-10-0179 (2010).
- 75 Miki, Y. *et al.* Immunolocalization of liver receptor homologue-1 (LRH-1) in human breast carcinoma: possible regulator of insitu steroidogenesis. *Cancer Lett* **244**, 24-33, doi:10.1016/j.canlet.2005.11.038 (2006).
- 76 Clyne, C. D., Speed, C. J., Zhou, J. & Simpson, E. R. Liver receptor homologue-1 (LRH-1) regulates expression of aromatase in preadipocytes. *J Biol Chem* **277**, 20591-20597, doi:10.1074/jbc.M201117200 (2002).
- 77 Thiruchelvam, P. T. *et al.* The liver receptor homolog-1 regulates estrogen receptor expression in breast cancer cells. *Breast Cancer Res Treat* **127**, 385-396, doi:10.1007/s10549-010-0994-9 (2011).
- 78 Hummelke, G. C. & Cooney, A. J. Germ cell nuclear factor is a transcriptional repressor essential for embryonic development. *Front Biosci* **6**, D1186-1191, doi:10.2741/hummelke (2001).
- 79 Mangelsdorf, D. J. *et al.* The nuclear receptor superfamily: the second decade. *Cell* **83**, 835-839, doi: 10.1016/0092-8674(95)90199-x, (1995).
- 80 Porter, B. A., Ortiz, M. A., Bratslavsky, G. & Kotula, L. Structure and Function of the Nuclear Receptor Superfamily and Current Targeted Therapies of Prostate Cancer. *Cancers (Basel)* **11**, doi:10.3390/cancers11121852 (2019).
- 81 Olefsky, J. M. Nuclear receptor minireview series. *J Biol Chem* **276**, 36863-36864, doi:10.1074/jbc.R100047200 (2001).
- 82 Pawlak, M., Lefebvre, P. & Staels, B. General molecular biology and architecture of nuclear receptors. *Curr Top Med Chem* **12**, 486-504, doi: 10.2174/156802612799436641 (2012).
- 83 Dawson, M. I. & Xia, Z. The retinoid X receptors and their ligands. *Biochim Biophys Acta* **1821**, 21-56, doi:10.1016/j.bbali.2011.09.014 (2012).

- 84 Anbalagan, M., Huderson, B., Murphy, L. & Rowan, B. G. Post-translational modifications of nuclear receptors and human disease. *Nucl Recept Signal* **10**, e001, doi:10.1621/nrs.10001 (2012).
- 85 Vivat-Hannah, V., Bourguet, W., Gottardis, M. & Gronemeyer, H. Separation of retinoid X receptor homo- and heterodimerization functions. *Mol Cell Biol* **23**, 7678-7688, doi: 10.1128/MCB.23.21.7678-7688.2003 (2003).
- 86 Rastinejad, F., Wagner, T., Zhao, Q. & Khorasanizadeh, S. Structure of the RXR-RAR DNA-binding complex on the retinoic acid response element DR1. *EMBO J* **19**, 1045-1054, doi:10.1093/emboj/19.5.1045 (2000).
- 87 Khorasanizadeh, S. & Rastinejad, F. Nuclear-receptor interactions on DNA-response elements. *Trends Biochem Sci* **26**, 384-390, doi: 10.1016/s0968-0004(01)01800-x (2001).
- 88 Chatagnon, A. *et al.* RAR/RXR binding dynamics distinguish pluripotency from differentiation associated cis-regulatory elements. *Nucleic Acids Res* **43**, 4833-4854, doi:10.1093/nar/gkv370 (2015).
- 89 Huang, P., Chandra, V. & Rastinejad, F. Structural overview of the nuclear receptor superfamily: insights into physiology and therapeutics. *Annu Rev Physiol* **72**, 247-272, doi:10.1146/annurev-physiol-021909-135917 (2010).
- 90 Merkulov, V. M., Klimova, N. V. & Merkulova, T. I. Glucocorticoid receptor: Translocation from the cytoplasm to the nuclei; chromatin and intranuclear chaperone cycles. *Russian Journal of Genetics: Applied Research* **6**, 297-306, doi:10.1134/S2079059716030096 (2016).
- 91 Galigniana, M. D. Steroid receptor coupling becomes nuclear. *Chem Biol* **19**, 662-663, doi:10.1016/j.chembiol.2012.06.001 (2012).
- 92 Galigniana, M. D., Erlejman, A. G., Monte, M., Gomez-Sanchez, C. & Piwien-Pilipuk, G. The hsp90-FKBP52 complex links the mineralocorticoid receptor to motor proteins and persists bound to the receptor in early nuclear events. *Mol Cell Biol* **30**, 1285-1298, doi:10.1128/MCB.01190-09 (2010).
- 93 Echeverria, P. C. *et al.* Nuclear import of the glucocorticoid receptor-hsp90 complex through the nuclear pore complex is mediated by its interaction with Nup62 and importin beta. *Mol Cell Biol* **29**, 4788-4797, doi:10.1128/MCB.00649-09 (2009).

- 94 Gallo, L. I., Ghini, A. A., Piwien Pilipuk, G. & Galigniana, M. D. Differential recruitment of tetratricopeptide repeat domain immunophilins to the mineralocorticoid receptor influences both heat-shock protein 90-dependent retrotransport and hormone-dependent transcriptional activity. *Biochemistry* **46**, 14044-14057, doi:10.1021/bi701372c (2007).
- 95 Pratt, W. B., Galigniana, M. D., Harrell, J. M. & DeFranco, D. B. Role of hsp90 and the hsp90-binding immunophilins in signalling protein movement. *Cell Signal* **16**, 857-872, doi:10.1016/j.cellsig.2004.02.004 (2004).
- 96 Pratt, W. B., Galigniana, M. D., Morishima, Y. & Murphy, P. J. Role of molecular chaperones in steroid receptor action. *Essays Biochem* **40**, 41-58, doi:10.1042/bse0400041 (2004).
- 97 Dong, D. & Noy, N. Heterodimer formation by retinoid X receptor: regulation by ligands and by the receptor's self-association properties. *Biochemistry* **37**, 10691-10700, doi:10.1021/bi980561r (1998).
- 98 Nagy, L. & Schwabe, J. W. Mechanism of the nuclear receptor molecular switch. *Trends in biochemical sciences* **29**, 317-324, doi: doi: 10.1016/j.tibs.2004.04.006, (2004).
- 99 Egea, P. F., Mitschler, A. & Moras, D. Molecular recognition of agonist ligands by RXRs. *Mol Endocrinol* **16**, 987-997, doi:10.1210/mend.16.5.0823 (2002).
- 100 Pissios, P., Tzameli, I., Kushner, P. & Moore, D. D. Dynamic stabilization of nuclear receptor ligand binding domains by hormone or corepressor binding. *Mol Cell* **6**, 245-253, doi:10.1016/s1097-2765(00)00026-5 (2000).
- 101 Kallenberger, B. C., Love, J. D., Chatterjee, V. K. & Schwabe, J. W. A dynamic mechanism of nuclear receptor activation and its perturbation in a human disease. *Nat Struct Biol* **10**, 136-140, doi:10.1038/nsb892 (2003).
- 102 Johnson, B. A. *et al.* Ligand-induced stabilization of PPARgamma monitored by NMR spectroscopy: implications for nuclear receptor activation. *J Mol Biol* **298**, 187-194, doi:10.1006/jmbi.2000.3636 (2000).
- 103 Bulynko, Y. A. & O'Malley, B. W. Nuclear receptor coactivators: structural and functional biochemistry. *Biochemistry* **50**, 313-328, doi:10.1021/bi101762x (2011).
- 104 Fadel, L. *et al.* Agonist binding directs dynamic competition among nuclear receptors for heterodimerization with retinoid X receptor. *J Biol Chem* **295**, 10045-10061, doi:10.1074/jbc.RA119.011614 (2020).

- 105 Brazda, P. *et al.* Live-cell fluorescence correlation spectroscopy dissects the role of coregulator exchange and chromatin binding in retinoic acid receptor mobility. *J Cell Sci* **124**, 3631-3642, doi:10.1242/jcs.086082 (2011).
- 106 Brazda, P. *et al.* Ligand binding shifts highly mobile retinoid X receptor to the chromatin-bound state in a coactivator-dependent manner, as revealed by single-cell imaging. *Molecular and cellular biology* **34**, 1234-1245, doi:10.1128/MCB.01097-13 (2014).
- 107 Varala, K., Li, Y., Marshall-Colon, A., Para, A. & Coruzzi, G. M. "Hit-and-Run" leaves its mark: catalyst transcription factors and chromatin modification. *Bioessays* **37**, 851-856, doi:10.1002/bies.201400205 (2015).
- 108 Schaffner, W. Gene regulation. A hit-and-run mechanism for transcriptional activation? *Nature* **336**, 427-428, doi:10.1038/336427a0 (1988).
- 109 Prufer, K., Racz, A., Lin, G. C. & Barsony, J. Dimerization with retinoid X receptors promotes nuclear localization and subnuclear targeting of vitamin D receptors. *J Biol Chem* **275**, 41114-41123, doi:10.1074/jbc.M003791200 (2000).
- 110 Cao, X. *et al.* Retinoid X receptor regulates Nur77/TR3-dependent apoptosis [corrected] by modulating its nuclear export and mitochondrial targeting. *Mol Cell Biol* **24**, 9705-9725, doi:10.1128/MCB.24.22.9705-9725.2004 (2004).
- 111 Dash, A. K., Yende, A. S., Jaiswal, B. & Tyagi, R. K. Heterodimerization of Retinoid X Receptor with Xenobiotic Receptor partners occurs in the cytoplasmic compartment: Mechanistic insights of events in living cells. *Exp Cell Res* **360**, 337-346, doi:10.1016/j.yexcr.2017.09.024 (2017).
- 112 Reho, B. *et al.* Simultaneous Mapping of Molecular Proximity and Comobility Reveals Agonist-Enhanced Dimerization and DNA Binding of Nuclear Receptors. *Anal Chem* **92**, 2207-2215, doi:10.1021/acs.analchem.9b04902 (2020).
- 113 Kilu, W., Merk, D., Steinhilber, D., Proschak, E. & Heering, J. Heterodimer formation with retinoic acid receptor RXRalpha modulates coactivator recruitment by peroxisome proliferator-activated receptor PPARgamma. *J Biol Chem* **297**, 100814, doi:10.1016/j.jbc.2021.100814 (2021).
- 114 García, P., Lorenzo, P. & de Lera, A. R. Natural ligands of RXR receptors. *Methods in enzymology* **637**, 209-234, doi:10.1016/bs.mie.2020.02.006 (2020).

- 115 Kojetin, D. J. *et al.* Structural mechanism for signal transduction in RXR nuclear receptor heterodimers. *Nat Commun* **6**, 8013, doi:10.1038/ncomms9013 (2015).
- 116 Elbel, E. E. *et al.* Hepatic Nuclear Receptor Expression Associates with Features of Histology in Pediatric Nonalcoholic Fatty Liver Disease. *Hepatol Commun* **2**, 1213-1226, doi:10.1002/hep4.1232 (2018).
- 117 De Bosscher, K., Desmet, S. J., Clarisse, D., Estebanez-Perpina, E. & Brunsveld, L. Nuclear receptor crosstalk - defining the mechanisms for therapeutic innovation. *Nat Rev Endocrinol* **16**, 363-377, doi:10.1038/s41574-020-0349-5 (2020).
- 118 Alimirah, F. *et al.* Crosstalk between the peroxisome proliferator-activated receptor gamma (PPARgamma) and the vitamin D receptor (VDR) in human breast cancer cells: PPARgamma binds to VDR and inhibits 1alpha,25-dihydroxyvitamin D3 mediated transactivation. *Exp Cell Res* **318**, 2490-2497, doi:10.1016/j.yexcr.2012.07.020 (2012).
- 119 Hunter, J., Kassam, A., Winrow, C. J., Rachubinski, R. A. & Capone, J. P. Crosstalk between the thyroid hormone and peroxisome proliferator-activated receptors in regulating peroxisome proliferator-responsive genes. *Mol Cell Endocrinol* **116**, 213-221, doi: 10.1016/0303-7207(95)03717-9, doi: https://www.ncbi.nlm.nih.gov/pmc/articles/PMC413346/ (1996).
- 120 Baretino, D. *et al.* Unliganded T3R, but not its oncogenic variant, v-erbA, suppresses RAR-dependent transactivation by titrating out RXR. *EMBO J* **12**, 1343-1354 (1993).
- 121 Chen, Y., Wei, L. N. & Muller, J. D. Probing protein oligomerization in living cells with fluorescence fluctuation spectroscopy. *Proc Natl Acad Sci U S A* **100**, 15492-15497, doi:10.1073/pnas.2533045100 (2003).
- 122 Simandi, Z. *et al.* RXR heterodimers orchestrate transcriptional control of neurogenesis and cell fate specification. *Mol Cell Endocrinol* **471**, 51-62, doi:10.1016/j.mce.2017.07.033 (2018).
- 123 Masia, S., Alvarez, S., de Lera, A. R. & Baretino, D. Rapid, nongenomic actions of retinoic acid on phosphatidylinositol-3-kinase signaling pathway mediated by the retinoic acid receptor. *Mol Endocrinol* **21**, 2391-2402, doi:10.1210/me.2007-0062 (2007).
- 124 Zhu, X. *et al.* All-Trans Retinoic Acid-Induced Deficiency of the Wnt/beta-Catenin Pathway Enhances Hepatic Carcinoma Stem Cell Differentiation. *PLoS One* **10**, e0143255, doi:10.1371/journal.pone.0143255 (2015).

- 125 Garcia-Regalado, A., Vargas, M., Garcia-Carranca, A., Arechaga-Ocampo, E. & Gonzalez-De la Rosa, C. H. Activation of Akt pathway by transcription-independent mechanisms of retinoic acid promotes survival and invasion in lung cancer cells. *Mol Cancer* **12**, 44, doi:10.1186/1476-4598-12-44 (2013).
- 126 Roa, L. A., Bloemen, M., Carels, C. E. L., Wagener, F. & Von den Hoff, J. W. Retinoic acid disrupts osteogenesis in pre-osteoblasts by down-regulating WNT signaling. *Int J Biochem Cell Biol* **116**, 105597, doi:10.1016/j.biocel.2019.105597 (2019).
- 127 Fretz, J. A., Zella, L. A., Kim, S., Shevde, N. K. & Pike, J. W. 1,25-Dihydroxyvitamin D3 induces expression of the Wnt signaling co-regulator LRP5 via regulatory elements located significantly downstream of the gene's transcriptional start site. *J Steroid Biochem Mol Biol* **103**, 440-445, doi:10.1016/j.jsbmb.2006.11.018 (2007).
- 128 Evans, J. L., Lin, J. J. & Goldfine, I. D. Novel approach to treat insulin resistance, type 2 diabetes, and the metabolic syndrome: simultaneous activation of PPARalpha, PPARgamma, and PPARdelta. *Curr Diabetes Rev* **1**, 299-307, doi:10.2174/157339905774574365 (2005).
- 129 Chen, Z. P. *et al.* Ligand- and DNA-induced dissociation of RXR tetramers. *J Mol Biol* **275**, 55-65, doi:10.1006/jmbi.1997.1413 (1998).
- 130 Wood, R. J. Vitamin D and adipogenesis: new molecular insights. *Nutr Rev* **66**, 40-46, doi:10.1111/j.1753-4887.2007.00004.x (2008).
- 131 Yang, F., Teves, S. S., Kemp, C. J. & Henikoff, S. Doxorubicin, DNA torsion, and chromatin dynamics. *Biochim Biophys Acta* **1845**, 84-89, doi:10.1016/j.bbcan.2013.12.002 (2014).
- 132 Yang, L. *et al.* All-trans retinoic acid protects against doxorubicin-induced cardiotoxicity by activating the ERK2 signalling pathway. *Br J Pharmacol* **173**, 357-371, doi:10.1111/bph.13377 (2016).
- 133 Ruiz-Arguelles, G. J. *et al.* Treatment of acute promyelocytic leukemia: a single institution experience. *Rev Invest Clin* **57**, 415-419, doi: <https://pubmed.ncbi.nlm.nih.gov/16187701/> (2005).
- 134 Prufer, K. & Barsony, J. Retinoid X receptor dominates the nuclear import and export of the unliganded vitamin D receptor. *Mol Endocrinol* **16**, 1738-1751, doi:10.1210/me.2001-0345 (2002).

- 135 Barik, S. Site-directed mutagenesis by double polymerase chain reaction : megaprimer method. *Methods Mol Biol* **15**, 277-286, doi:10.1385/0-89603-244-2:277 (1993).
- 136 Sinha, S., Grewal, R. K. & Roy, S. Modeling Bacteria-Phage Interactions and Its Implications for Phage Therapy. *Adv Appl Microbiol* **103**, 103-141, doi:10.1016/bs.aambs.2018.01.005 (2018).
- 137 Welshons, W. V., Wolf, M. F., Murphy, C. S. & Jordan, V. C. Estrogenic activity of phenol red. *Mol Cell Endocrinol* **57**, 169-178, doi: [10.1016/0303-7207\(88\)90072-X](https://doi.org/10.1016/0303-7207(88)90072-X) (1988).
- 138 Huisken, J., Swoger, J., Del Bene, F., Wittbrodt, J. & Stelzer, E. H. Optical sectioning deep inside live embryos by selective plane illumination microscopy. *Science* **305**, 1007-1009, doi:10.1126/science.1100035 (2004).
- 139 Ries, J., Chiantia, S. & Schwille, P. Accurate determination of membrane dynamics with line-scan FCS. *Biophys J* **96**, 1999-2008, doi:10.1016/j.bpj.2008.12.3888 (2009).
- 140 Sankaran, J., Shi, X., Ho, L. Y., Stelzer, E. H. & Wohland, T. ImFCS: a software for imaging FCS data analysis and visualization. *Opt Express* **18**, 25468-25481, doi:10.1364/OE.18.025468 (2010).
- 141 Krieger, J. W. *et al.* Imaging fluorescence (cross-) correlation spectroscopy in live cells and organisms. *Nat Protoc* **10**, 1948-1974, doi:10.1038/nprot.2015.100 (2015).
- 142 Szalóki, N., Krieger, J. W., Komáromi, I., Tóth, K. & Vámosi, G. Evidence for Homodimerization of the c-Fos Transcription Factor in Live Cells Revealed by Fluorescence Microscopy and Computer Modeling. *Molecular and Cellular Biology* **35**, 3785-3798, doi:doi:10.1128/MCB.00346-15 (2015).
- 143 Li, H. *et al.* The Sequence Alignment/Map format and SAMtools. *Bioinformatics* **25**, 2078-2079, doi:10.1093/bioinformatics/btp352 (2009).
- 144 Li, H. & Durbin, R. Fast and accurate short read alignment with Burrows-Wheeler transform. *Bioinformatics* **25**, 1754-1760, doi:10.1093/bioinformatics/btp324 (2009).
- 145 Heinz, S. *et al.* Simple combinations of lineage-determining transcription factors prime cis-regulatory elements required for macrophage and B cell identities. *Mol Cell* **38**, 576-589, doi:10.1016/j.molcel.2010.05.004 (2010).

- 146 Dunham, I. *et al.* An integrated encyclopedia of DNA elements in the human genome. *Nature* **489**, 57-74, doi:10.1038/nature11247 (2012).
- 147 Kanehisa, M. & Goto, S. KEGG: kyoto encyclopedia of genes and genomes. *Nucleic Acids Res* **28**, 27-30, doi:10.1093/nar/28.1.27 (2000).
- 148 Saldanha, A. J. Java Treeview--extensible visualization of microarray data. *Bioinformatics* **20**, 3246-3248, doi:10.1093/bioinformatics/bth349 (2004).
- 149 Hulsen, T., de Vlieg, J. & Alkema, W. BioVenn - a web application for the comparison and visualization of biological lists using area-proportional Venn diagrams. *BMC Genomics* **9**, 488, doi:10.1186/1471-2164-9-488 (2008).
- 150 Thorvaldsdottir, H., Robinson, J. T. & Mesirov, J. P. Integrative Genomics Viewer (IGV): high-performance genomics data visualization and exploration. *Brief Bioinform* **14**, 178-192, doi:10.1093/bib/bbs017 (2013).
- 151 Phair, R. D., Gorski, S. A. & Misteli, T. Measurement of dynamic protein binding to chromatin in vivo, using photobleaching microscopy. *Methods Enzymol* **375**, 393-414, doi:10.1016/s0076-6879(03)75025-3 (2004).
- 152 Philippe, L., van den Elzen, A. M. G., Watson, M. J. & Thoreen, C. C. Global analysis of LARP1 translation targets reveals tunable and dynamic features of 5' TOP motifs. *Proc Natl Acad Sci U S A* **117**, 5319-5328, doi:10.1073/pnas.1912864117 (2020).
- 153 Tyagi, R. K., Amazit, L., Lescop, P., Milgrom, E. & Guiochon-Mantel, A. Mechanisms of progesterone receptor export from nuclei: role of nuclear localization signal, nuclear export signal, and ran guanosine triphosphate. *Mol Endocrinol* **12**, 1684-1695, doi:10.1210/mend.12.11.0197 (1998).
- 154 Daniel, B. *et al.* The Nuclear Receptor PPARgamma Controls Progressive Macrophage Polarization as a Ligand-Insensitive Epigenomic Ratchet of Transcriptional Memory. *Immunity* **49**, 615-626 e616, doi:10.1016/j.immuni.2018.09.005 (2018).
- 155 Chen, Y., Wei, L. N. & Muller, J. D. Unraveling protein-protein interactions in living cells with fluorescence fluctuation brightness analysis. *Biophys J* **88**, 4366-4377, doi:10.1529/biophysj.105.059170 (2005).
- 156 Nanasi, P., Jr. *et al.* Doxorubicin induces large-scale and differential H2A and H2B redistribution in live cells. *PLoS One* **15**, e0231223, doi:10.1371/journal.pone.0231223 (2020).

- 157 Imre, L. *et al.* Nucleosome stability measured in situ by automated quantitative imaging. *Sci Rep* **7**, 12734, doi:10.1038/s41598-017-12608-9 (2017).
- 158 Feige, J. N. *et al.* Fluorescence imaging reveals the nuclear behavior of peroxisome proliferator-activated receptor/retinoid X receptor heterodimers in the absence and presence of ligand. *J Biol Chem* **280**, 17880-17890, doi:10.1074/jbc.M500786200 (2005).
- 159 van Royen, M. E., van de Wijngaart, D. J., Cunha, S. M., Trapman, J. & Houtsmuller, A. B. A multi-parameter imaging assay identifies different stages of ligand-induced androgen receptor activation. *Cytometry A* **83**, 806-817, doi:10.1002/cyto.a.22284 (2013).
- 160 Mikuni, S., Yamamoto, J., Horio, T. & Kinjo, M. Negative Correlation between the Diffusion Coefficient and Transcriptional Activity of the Glucocorticoid Receptor. *Int J Mol Sci* **18**, doi:10.3390/ijms18091855 (2017).
- 161 Maruvada, P., Baumann, C. T., Hager, G. L. & Yen, P. M. Dynamic shuttling and intranuclear mobility of nuclear hormone receptors. *J Biol Chem* **278**, 12425-12432, doi:10.1074/jbc.M202752200 (2003).
- 162 Jankevics, H. *et al.* Diffusion-time distribution analysis reveals characteristic ligand-dependent interaction patterns of nuclear receptors in living cells. *Biochemistry* **44**, 11676-11683, doi:10.1021/bi050744v (2005).
- 163 Lionnet, T., Wu, B., Grunwald, D., Singer, R. H. & Larson, D. R. Nuclear physics: quantitative single-cell approaches to nuclear organization and gene expression. *Cold Spring Harb Symp Quant Biol* **75**, 113-126, doi:10.1101/sqb.2010.75.057 (2010).
- 164 Savatier, J., Jalaguier, S., Ferguson, M. L., Cavailles, V. & Royer, C. A. Estrogen receptor interactions and dynamics monitored in live cells by fluorescence cross-correlation spectroscopy. *Biochemistry* **49**, 772-781, doi:10.1021/bi9013006 (2010).
- 165 Hendrix, J. *et al.* The transcriptional co-activator LEDGF/p75 displays a dynamic scan-and-lock mechanism for chromatin tethering. *Nucleic Acids Res* **39**, 1310-1325, doi:10.1093/nar/gkq933 (2011).
- 166 Sessler, R. J. & Noy, N. A ligand-activated nuclear localization signal in cellular retinoic acid binding protein-II. *Mol Cell* **18**, 343-353, doi:10.1016/j.molcel.2005.03.026 (2005).
- 167 Kumar, S., Saradhi, M., Chaturvedi, N. K. & Tyagi, R. K. Intracellular localization and nucleocytoplasmic trafficking of steroid receptors: an overview. *Mol Cell Endocrinol* **246**, 147-156, doi:10.1016/j.mce.2005.11.028 (2006).

- 168 Wagstaff, K. M. & Jans, D. A. Importins and beyond: non-conventional nuclear transport mechanisms. *Traffic* **10**, 1188-1198, doi:10.1111/j.1600-0854.2009.00937.x (2009).
- 169 Georgiadi, A. & Kersten, S. Mechanisms of gene regulation by fatty acids. *Adv Nutr* **3**, 127-134, doi:10.3945/an.111.001602 (2012).
- 170 Kersten, S. *et al.* Peroxisome proliferator-activated receptor alpha mediates the adaptive response to fasting. *J Clin Invest* **103**, 1489-1498, doi:10.1172/JCI6223 (1999).
- 171 Zhao, C. & Dahlman-Wright, K. Liver X receptor in cholesterol metabolism. *J Endocrinol* **204**, 233-240, doi:10.1677/JOE-09-0271 (2010).
- 172 Wang, B. & Tontonoz, P. Liver X receptors in lipid signalling and membrane homeostasis. *Nat Rev Endocrinol*, doi:10.1038/s41574-018-0037-x (2018).
- 173 Ide, T. *et al.* Cross-talk between peroxisome proliferator-activated receptor (PPAR) alpha and liver X receptor (LXR) in nutritional regulation of fatty acid metabolism. II. LXRs suppress lipid degradation gene promoters through inhibition of PPAR signaling. *Mol Endocrinol* **17**, 1255-1267, doi:10.1210/me.2002-0191 (2003).
- 174 Gonnord, P. *et al.* A hierarchy of affinities between cytokine receptors and the common gamma chain leads to pathway cross-talk. *Sci Signal* **11**, doi:10.1126/scisignal.aal1253 (2018).
- 175 Vámosi, G. *et al.* IL-2 and IL-15 receptor alpha-subunits are coexpressed in a supramolecular receptor cluster in lipid rafts of T cells. *Proceedings of the National Academy of Sciences of the United States of America* **101**, 11082-11087, doi: <https://doi.org/10.1073/pnas.0403916101> (2004).
- 176 Yasmin, R., Williams, R. M., Xu, M. & Noy, N. Nuclear import of the retinoid X receptor, the vitamin D receptor, and their mutual heterodimer. *J Biol Chem* **280**, 40152-40160, doi:10.1074/jbc.M507708200 (2005).
- 177 Michigami, T. *et al.* Identification of amino acid sequence in the hinge region of human vitamin D receptor that transfers a cytosolic protein to the nucleus. *J Biol Chem* **274**, 33531-33538, <https://doi.org/10.1074/jbc.274.47.33531> (1999).
- 178 Gocek, E., Bauriska, H., Marchwicka, A. & Marcinkowska, E. Regulation of Leukemic Cell Differentiation through the Vitamin D Receptor at the Levels of Intracellular Signal Transduction, Gene Transcription, and Protein Trafficking and Stability. *Leuk Res Treatment* **2012**, 713243, doi:10.1155/2012/713243 (2012).

- 179 Guiochon-Mantel, A. *et al.* Nucleocytoplasmic shuttling of the progesterone receptor. *EMBO J* **10**, 3851-3859, <https://doi.org/10.1002/j.1460-2075.1991.tb04954.x> (1991).
- 180 Hanel, A., Malmberg, H. R. & Carlberg, C. Genome-wide effects of chromatin on vitamin D signaling. *J Mol Endocrinol* **64**, R45-R56, doi:10.1530/JME-19-0246 (2020).
- 181 Octavia, Y. *et al.* Doxorubicin-induced cardiomyopathy: from molecular mechanisms to therapeutic strategies. *J Mol Cell Cardiol* **52**, 1213-1225, doi:10.1016/j.yjmcc.2012.03.006 (2012).
- 182 Aminkeng, F. *et al.* A coding variant in RARG confers susceptibility to anthracycline-induced cardiotoxicity in childhood cancer. *Nat Genet* **47**, 1079-1084, doi:10.1038/ng.3374 (2015).
- 183 Baudendistel, N., Muller, G., Waldeck, W., Angel, P. & Langowski, J. Two-hybrid fluorescence cross-correlation spectroscopy detects protein-protein interactions in vivo. *Chemphyschem : a European journal of chemical physics and physical chemistry* **6**, 984-990, doi:10.1002/cphc.200400639 (2005).
- 184 Vámosi, G. *et al.* Conformation of the c-Fos/c-Jun Complex In Vivo: A Combined FRET, FCCS, and MD-Modeling Study. *Biophys J* **94**, 2859-2868, doi:<https://doi.org/10.1529/biophysj.107.120766> (2008).
- 185 Pernus, A. & Langowski, J. Imaging Fos-Jun transcription factor mobility and interaction in live cells by single plane illumination-fluorescence cross correlation spectroscopy. *PLoS One* **10**, e0123070, doi:10.1371/journal.pone.0123070 (2015).
- 186 Greene, R. F., Collins, J. M., Jenkins, J. F., Speyer, J. L. & Myers, C. E. Plasma pharmacokinetics of adriamycin and adriamycinol: implications for the design of in vitro experiments and treatment protocols. *Cancer Res* **43**, 3417-3421, doi: <https://pubmed.ncbi.nlm.nih.gov/6850648/> (1983).
- 187 Silva, E. F., Bazoni, R. F., Ramos, E. B. & Rocha, M. S. DNA-doxorubicin interaction: New insights and peculiarities. *Biopolymers* **107**, doi:10.1002/bip.22998 (2017).
- 188 Neema, S. *et al.* Vitamin D Deficiency After Oral Retinoid Therapy for Ichthyosis. *Pediatr Dermatol* **32**, e151-155, doi:10.1111/pde.12614 (2015).
- 189 Johansson, S. & Melhus, H. Vitamin A antagonizes calcium response to vitamin D in man. *J Bone Miner Res* **16**, 1899-1905, doi:10.1359/jbmr.2001.16.10.1899 (2001).

APPENDICES

I. LIST OF THE FIGURES

FIGURE 1. NUCLEAR RECEPTORS CLASSICAL CLASSIFICATION INTO FOUR SUBFAMILIES	20
FIGURE 2. SCHEMATIC REPRESENTATION OF NUCLEAR RECEPTORS	23
FIGURE 3. SCHEMATIC REPRESENTATION OF RES RECOGNIZED BY RXR HETERODIMERS.....	24
FIGURE 4. ACTIVATION MECHANISM OF RXR PARTNERS SUBFAMILY ACCORDING TO THE MOLECULAR SWITCH MODEL	26
FIGURE 5: SCHEMATIC REPRESENTATION FOR SEVERAL RXR PARTNERS SHARING A LIMITING POOL OF RXR.	29
FIGURE 6. THE RESTRICTION MAP AND MULTIPLE CLONING SITE (MCS) OF THE pEGFP-C3 VECTOR	35
FIGURE 7. THE RESTRICTION MAP AND MULTIPLE CLONING SITE (MCS) OF THE pRSET-B- MCHERRY C-1	36
FIGURE 8. SCHEMATIC REPRESENTATION OF THE RXRA DNA BINDING DOMAIN.	47
FIGURE 9. SCHEMATIC REPRESENTATION OF THE TRANSLOCATION ASSAY IN A THREE-COLOR IMAGING MODEL SYSTEM.	50
FIGURE 10. SCHEMATIC REPRESENTATION OF THE TRANSFECTION CONDITIONS YIELDING EITHER	55
FIGURE 11. SCHEMATIC REPRESENTATION OF IMAGE ANALYSIS AND NCR CALCULATION.....	57
FIGURE 12. SCHEMATIC REPRESENTATION OF THE CHIP-SEQ EXPERIMENT WORKFLOW.	66
FIGURE 13. AN IDEALIZED PLOT OF A FRAP RECOVERY CURVE.....	69
FIGURE 14. REPRESENTATIVE CONFOCAL MICROSCOPIC IMAGES SHOWING THE APPLIED FRAP SETTINGS.....	71
FIGURE 15. GENE EXPRESSION LEVEL OF NRs IN HEK293 T CELL LINE.	74
FIGURE 16. ENDOGENOUS EXPRESSION OF THE RXR IN CELLS INVOLVED IN THE STUDY.	75
FIGURE 17. SUBCELLULAR DISTRIBUTION OF NRs INVOLVED IN THIS STUDY.	77
FIGURE 18. RXR-DEPENDENT NUCLEAR ENRICHMENT OF NR1 IS MEDIATED BY HETERODIMERIZATION.	79
FIGURE 19. COMPETITION BETWEEN PPAR γ AND RARA: RXRA IS MORE PRONE TO HETERODIMERIZE WITH RARA THAN WITH PPAR γ UNLESS PPAR γ GETS LIGANDED.	81
FIGURE 20. RXRA PARTNER SELECTION IS DOSE DEPENDENT.	82
FIGURE 21. COMPETITION BETWEEN RARA AND VDR: RXRA IS MORE PRONE TO HETERODIMERIZE WITH RARA THAN WITH VDR UNLESS VDR GETS LIGANDED.	84

FIGURE 22. COMPETITION BETWEEN PPAR γ AND VDR: RXRA IS MORE LIKELY TO HETERODIMERIZE WITH PPAR γ THAN WITH VDR UNLESS VDR GETS LIGANDED.	86
FIGURE 23. ENDOGENOUS LIGAND DOES NOT CONTRIBUTE TO THE COMPETITION IN OUR MODEL SYSTEM.	87
FIGURE 24. EGFP-VDR/NLSM AS NR1 IN COMPETITION WITH RARA AND PPAR γ	89
FIGURE 25. INCREASED AVAILABILITY OF RXRA ABOLISHES THE COMPETITION BETWEEN NRs FOR RXRA HETERODIMERIZATION.	91
FIGURE 26. VALIDATION OF THE SPIM-ALEX-FRET-FCCS METHOD WITH CONTROL SAMPLES.	93
FIGURE 27. SPIM-ALEX-FRET-FCCS MEASUREMENT REVEAL LIGAND DEPENDENT HOMODIMERIZATION OF RXR.	95
FIGURE 28. GENOMIC BINDING SITES OF VDR CLASSIFIED INTO THREE GROUPS.	96
FIGURE 29. CLUSTERING THE GENOMIC BINDING SITES (GBSs) ACCORDING TO THEIR TAG DENSITIES AND RESPONSE TO CALCITRIOL TREATMENT REVEALED TWO CLUSTERS WITHIN EACH GBS GROUP.	97
FIGURE 30. DE NOVO MOTIF ENRICHMENT ANALYSIS OF VDR GENOMIC BINDING SITES.	98
FIGURE 31. CALCITRIOL REGULATED GENES IN ENHANCER AND PROMPTER REGIONS.	99
FIGURE 32. REPRESENTATIVE TWO-COMPONENT EXPONENTIAL FITS OF EGFP-RARA NORMALIZED INTENSITIES.	101
FIGURE 33. DOXORUBICIN (DOX) REDUCES RARA BINDING TO DNA IN VIVO.	102
FIGURE 34. NUCLEAR MOBILITY OF EGFP DIMER IS UNAFFECTED BY DOX TREATMENT.	103
FIGURE 35. SCHEMATIC REPRESENTATION OF FATTY ACID METABOLISM REGULATION MEDIATED BY TWO NRs.	107
FIGURE 36. SUMMARY OF THE RESULTS REPRESENTED AS CHEMICAL EQUATIONS. REACTANTS, THE TWO COMPETING PARTNERS AND RXR.	108
FIGURE 37. SCHEMATIC REPRESENTATION OF THE STUDY RESULTS.	114
FIGURE 38. SCHEMATIC REPRESENTATION OF THE CLINICAL OR BIOLOGICAL CONSEQUENCES OF OUR RESULTS.	115

II. LIST OF THE TABLES

TABLE 1. MAMMALIAN NUCLEAR RECEPTORS AND THEIR COGNATE LIGANDS.	11
TABLE 2. NUCLEAR RECEPTORS CLASSIFICATION INTO 7 SUBFAMILIES ⁷⁰	21
TABLE 3. PCR SETTING.....	37
TABLE 4. PRIMERS USED TO CLONE NRs INTO pCMV-C3 VECTORS	40
TABLE 5. PRIMERS USED TO CLONE NR/NLSM INTO pCMV-C3 VECTORS.	41
TABLE 6. PRIMERS USED TO CLONE RXR/NLSM INTO pCMV-C3 VECTORS.....	44
TABLE 7. SUMMARY OF THE MUTATIONS INDUCED IN NRs	48
TABLE 8. PRIMERS USED TO CLONE RXRLBD INTO pCMV-C3 VECTORS.....	49
TABLE 9. EXPERIMENTAL DETECTION OF MOI IN HEK293 CELLS.	52
TABLE 10. NRs LIGANDS USED IN THE STUDY	56
TABLE 11. RECIPE FOR WASHING BUFFERS USED IN CHIP.	65
TABLE 12. CONTROL SAMPLES USED IN SPIM-ALEX-FRET-FCCS EXPERIMENTS.	92
TABLE 13. PARAMETERS DETERMINED FROM SPIM-ALEX-FRET-FCCS AND THEIR MEANING...	94

III. KEYWORDS

- Nuclear receptor (NR)
- Retinoic Acid Receptor (RAR)
- Retinoid X Receptor (RXR)
- Peroxisome Proliferator-Activated Receptor (PPAR)
- Vitamin D Receptor (VDR)
- Transcription factor (TF)
- RXR partners
- ChIP-seq
- Nuclear localization
- Nuclear transport
- Heterodimerization
- Confocal microscopy
- Competition
- Crosstalk
- FRAP
- Calcitriol
- AM580
- LG268
- Rosiglitazone (RSG)
- GW9662
- Nuclear receptor agonist
- Nuclear receptor antagonist
- Metabolism
- Genetics
- Protein-protein interaction
- Doxorubicin
- Intercalator
- Chemotherapeutics

IV. Authenticated list of candidate's publications



UNIVERSITY of
DEBRECEN

UNIVERSITY AND NATIONAL LIBRARY
UNIVERSITY OF DEBRECEN

H-4002 Egyetem tér 1, Debrecen
Phone: +3652/410-443, email: publikaciok@lib.unideb.hu

Registry number: DEENK/503/2021.PL
Subject: PhD Publication List

Candidate: Lina Fadel
Doctoral School: Doctoral School of Molecular Medicine

List of publications related to the dissertation

1. **Fadel, L.**, Rehá, B., Volkó, J., Bojcsuk, D., Kolostyák, Z., Nagy, G., Müller, G., Simándi, Z., Hegedűs, É., Szabó, G., Tóth, K., Nagy, L., Vámosi, G.: Agonist binding directs dynamic competition among nuclear receptors for heterodimerization with retinoid X receptor. *J. Biol. Chem.* 295 (29), 10045-10061, 2020.
DOI: <http://dx.doi.org/10.1074/jbc.RA119.011614>
IF: 5.157
2. Rehá, B., Lau, L., Mocsár, G., Müller, G., **Fadel, L.**, Brázda, P., Nagy, L., Tóth, K., Vámosi, G.: Simultaneous Mapping of Molecular Proximity and Comobility Reveals Agonist-Enhanced Dimerization and DNA Binding of Nuclear Receptors. *Anal. Chem.* 92 (2), 2207-2215, 2020.
DOI: <http://dx.doi.org/10.1021/acs.analchem.9b04902>
IF: 6.986

Total IF of journals (all publications): 12,143

Total IF of journals (publications related to the dissertation): 12,143

The Candidate's publication data submitted to the iDEa Tudóstér have been validated by DEENK on the basis of the Journal Citation Report (Impact Factor) database.

24 November, 2021



V. Conferences' presentations and posters related to the dissertation topic

- Hungarian Molecular life sciences 2021, 05- 07 November, Hotel Eger & Park, Eger, Hungary.

Poster: *“Agonist binding directs dynamic competition among nuclear receptor for heterodimerization with retinoid X receptor”.*

- MBFT 2019, Magyar Biofizikai Társaság. 26-29 Aug 2019, department of Biophysics and Cell Biology, Debrecen, Hungary.

Short talk: *“Impact of agonist treatment on RXR partner selection”.*

- EMBO Workshop on Nuclear receptors and biological networks (w18-79). 11-14 September 2018, Avra Imperial Hotel, Kolymbari, Crete, Greece.

Poster: *“Competition between nuclear receptors LBDs for binding to RXR”.*

- 33rd congress of the international society for advancement of cytometry, 28 April - 02 May 2018, Prague Congress Centre, Prague, Czech Republic.

Poster: *“Effect of Agonist binding and heterodimerization with RXR on the localization of nuclear receptor LBDs”.*

- Nuclear receptors and epigenomic mechanisms in human disease and aging, FEBS advanced lecture course. 27 Aug- 01 Sep 2017, Spetses, Greece.

Poster: *“Effect of Agonist binding and heterodimerization with RXR on the localization of nuclear receptor LBDs”.*

- Hungarian Molecular life sciences 2017, 31 March - 02 Apr 2017, Hotel Eger & Park, Eger, Hungary.

Poster: *“The modulation of nuclear receptor dimerization upon ligand binding followed by localization”.*

VI. ACKNOWLEDGMENT

I would like to thank the Tempus Public Foundation and the Stipendium Hungaricum scholarship for offering me and thousands of students over the world the chance to pursue our study at reputative universities like the University of Debrecen.

I appreciate my supervisor, Dr. György Vámosi, for his support over the five years of my PhD. For the time, the experiences and the knowledge he invested in supervising this scientific work... For all the doors he opened for me and the experiences and skills I acquired in his lab. For his big trust ... and for giving me enough space to think, to learn and to structure my work according to my own vision and interest.

I also would like to thank all the kind and collaborative colleagues in our lab “Protein dynamics and interaction research group”. Special thanks to Dr. Julianna Volkó for giving me a hand since I joined the lab and for her precious friendship. And to our golden assistance Ms. Edina Nagy who makes great efforts to set our working environment always to perfect.

A big thank to my co-supervisor Prof. Gábor Szabó who first picked my application to the PhD scholarship and since then he was a big support. Thanks for your kindness, for the quality discussions and for the very nice collaborative work.

Much gratitude to our great collaborator, Prof. Laszlo Nagy, for all the golden chances he generously offered me. Your contribution to my work was like a shelter and wings; it raised the quality of my research, expanded my scientific skills and broaden my vision as junior research seeking for a bright future. I also would like to extend my appreciation to all the people working in his lab, in N-Lab; thanks for always making me feel like a member of your lab, I enjoyed our collaborative work, and I learnt a lot from you.

Big thank to our collaborators at the DKFZ in Heidelberg, Division Biophysics of Macromolecule research group, to Prof. Jörg Langowski and Dr. Katalin Tóth for welcoming me for a short internship, for their kindness, hospitality and big support. I am so grateful to Ms. Gabriele Müller who generously instructed and assisted me in cloning all the needed plasmids to do my study.

Thanks for the workers at the faculty of Medicine, Doctoral School of Molecular Medicine, and especially at the department of Biophysics and Cell Biology for offering the researchers a great environment to do their research; equipped labs and qualified staff.

This scientific work to obtain a PhD in Medical Sciences is dedicated to my dear wounded country Syria, the cradle of civilization ... the land of the first alphabet, the first musical note, the first scale for gold and the first grain of wheat...

All thanks and gratitude to our teachers, professors and students who insisted on pursuing the education despite of the horrors of the war. With a great determination our schools and universities have never closed its doors in front of an ambitious generation believes that only by education and hardworking our wounds will heal up and the future of Syrians will prosper on their land. From Syria, the love, peace and civilization will prevail all over the world again and this 9000 years old civilization will definitely prosper and flourish again.

I would like to thank and appreciate my teachers and professors, at Al-Karamah elementary school and at the high school for Excellent students in my hometown Tartous, at Tishreen University in Latakia where I graduated as a pharmacist and at Damascus University where I obtained a master of specialization in Medical Laboratory Diagnostics.

The biggest thank is to my beloved family, your love and support always pave my way to success. My dear papa, Malek Fadel, I look into your eyes and the whole world gets expanded in my eyes... I listen to your philosophy in life, to your rich and deep thoughts, and I feel like my soul rises, my mind matures and my heart flourishes with goodness, kindness and love. I am grateful for your infinite support, unconditional love and your precious trust. Thanks for your presence in all the details of our life, for being an affectionate and loving father and a wonderful friend.

My dear mama, Victoria Saoud, I learned from you the honesty and the sincerity in work... I learned that the core of success is the patience and the hardworking and as far as our dreams go, the earth expands. I acquired from you the mentality of a passionate and dedicated researcher who believes that science and knowledge are responsibilities where sharing is a duty and acquiring is a right and that excellence and mastery are a blessing and a grace; it is possessed by people who practice it in every little detail. All the love, appreciation and admiration for an outstanding pediatrician, a talented writer, an ideal mother and a wonderful friend.

My dear sisters, Rima & Dima, thanks for your precious presence in my life... you are a blessing, a refuge and a big support ... my shining diamond and my parents gift... my closest friends and my precious treasure. I would like to express my gratitude to with whom my dreams get bigger, get sweeter, fly further and become true.

Science is owned by the universe, and it is the core of its structure. By adding to science, you increase your links with the universe.

Let science grow and prosper governed by honesty, trust and good deeds...

Strive to contribute with your knowledge to building a more just, safe and beautiful society...

Lina Fadel

July 2021